MOLECULAR DYNAMICS STUDIES OF MIXED GAS HYDRATE MELTS AND AQUEOUS INTERFACES

Ph.D. THESIS

by

SUJITH K S

DEPARTMENT OF CHEMISTRY
INDIAN INSTITUTE OF TECHNOLOGY ROORKEE
ROORKEE – 247667, INDIA
MAY, 2018

MOLECULAR DYNAMICS STUDIES OF MIXED GAS HYDRATE MELTS AND AQUEOUS INTERFACES

A THESIS

Submitted in partial fulfilment of the requirements for the award of the degree

of

DOCTOR OF PHILOSOPHY

in

CHEMISTRY

by

SUJITH K S

DEPARTMENT OF CHEMISTRY
INDIAN INSTITUTE OF TECHNOLOGY ROORKEE
ROORKEE – 247667, INDIA
MAY, 2018

INDIAN INSTITUTE OF TECHNOLOGY ROORKEE
ROORKEE

CANDIDATE'S DECLARATION

I hereby certify that the work which is being presented in the thesis entitled, **"MOLECULAR DYNAMICS STUDIES OF MIXED GAS HYDRATE MELTS AND AQUEOUS INTERFACES"** in partial fulfilment of the requirements for the award of the Degree of Doctor of Philosophy and submitted in the Department of Chemistry of the Indian Institute of Technology Roorkee, Roorkee is an authentic record of my own work carried out during a period from July, 2014 to May, 2018 under the supervision of Dr. Ramachandran C. N., Assistant Professor, Department of Chemistry, Indian Institute of Technology Roorkee, Roorkee.

The matter presented in this thesis has not been submitted by me for the award of any other degree of this or any other institution.

(SUJITH K S)

This is to certify that the above statement made by the candidate is correct to the best of my knowledge.

(Ramachandran C. N.)
Supervisor

Dated:

Abstract

Increasing global energy demand has necessitated the search for energy resources which can substitute the fast depleting conventional reserves. In the last few decades, gas hydrates have gained significant attention as a promising future energy resource. The advantages of gas hydrates as an energy resource includes their abundance in under ocean and permafrost regions and the low level of CO_2 emission during the combustion of natural gas compared to other carbon based fuels. Several techniques for the extraction of natural gas from hydrate sediments have been developed. All these techniques involve the dissociation of the crystalline hydrate structure which is accompanied by the release of large amount of gas and water. The liquid phase formed during hydrate dissociation contains hydrate forming gas molecules dissolved in it at high concentrations. The evolution of dissolved gas molecules from this liquid is known to have a significant effect on the kinetics of hydrate dissociation. Earlier studies on the evolution of dissolved gas from the hydrate melt were limited to the case of only one type of gas molecule in the melt. The effect of thermodynamic hydrate inhibitors on the evolution of dissolved gas is also not well understood. The present thesis attempts to apply molecular dynamics simulations to study the process of dissolved gas evolution from aqueous solutions containing one or more types of the hydrate forming gases at conditions typical to natural gas extraction.

An important physical system which is of significance to gas hydrate formation as well as atmospheric chemistry is the interface between liquid and gas. One of the most studied liquid-gas interface is the one between water and methane which is known to act as preferred sites for hydrate nucleation due to the high concentration of dissolved gas at the interface. The interaction of methane with water at their interface also has an important role in atmospheric processes such as adsorption of methane on aqueous aerosols. Despite this, the current understanding of structure and dynamics of this interface is insufficient to explain important interfacial processes such as methane dissolution. In the present thesis, molecular dynamics simulations are applied to study the structure of methane-water interface at a molecular level. The role of interfacial structure and the presence of an amphiphilic cosolvent on the adsorption and dissolution of methane at the interface is also examined.

In Chapter 1 of the thesis, various methods for natural gas extraction through hydrate dissociation and the factors affecting the rate of dissociation are discussed. The chapter also reviews earlier studies on the evolution of dissolved gas molecules and its effect on hydrate

dissociation. Following this, findings from reported studies on the structure and dynamics of the liquid-gas interface are briefly reviewed.

The second chapter briefly discusses the computational methods applied in the present work. The functional forms of the various interaction potentials and integrator algorithms applied in molecular dynamics simulations are discussed and a brief outline of the simulation procedure is given.

In chapter 3, evolution of dissolved gas in the CH_4-CO_2-H_2O ternary mixture is investigated. The study of CH_4-CO_2-H_2O mixture is important since it is formed during the extraction of methane from hydrate sediments by its replacement in hydrate cages with CO_2. Classical molecular dynamics simulations of the ternary mixture of varying compositions were performed which revealed that evolution of gas molecules from the mixture involves the formation of nanobubbles. The study also revealed that an increase in the concentration of CO_2 enhanced the formation of bubbles in the mixture. To understand the role of CO_2 in promoting bubble formation, the structure and composition of the nanobubbles formed were examined in terms of the average distribution of gas molecules. The analysis revealed that bubbles formed in the mixture are of mixed type with both gas molecules present inside them. The average distribution of gas molecules in the bubble indicated that CO_2 molecules accumulate at the interface between the bubble and the surrounding liquid phase. The CO_2 molecules at the interface interact with CH_4 through direct contact which is energetically favorable than gas-water interactions. The value of surface tension at the bubble-water interface was calculated which revealed that the presence of CO_2 reduces the surface tension thereby enhancing the stability of the interface. The greater stability of the interface decreases the critical size of the bubble nuclei leading to rapid bubble formation. The results suggest that an increase in concentration of CO_2 assists the evolution of dissolved gas from the CH_4-CO_2-H_2O mixture thereby preventing the accumulation of methane in the liquid phase. Thus, the presence of CO_2 assists the decomposition of methane hydrates in the initial stages of the replacement process.

Chapter 4 investigates the effect of thermodynamic hydrate inhibitors on natural gas evolution from a hydrate melt. The effect of two common hydrate inhibitors, NaCl and CH_3OH on the formation of nanobubbles by dissolved gas molecules was studied. Both types of inhibitors considered are found to assist the formation of methane nanobubbles in the CH_4-H_2O system. NaCl promotes bubble formation by enhancing hydrophobic interaction bewteen aqueous gas molecules. Whereas, enhanced bubble formation in the presence of CH_3OH is

attributed to its amphiphilic nature. These molecules are found to accumulate at the interface between bubble and water with the methyl group oriented towards the gas phase. The presence of CH_3OH at the interface makes the nanobubble more stable by reducing the excess pressure inside the bubble as well as surface tension at the interface. The evolution of dissolved gas from the CH_4-CO_2-H_2O mixture containing hydrate inhibitor was also examined. It is observed that, for a given concentration of the inhibitor, nanobubble nucleation is more rapid in the CH_4-CO_2-H_2O ternary system compared to that in CH_4-H_2O system. The nanobubble formed in the ternary system contains both CH_4 and CO_2 in it and the composition of the bubble is found to be influenced by the type and concentration of the inhibitor molecules present. The stability and properties of the nanobubble is related to its interaction with the surrounding liquid. A quantitative analysis of the bubble-liquid interaction revealed that a frequent exchange of gas molecules takes place between the bubble and the surrounding liquid. The frequency of this gas exchange is found to decrease with an increase in the concentration of hydrate inhibitor and also with an increase in the radius of the bubble. The observed trends in bubble-liquid interaction are explained in terms of the excess pressure inside the bubble and the solubility of gas molecule in the surrounding liquid phase.

Considering the significance of methane-water interface to gas hydrates and atmospheric chemistry, the molecular level structure of this interface was investigated. The results of the study are discussed in chapter 5. Earlier studies on the adsorption of methane molecules on the water surface did not consider the effect of the inherent molecular level roughness of the surface on gas adsorption. Therefore, adsorption of methane on water surface was examined by taking into account the roughness of the surface. A quantitative analysis of roughness was performed in which the extend of roughness was expressed in terms of the amplitude of humps and wells of the surface as well as the frequency at which these are present at the surface. The simulation of methane-water interface at different pressures indicated that an increase in the pressure makes the water surface more rough in terms of amplitude of the humps and wells. The adsorption of methane on the rough water surface was analyzed by identifying the methane molecules in direct contact with the surface as well as those which are held slightly above the surface by attractive non-covalent methane-water interactions. The analysis revealed that a greater fraction of methane molecules in direct contact with the surface are present at the humps of the surface. In contrast, the density of methane molecules above the surface is higher near the wells compared to the humps. The results indicate a clear preference for methane to come in direct contact with

the water surface at the humps rather than at the wells. This is caused by a lower density of water at the humps of the surface layer which reduces the free energy penalty associated with the formation of a cavity between water molecules which methane can occupy.

In chapter 6, dissolution of methane at its interface with methanol-water liquid mixture is investigated. Methanol is a commonly used hydrate inhibitor and is also known to act as a cosolvent for methane in water. The entry of methane into the bulk liquid region of the methanol-water mixture is examined by determining the average density profile of methane along the direction perpendicular to the interface. The results indicate that molecular level surface roughness of the methanol-water liquid mixture has a role in methane dissolution with humps of the surface acting as preferred channels for the entry of methane into the bulk liquid. Analysis of surface roughness of the methanol-water mixture indicates that the surface becomes more rough with an increase in the concentration of methanol. The humps and wells at the surface of methanol rich mixtures are larger in terms of their amplitude compared to the case of mixtures with lower concentrations of methanol. The larger humps on the surface of methanol rich mixtures can assist the entry of methane into the liquid by acting as channels for methane dissolution. The results suggest that the effect of methanol on roughness of liquid surface has a role in the enhanced solubility of methane in aqueous methanol. The effect of methane on the orientation of the methanol molecules at the surface of the methanol-water mixture was also examined. The results indicate that the presence of methane significantly increases the tendency of surface methanol molecules to have their methyl group oriented towards the gas phase of the interface.

The summary and future scope of the present study is provided in chapter 7.

Acknowledgement

I express my deep sense of gratitude and heartfelt thanks to my supervisor **Dr. C. N. Ramachandran**, for his esteemed guidance, invaluable suggestions, keen interest, constructive criticisms and constant encouragement during the course of the present study. I wholeheartedly acknowledge his full cooperation that I received from the very beginning of this work up to the completion in the form of this thesis.

I would also like to thank my research committee members, **Prof. Anil Kumar** (Chairman), **Dr. Pallavi Debnath** (Internal Expert) and **Dr. Ajay Y Deo** (External Expert) for providing valuable suggestions and knowledge throughout my Ph.D.

I take this opportunity to express my profound gratitude and deep regards to **Prof. M. R. Maurya,** Head of the Department of Chemistry, Indian Institute of Technology Roorkee and former head, **Prof. Anil Kumar** for providing the essential infrastructure to carry out my research.

I am also grateful to **Mr. S. P. Singh**, **Mr. Ankur Sharma**, **Mr. Madan Pal**, **Mr. K.C. Tiwari** and other staff members of the Department of Chemistry for their kind co-operation and invaluable help during the official work.

I wish to thank my lab-mates **Surinder Pal Kaur**, **Vinit**, **Ankita Joshi**, **Mohan Tiwari**, **V. Shilpi**, **Sakshi Ganotra**, **Bhawna Singh Tomar**, **Km Suman Lata, Manisha Singh**, **Rajdeep** and **Laukesh Sharma** for their constant support, timely motivation and unfailing help during the course of my Ph.D. I am also grateful to **Dr. P. Smitha** for her constant motivation and support.

I am thankful to Indian Institute of Technology Roorkee (**IITR**) for providing infrastructure for my research work. The financial support provided by Science and Engineering Research Board (**SERB**), Department of Science and Technology (**DST**), India and the Ministry of Human Resource Development (**MHRD**), Government of India are gratefully acknowledged.

I would like to humbly dedicate this thesis to my parents for their love and blessings during this research work. My wife, Anjali has been extremely supportive of me throughout this entire process and has made countless sacrifices to help me get to this point. My special gratitude is due to my brothers for their loving support and encouragement. I would like to express my

reverence and great admiration for my parents-in-law, and brothers-in-law, who have always been the inspiring and encouraging force for me.

Above all, I owe it all to Almighty God for granting me the wisdom, health and strength to undertake this research task and enabling me to its completion.

Sujith K S
IIT Roorkee
May 2018

Table of Contents

LIST OF TABLES

LIST OF FIGURES

List of Publications

Publications from the thesis

1. **K. S. Sujith**, C. N. Ramachandran. Carbon Dioxide Induced Bubble Formation in a CH_4-CO_2-H_2O Ternary System: A Molecular Dynamics Simulation Study. *Phys. Chem. Chem. Phys.*, 2016, **18**, 3746-3754.
2. **K. S. Sujith**, C. N. Ramachandran. Natural Gas Evolution in a Gas Hydrate Melt: Effect of Thermodynamic Hydrate Inhibitors. *J. Phys. Chem. B*, 2017, **121**,153-163.
3. **K. S. Sujith**, C. N. Ramachandran. Effect of Surface Roughness on Adsorption and Distribution of Methane at the Water-Methane Interface. *J. Mol. Liq.* (**under review**)
4. **K. S. Sujith**, Km Suman Lata, C. N. Ramachandran. Adsorption and Dissolution of Methane at the Surface of the Methanol-Water Mixture. *Fluid Phase Equilib.* (**under review**)

Other publications

1. S. P. Kaur, **K. S. Sujith**, C. N. Ramachandran. Formation of a Nanobubble and its Effect on the Structural Ordering of Water in a CH_4-N_2-CO_2-H_2O Mixture. *Phys. Chem. Chem. Phys.*, 2018, **20**, 9157-9166.
2. Vinit, **K. S. Sujith,** C. N. Ramachandran. Spin–Spin Coupling in Nitrogen Atom Encapsulated C_{60}, $C_{59}N$, and Their Respective Dimers. *J. Phys. Chem. A*, 2016, **120** , 6990-6997.

List of Conferences/Workshops

1. *8th USPEX workshop* organized by Shiv Nadar University and Stony Brook University at Shiv Nadar University, Greater Noida, January 20-24, 2015.
2. *CHEMCON 2015, 68th Annual Session of Indian Institute of Chemical Engineers* organized by Indian Institute of Technology, Guwahati and Indian Institute of Chemical Engineers at Indian Institute of Technology, Guwahati, December 27-30, 2015.
3. *18th CRSI National Symposium in Chemistry* organized by Panjab University and Institute of Nano Science and Technology at Panjab University Chandigarh, February 5-7, 2016.
4. *15th Theoretical Chemistry Symposium* organized by University of Hyderabad and Indian Institute of Chemical Technology, Hyderabad, December 14-17, 2016.
5. *ACS on Campus* organized by IIT Roorkee on February 7, 2018.

Chapter 1
Introduction

Global energy consumption is estimated to grow by more than 50% in the next three decades with rapidly increasing energy demand from developing countries [1]. In spite of significant advances in exploring renewable energy resources, it is forecasted that more than 76% of the energy demand in 2040 will be met from carbon based fuels [1]. The common carbon based fuel sources are oil, coal and natural gas among which natural gas is being increasingly favored as indicated by a recent report by the International Energy Agency (IEA) [2]. The preference for natural gas over oil and coal is driven primarily by concerns of increasing CO_2 emission accompanying the rising energy consumption. The amount of CO_2 emitted during the combustion of natural gas is significantly lower compared to the case of oil and coal [1, 3]. This has stimulated efforts towards the extraction of natural gas from conventional as well as unconventional sources. With rapid depletion of readily accessible gas reserves, recent years witnessed the emergence of unconventional sources such as shale gas and coal bed methane [1]. A more attractive natural gas resource which came to prominence in the last few decades is Natural Gas Hydrate which are ice like sediments present in the marine and permafrost regions [1, 3]. It is estimated that the amount of natural gas stored in gas hydrate reserves is more than twice the amount stored in all other resources combined [4]. The diverse geographical distribution of hydrate reserves combined with their abundance has kindled research into various aspects of gas hydrates in the recent years. A brief overview of the history and importance of natural gas hydrates is presented below.

1. 1 Gas Hydrates

Gas hydrates were first discovered by Sir Humphrey Davy in 1810 who reported the formation of a solid compound when chlorine gas was dissolved into water above the ice point [5]. However, significance of gas hydrates was not realized until the discovery by Hammerschmidt in 1934 that the blockage of gas transmission pipelines is due to the formation of gas hydrate plugs [6]. The cost and safety concerns regarding the formation of gas hydrate in pipelines motivated the study of these compounds in greater detail. Besides their role in flow assurance in gas pipelines, gas hydrates have a significant role as a future energy resource and an

efficient means for the storage and transporation of natural gas [3]. The importance of gas hydrates in addressing the problems of global warming and climate change is also being realized and has developed into an active area of research [3]. A brief discussion of various important aspects of gas hydrates is given below.

Gas hydrates were initially considered as a nuisance to the petroleum industry due to their role in pipe line blockage leading to significant delay in gas production and subsequent economic loss. This inspired research aimed at mitigating the problems caused by formation of hydrate plug in natural gas pipelines. Several methods have been developed for flow assurance in pipelines which includes depressurization of the pipeline, heating and injection of chemicals which can inhibit or delay hydrate formation [4]. Considerable progress has been made in the development of hydrate inhibitors which can prevent hydrate plug formation in gas pipelines [3].

Although gas hydrates were initially considered as a hazard to natural gas industry, later discovery of vast reserves of naturally occuring gas hydrates has made them attractive as an energy resource [3, 4]. The gas concentraion in hydrates is very high such that a unit volume of methane hydrate when dissociated produces ~180 volumes of methane at standard temperature and pressure [3]. Efforts are underway for safe and economic recovery of the natural gas trapped inside the hydrate sediments.

The ability of gas hydrates to store gas in highly compressed form implies that these compounds have immense application in the field of gas storage and transportation. The application of hydrates in gas storage was first suggested by Gudmundsson *et al.* whose work led to further development of this idea [4, 7]. Stern *et al.* reported an anomalous self preservation in gas hydrates which enables them to remain stable for long periods under moderate refrigeration at atmospheric pressure [8]. Studies on gas storage in hydrates have also been extended to the case of hydrogen [9-13].

Apart from its role in natural gas industry, the importance of gas hydrates in influencing global warming and climate change has been increasingly recognized due to the huge volume of green house gases entrapped within the hydrate sediment. A spontaneous dissociation of the hydrate sediments can increase the amount of methane in the atmosphere to dangerous levels [14, 15]. Another topic of interest in relation to the role of gas hydrates in global warming is the possibility of using these compounds as a means to sequester green house active gases. Recent studies in this direction have been mostly focussed on the sequestration of CO_2 through hydrate

formation [16-18].

The advances in various applications of gas hydrates mentioned above have been possible due to a detailed understanding of the structural and dynamic properties of these compounds. Significant advances have been made in the last two decades in the study of various aspects of gas hydrates. A brief review of the studies on the molecular level structure of gas hydrates is given in the following section.

1.2 Structure and Composition of Gas Hydrates

Gas hydrates form from water and small gas molecules such as CH_4, CO_2, N_2 etc. under conditions of low temperature and high pressure. Experiments have revealed the crystalline nature of gas hydrates in which gas molecules are accommodated inside cage like cavities formed by hydrogen bonded network of water molecules [3, 19]. Three main structures of gas hydrates are known which are cubic structure I (sI), cubic structure II and hexagonal structure (sH) [1, 3, 19, 20]. The building blocks of crystal structure of gas hydrates are the different types of water cages which encapsulate various gas molecules. The water cavities found in gas hydrates include pentagonal dodecahedral (5^{12}), tetrakaidecahedral ($5^{12}6^2$), hexakaidecahedral ($5^{12}6^4$) , icosahedral ($5^{12}6^8$) and irregular dodecahedral ($4^35^66^3$) cages. The sI hydrate unit cell is made two 5^{12} cages and six $5^{12}6^2$ cages. The sII unit cell consists of sixteen 5^{12} and eight $5^{12}6^4$ cages and the unit cell of the third hydrate structure, sH is composed of three 5^{12}, two $4^35^66^3$ and a $5^{12}6^8$ cages. The water cages constituting the hydrate structure are occupied by guest atoms or molecules of suitable size.

Several quantum mechanical studies revealed that the presence of guest molecules inside water cages enhances the stability of hydrates through dispersion interactions between the guest and host water molecules [21-32]. Another finding about host-guest interaction in gas hydrates is that for a given cage size, this interaction is most favorable for an optimum size of the guest molecule [21, 26, 28, 32]. Thus, the size of guest molecule is a crucial factor in determining the stability of hydrate structure formed.

An important aspect of gas hydrates which differentiates them from inorganic hydrates is the stoichiometry of these compounds. Unlike inorganic hydrates which has a definite stoichiometry, gas hydrates are non-stoichiometric compounds due to the variable occupancy of the water cages present in hydrates. Experiments have shown the methane hydrate has a variable

H_2O:CH_4 ratio depending on the conditions in which the hydrate is formed [33]. This suggests that some of the cavities in the hydrate structure are not occupied by gas molecules. The non-stoichiometry of gas hydrates can also arise from the multiple occupancy of water cages by guest molecules [23, 24, 34, 35].

A molecular level understanding about the structure and composition of gas hydrates has served as guidelines to the natural gas industry. One of the major objectives of the studies on gas hydrates has been to develop methods for the extraction of natural gas trapped in the hydrate sediments. Several techniques have been developed for natural gas extraction and studies are being carried out to make the extraction process more efficient and safe. Various techniques for natural gas extraction from gas hydrates are briefly discussed in the following section.

1.3 Natural Gas Extraction from Gas Hydrates

A large fraction of the naturally occurring gas hydrate deposits is present at the ocean floor [3]. The recovery of natural gas from gas hydrates within the ocean sediments is a technically challenging process. The major concern that must be addressed in the development of natural gas extraction techniques is that the reservoir stability should be preserved while gas is extracted at a rate which is profitable for the industry. An uncontrolled dissociation of hydrates in the sediments can be disastrous for the environment as well as for the stability of the sea floor [1, 3]. Natural gas is extracted from hydrates by inducing the dissociation of the hydrate structure causing the release of large quantities of gas which were trapped within the hydrate structure. The various extraction techniques which are applied in inducing gas hydrate dissociation are thermal stimulation, depressurization and inhibitor injection [1]. These techniques are briefly discussed below.

Thermal stimulation involves heating of natural gas sediments to a temperature at which the gas hydrate structure is unstable and undergoes dissociation. The process is carried out by the injection of hot water or brine into the hydrate bearing sediment [36-40]. Thermal stimulation by hot water injection has been found to be inefficient due to significant heat loss during the delivery of the hot fluid from the ocean surface to the hydrate sediment. This has lead to the application of alternate methods for thermal stimulation. In one such method, an electromagnetic heat source is introduced into the hydrate sediment which was reported to provide significanly higher efficiency than hot water injection [41, 42]. A method called *in situ* combustion has also

been developed which involves the combustion of methane inside the hydrate sediment thereby providing heat necessary for hydrate dissociation [43-45].

Another technique for natural gas extraction from hydrate sediments is depressurization, in which the pressure in the sediments is reduced to a level at which the hydrate phase dissociates [46-49]. Molecular dynamics simulations indicated that extraction of natural gas by depressurization is slower compared to that by thermal stimulation [50]. It has also been shown that dissociation of hydrates by depressurization is limited by heat transfer as hydrate dissociation is an endothermic process [1, 51]. Thus, it has been suggested that depressurization may be combined with other techniques such as thermal stimulation for efficient gas extraction [1].

In addition to the mechanical methods discussed above, chemical methods for natural gas extraction from hydrates have also been developed. One of the chemical methods involves the injection of thermodynamic inhibitors into the hydrate sediments [52-57]. Thermodynamic hydrate inhibitors shift the hydrate equilibrium to high pressure and low temperature thereby making the hydrate structure unstable in their natural conditions. The most common hydrate inhibitors for natural gas extraction are methanol and ethylene glycol among which the latter is preferred due to its low toxicity and higher availability [52, 55]. Another hydrate inhibitor that has been considered is NaCl due to its high availability in nature [53, 54]. The major advantage of chemical injection is that it induces dissociation throughout the hydrate sediment while other extraction techniques cause localized dissociation of the hydrate [56].

An attractive chemical technique for natural gas extraction which has been gaining attention is the replacement of CH_4 from the hydrate sediment by another gas molecule, CO_2. [16-18, 57-62]. In this technique, CO_2 is injected into the hydrate sediment in gaseous or liquid form or in some cases as an emulsion in water. Compared to other natural gas extraction techniques, the replacement method is environmentally friendly as it involves the sequesteration of CO_2 which is a green house gas along with the extraction of CH_4. Another advantage of this method lies in its self sustainability, since the heat released during the formation of CO_2 hydrate is sufficient to dissociate the CH_4 hydrate present in the sediment [63]. In addition to this, the formation of CO_2 hydrate during the replacement process ensures the stability of the under ocean sediment unlike in other extraction techniques. The replacement method is based on the fact that at low temperatures, CO_2 hydrate is thermodynamically more stable than the CH_4 hydrate [62].

The feasibility of replacing CH_4 in its hydrates with CO_2 has also been supported by molecular dynamics simulations [64-66] and *ab initio* calculations [21, 22]. Though the replacement process has several advantages over other natural gas extraction techniques, various factors limiting the replacement efficiency are to be addressed to make the process economical. One of the reasons for limited efficiency of the replacement method is the formation of a CH_4-CO_2 mixed hydrate layer which can hinder the mass transfer of molecules thereby slowing down the guest replacement [67-69]. Another factor which affects replacement efficiency is the reoccupation of CH_4 molecules into the hydrate phase thereby reducing the yield of CH_4 extraction [59, 70].

One of the key steps of all the natural gas extraction techniques discussed above is the dissociation of the gas hydrate stucture to release the guest gas molecules encapsulated in water cavities. A detailed understanding of the mechanism and various factors which affect hydrate dissociation is essential for the safe and efficient extraction of natural gas from hydrates. Several experimental as well as accurate molecular dynamics simulation studies have been reported which has significantly improved our understanding of hydrate dissociation. A brief review of the recent studies reported on this topic is given below.

1.4 Dissociation of Gas Hydrates

Gas hydrate dissociation is one of the most crucial steps in all the natural gas extraction processes discussed above. The dissociation of gas hydrate is an endothermic process which involves the break down of water cages at an interface of the hydrate solid with a liquid. During this process gas molecules encapsulated in the hydrate lattice are released into the surrounding liquid phase along with water molecules from the dissociated hydrate structure. Several experimental studies have been reported on natural gas hydrate dissociation induced by various techniques such as thermal stimulation, depressurization and inhibitor injection [36, 37, 42, 46, 51, 52, 55, 71-79]. While experiments provide information about various factors affecting the dissociation process, the application of molecular dynamics simulations in the recent years have provided significant insight into the molecular level details of hydrate dissociation [80-89, 94-99].

The simulation studies on the mechanism of hydrate dissociation showed that dissociation proceeds in a sequential manner starting with the outermost layer of water cages at

the surface of the hydrate crystal [80-84]. The dissociation of the outer layer of the hydrate structure is followed by that of the next layer of water cages and continues in a similar fashion towards the inner hydrate layers eventually leading to complete dissociation of the hydrate. Another important observation reported about hydrate dissociation is that the dissociation of a layer of the hydrate structure takes place in a concerted manner in which the entire layer breaks down simultaneously in a single step [80, 81].

In addition to the mechanism of hydrate dissociation, studies have been reported on the various factors affecting the rate of hydrate dissociation. One of the determinants of hydrate dissociation rate is the occupancy of the hydrate cavities with guest molecules [85-88]. Molecular dynamics simulation studies reported by English *et al.* and Myshakin *et al.* showed that partially occupied methane hydrates dissociated faster compared to the dissociation of hydrate structure with all the cages occupied by guest molecules [85, 86]. Similar studies on carbon dioxide hydrates by Sarupria *et al.* and Liu *et al.* showed that the rate of hydrate dissociation depends not only on cage occupancy, but also on the distribution of the guests among the 5^{12} and $5^{12}6^2$ cages of the hydrate structure [87, 88]. The effect of guest-water interaction on hydrate dissociation was also investigated by Das *et al.* who reported that for a given size of the guest molecule, stronger guest-water interaction will lead to slower hydrate dissociation [89]. Thus, the composition of gas hydrates has a significant effect on the rate at which the hydrate dissociates. Hydrate dissociation is also known to be influenced by several external factors such as heat and mass transfer, presence of sediments and various chemical species. The role of these factors in determining the rate of gas hydrate dissociation is briefly discussed below.

Dissociation of gas hydrates is an endothermic process which indicates that a continuous supply of heat to the hydrate surface is necessary for sustained hydrate dissociation. Several experimental studies on hydrate dissociation showed that heat transfer has a significant effect on the rate of hydrate dissociation [37, 71-76]. The role of heat transfer in the dissociation of gas hydrates has also been investigated using molecular dynamics simulations [80-82, 84]. Bagherzdeh *et al.* performed NVE simulations of methane hydrate dissociation and reported that the system undergoes cooling as the kinetic energy of the molecules is utilized in the melting of hydrate structure [80]. The formation of localized cold and hot regions during hydrate dissociation has also been reported [80-82] which confirms that insufficient heat transfer from

the liquid to the hydrate phase has a negative effect on dissociation rate [84].

In addition to the above studies, the effect of porous sediments containing several organic and inorganic chemical species on hydrate dissociation has also been investigated. The porous sediments and the presence of chemicals in them are known to influence the thermodynamic properties of gas hydrates [90-93]. Molecular dynamics simulation studies have been reported which provide insight into the effect of sediment surfaces and chemicals on hydrate dissociation [94-96]. One of the major findings of these studies is that hydrate structure confined between hydroxylated silica surfaces dissociates faster than that in hydrate-water systems [94, 95]. It was also reported that the presence of organic matter such as fatty acids in sediments accelerate the disintegration of hydrate structure even at low dissociation temperatures [96].

Apart from cage occupancy, heat transfer and the presence of porous sediments containing various chemicals, mass transfer also has a significant effect on hydrate dissociation. Mass transfer refers to the migration of molecules which are released during the dissociation of the hydrate structure. The evolution of dissolved gas molecules from the liquid hydrate melt formed during dissociation has a significant effect on the rate of dissociation. A brief summary of the recent studies reported on the evolution of gas molecules from the hydrate melt and the effect of the resulting mass transfer on dissociation is given below.

1.4.1 Evolution of Dissolved Gas from the Hydrate Melt

Earlier studies about the mechanism of gas hydrate dissociation showed that dissociation occur in a step wise manner where layers of hydrate structure disintegrate one after another [80-84]. These studies demonstrated that the hydrate layer dissociates in a concerted manner which involve simultaneous disintegration of the water cages of the layer. Duing this concerted dissociation, guest molecules along with water are released into the liquid phase. As the concentration of gas molecule in the hydrate phase is significantly higher than its solubility in water, the liqiud hydrate melt adjacent to the dissociating hydrate structure contains gas molecules dissolved in it at supersaturated concentrations [80-83]. Earlier reported simulation studies of hydrate dissociation indicated that the properties of the hydrate melt have a significant effect on the rate at which dissociation proceeds [80-86, 97-99]. Two important processes occuring in the hydrate melt are hydrate regeneration and bubble formation. Regeneration of hydrate cages from the hydrate melt has been reported by various simulation studies on hydrate

dissociation [80-83, 86, 97, 98]. The regeneration of hydrate structure from its melt is driven by the high concentration of gas molecules as well as by a decrease in temperature caused by endothermic hydrate dissociation and insufficient heat transfer. This indicates that a slow diffusion of gas molecules released into the liquid phase during dissociation can result in reversible hydrate growth. Another important phase change in the hydrate melt which affects the rate of dissociation is bubble formation. Formation of bubbles by the gas molecules released during hydrate melting has been reported by several molecular dynamics simulation studies [80-83, 97-99]. Bagherzadeh *et al.* showed by molecular dynamics simulations of methane hydrate dissociation that the methane molecules released into the liquid phase during dissociation aggregagte to form stable bubbles with radius of the order of nanometers [80, 82]. Similar observation was made by Alavi *et al.* who further reported that the diffusion of methane nanobubbles does not follow Fick's law and thereby affect mass transfer of molecules from the dissociating hydrate surface [81]. Another study on methane nanobubble formation during hydrate dissociation reported that a minimum concentration of dissolved methane above the saturation limit is necessary for the formation of stable bubbles [83]. The same study also reported that these nanobubbles remain in the hydrate melt and can cause 'memory effect' which refers to rapid regeneration of hydrate structures from aqueous phase formed during hydrate decomposition. The effect of bubble formation on the rate of gas hydrate dissociation was studied in detail by Yagasaki *et al.* [97, 98]. Their study on dissolved gas evolution during methane hydrate dissociation indicated an initial decrease in the rate of dissociation as the concentration of methane increases in the liquid phase surrounding the hydrate. However, on reaching the limit of supersaturation, methane bubbles start to form in the hydrate melt which rapidly absorbs dissolved methane molecules from the liquid. The formation of methane bubble results in a significant increase in the rate of dissociation of the methane hydrate [97]. The effect of aqueous NaCl solution on the rate of hydrate dissociation was also studied which showed that NaCl influenced the induction time and location of bubble nucleation in the hydrate melt. The bubbles formed in the presence of NaCl were closer to the hydrate interface compared to random location of methane bubbles formed in pure water [98]. In addition to the results from molecular dynamics simulations, the formation of nano and microbubbles during hydrate dissociation has also been reported by a recent experimental study [100]. The study also reported that the slow rise of these bubbles allowed them to stay for significantly long periods in the hydrate melt.

Thus, the formation of nanobubbles is expected to have a significant role in the regeneration of hydrate structure and 'memory effect'. The role of nanobubbles in causing the 'memory effect' observed in gas hydrates has also been observed [101]. Thus, from the above discussion it is clear that the evolution of gas molecules released into the liquid phase during hydrate dissociation has a crucial role in determining the rate and extend of dissociation.

The evolution of aqueous gas molecules from hydrate melt through bubble formation involves the formation of an interface between the resulting bubble and the surrounding liquid phase. The properties of this interface has a significant influence on the evolution of dissolved gas. In addition to natural gas evolution, the liquid-gas interface is of importance in several other areas such as gas hydrate nucleation and atmospheric chemistry. The importance of the interface between liquid and gas phase has motivated several experimental and theoretical studies on the structure and dynamics of this interface, a brief review of which is given below.

1.5 Structure and Dynamics of the Liquid-Gas Interface

The structure and dynamics of the interface between liquid and gas have gained considerable attention due to its importance in understanding several interfacial phenomena such as gas dissolution and hydrate formation as well as in addressing the problems of global warming and climate change [102]. Besides this, the study of this interface has industrial applications such as in the separation of solute molecules of different hydrophilicities from a mixture [103].

One of the most studied liquid-gas interfaces is the one beween methane and water due to its role in the process of methane hydrate nucleation. The formation of gas hydrates starts with a process known as nucleation which is followed by the growth of the hydrate nuclei leading to the formation of the hydrate crystal [19, 104]. The water-gas interface as the preferred location for gas hydrate nucleation has been proved by several experimental studies on hydrate formation [105-112]. These observations have inspired several molecular dynamics simulation studies of the water-gas interface at hydrate forming conditions [113-118]. The studies showed that the enhanced probability for hydrate nucleation at the interface is due to a high concentration of aqueous methane molecules. A high concentration of dissolved gas at the water-gas interface induce hydrate nucleation by facilitating the formation of water cages [114, 118-121]. Thus, the dissolution of gas molecules from the gas phase to water at the interface is a key step in hydrate nucleation. Besides its role in hydrate formation, the properties of water-gas interface has an

important role in addressing the problems of global warming and climate change. It has been reported that the adsorption of the green house gas, methane on atmospheric water clusters results in a change in their infrared absorbance thereby influencing the amount of radiation reaching the earth's surface [122]. Despite its role in hydrate formation and atmospheric chemistry, our understanding of the water-methane interface and important interfacial phenomena such as gas dissolution is incomplete. To gain insight into the mechanism of these processes, a molecular level understanding of the structure of this interface is essential. The findings of some of the recent studies about interaction of gas molecules with water surface are summarized below.

The thickness of the water-gas interface is reported to be of the order of angstroms making it experimentally challenging to study the structure and dynamics of this interface [115]. This has led to the application of computer simulations in studying the structure of this interface at a molecular level [115, 123-128]. One of the major findings of these studies is that the solute molecules get readily adsorbed on the water surface leading to the formation of a thin film [123-127]. This is supported by the observation of a free energy minimum when a gas molecule is present close to the surface of water. However, as the molecule tries to enter the bulk water region by crossing the water-gas interface, free energy increases again to reach a maximum [123, 126, 127]. A molecule must cross this free energy barrier in order to dissolve into the bulk liquid region. Based on the characteristics of water-gas interaction, it was proposed that the process of gas dissolution involves two steps [126]. The first step involves the adsorption of the gas molecule on the surface of water following which the adsorbed molecule is incorporated into the bulk liquid. Two contrasting descriptions of the dissolution process has been reported by recent studies of the water-methane interface [125, 127]. Ghoufi *et al.* reported that the dissolution of adsorbed methane molecules occurs through a progressive hydration of these molecules by water [125]. The water surface undergoes a structural change in this process due to the adsorption of methane molecules. A different mechanism for methane dissolution was proposed by Murina *et al.* according to which the molecular level configuration of the water surface is unaffected during the process [127]. In this mechanism, instead of a progressive hydration of methane, the methane molecules dissolve by occupying the cavities formed due to spontaneous density fluctuations in water. Thus, the actual mechanism of methane dissolution still remains uncertain. A better understanding of the structure of the water-gas interface is essential to get insight into these

important interfacial phenomena.

In addition to water-gas interface, the structure and dynamics of the interface of methanol-water mixture with its vapor has also been a subject of intense study [129-140]. Studying the surface properties of this mixture is of fundamental importance as methanol is the simplest amphiphilic molecule which resemble larger amphiphiles in several properties such as its enhanced concentration at the surface. The study of this interface involved the application of surface specific experimental techniques [132-136] such as sum frequency generation spectroscopy as well as molecular dynamics simulations [129-131, 137-140]. An important finding of these studies is that the methanol molecules have a tendency to remain at the surface even for mixtures which contain low methanol concentrations [129-140]. Matsumoto *et al.* reported that the surface layer of the methanol-water mixture is almost saturated with methanol [130]. The presence of a methanol depletion region following the adsorption layer has also been reported where the concentration of methanol is lower than its concentration in the bulk [137]. Another important characteristic of the water-methanol liquid surface is that the methanol molecules have a strong orientational preference with its methyl group pointing towards the vapor side of the interface. Partay *et al.* [129] and Darvas *et al.* [140] studied in further detail the orientation of molecules at the surface of the water-methanol mixture and reported that the orientational preference of molecules is limited only to the outermost molecular layer at the surface. In addition to the surface concentration and orientational preferences, several characterists of the surface molecules such as the residence time, heterogeneity and hydrogen bonding interactions were also studied in detail. The analysis of residence time of surface molecules of the methanol-water mixture by Partay *et al.* showed that a methanol molecule at the surface layer stays there for a significanlty longer time compared to a water molecule in the same layer [129]. Studies of this mixture also reported the presence of microscopic heterogeneties at the surface molecular layer where with an increase in the concentration of methanol, surface water molecules aggregate together to form clusters which are dispersed in a layer of methanol [129]. Hydrogen bond dynamics at the surface of the water-methanol mixture was studied in detail by Chandra *et al.* by applying molecular dynamics simulations [138, 139]. The studies revealed that the relaxation of hydrogen bonds in the interfacial region is slower than that in the bulk region of the liquid mixture. It was also showed that both water and methanol molecules at the interface have higher diffusivity compared to that in the bulk.

The above discussion indicates that significant progress has been made in understanding the structural and dynamical characteristics of the interface of water-methanol mixture with its vapor. However, the interaction of the surface of this mixture with another gas molecule has not been considered in detail by the earlier reported studies. The interaction of hydrophobic gas such as methane with the surface of the water-methanol mixture is of particular significance since methanol is a commonly used hydrate inhibitor which also act as a cosolvent for methane [141]. Hence, studying the interaction of hydrophobic gases with the surface of the water-methanol mixture can provide insight into the effect of a cosolvent on gas adsorption at an aqueous interface.

1.6 Objectives of the Thesis

An important process which occur during natural gas extraction from hydrates is the dissociation of the hydrate structure. Based on the above discussion, hydrate dissociation can be considered to involve the following stages. In the first stage, the solid hydrate dissociates leading to the formation of a liquid with gas molecules dissolved in it at high concentration. Following the first stage, gas molecules evolves from the hydrate melt thereby leading to the mass transfer of molecules during the dissociation process. Several studies have been reported on the process of hydrate dissociation and the evolution of gas from the liquid phase containing gas dissolved at high concentrations [80-89, 94-101]. The studies on dissolved gas evolution has been limited to systems containing only a single type of gas molecule. Also, the effect of chemical species such as hydrate inhibitors on the evolution of aqueous gas is not well understood.

One of the objectives of the thesis is to study the evolution of hydrophobic gas molecules dissolved in water at high concentrations which is similar to the liquid melt formed during the dissociation of gas hydrate. Particular attention is given to the case where the liquid contains two different types of gas molecules dissolved in it. The gas molecules considered in the present study are CH_4 and CO_2 which are the most important in the context of natural gas extraction. Although studies have been reported on the evolution of dissolved CH_4 from the liquid phase during hydrate dissociation [80-86, 97, 98], evolution of dissolved gas from a liquid containing both CH_4 and CO_2 has not been considered by earlier studies. Understanding dissolved gas evolution in CH_4-CO_2-H_2O ternary mixture is of significance to the extraction of CH_4 from its hydrate through replacement with CO_2. The aim of the thesis is to study at a molecular level the

evolution of aqueous gas from the CH_4-CO_2-H_2O of varying composition.

In addition to studying the evolution of gas from CH_4-CO_2-H_2O mixture, thesis also aims to understand the effect of thermodynamic hydrate inhibitors on dissolved gas evolution. The two common hydrate inhibitors used for natural gas extraction are NaCl and CH_3OH which when injected into the hydrate sediment induce hydrate dissociation [52-54]. As these inhibitors are present in significant amounts in the liqiud phase formed during hydrate dissociation, it is important to study their effect on the evolution of gas molecules from this liquid.

Another objective of the thesis is to study the interaction of gas molecules with the liquid surface which is of importance to several processes like hydrate nucleation as well as in understanding important interfacial phenomena such as gas dissolution. Several studies on the structure and dynamics of water-gas interface have been reported [115, 123-128]. However, the present understanding of the interaction of gas molecules with water surface is insufficient to explain important interfacial phenomena such as gas adsorption and dissolution. The aim of the thesis is to study the structure of this interface at a molecular level taking into account its several features such as the molecular level roughness which has not been considered in the previously reported studies. The thesis also aims at studying adsorption and distribution of gas molecules at the interface and the effect of various factors such as pressure, water-gas interaction and surface roughness on gas adsorption.

Earlier studies reported [123-127] on the process of adsorption and dissolution of gas molecules at the surface of water did not consider the effect of another aqueous molecule on the process. The thesis aims at understanding the effect of methanol on the adsorption and dissolution of methane at its interface with the methanol-water mixture. Understanding the interaction of methane with the surface of the methanol-water mixture is important since methanol is one of the most common hydrate inhibitors which also act as a cosolvent for methane [141]. Methanol is also the simplest amphiphilic molecule and is known to be present in large excess at the surface of the methanol-water mixture thereby influencing the surface charactersitics of the mixture [129-140].

1.7 Outline of the Thesis

The thesis consists of seven chapters. Chapter 1 gives an introduction to gas hydrates and a review of earlier reported studies on hydrate dissociation and evolution of gas molecules from

the resulting hydrate melt. A brief review of reported studies about the liquid-gas interface is also given with particular attention to the properties of the water-methane interface and the interface of methanol-water mixture with its vapor. Following this, the objectives of the thesis are stated which will improve the understanding about natural gas evolution from hydrate melts and interfacial phenomena such as gas adsorption and dissolution taking place at the liquid-gas interface.

The process of natural gas evolution and the adsorption and dissolution of gas moleclues at the liquid-gas interface are studied by applying classical molecular dynamics simulations. In chapter 2, a brief discussion of the theoretical aspects of molecular dynamics simulations is given. Various interaction potentials in molecular dynamics and technical details of steps involved in simulations are briefly explained.

In chapter 3, results from the study of dissolved gas evolution from the CH_4-CO_2-H_2O ternary mixture are presented. The evolution of aqueous gas moleclues from the mixture through formation of nanobubbles and the effect of composition of the mixture on gas evolution is discussed.

In chapter 4, we report findings from the study of natural gas evolution in the CH_4-H_2O and CH_4-CO_2-H_2O systems in presence of hydrate inhibitors, NaCl and CH_3OH. The various physicochemical factors influencing the formation of nanobubbles by dissolved gas molecules are discussed. The interaction of nanobubbles with the surrounding liquid is studied and the effect of hydrate inhibitors on this interaction is examined.

In chapter 5, results from the study of adsorption of hydrophobic gas at the water-gas interface are presented. The effect of various factors such as pressure, water-gas interaction and roughness of the liquid surface on the adsorption of gas molecules is discussed. The observations are explained in terms of the interaction between gas and water molecules at the liquid surface.

Chapter 6 presents findings from the study of dissolution of methane into the methanol-water mixture. The entry of methane into the bulk liquid across its interface with the methanol-water liquid mixture is examined and the effect of methanol on the structure of the interface is studied. The importance of interfacial structure of methanol-water mixture to the enhanced dissolution methane in methanol rich mixtures is discussed.

In chapter 7 the important findings of the thesis are summarized and future scope is discussed.

Chapter 2
Molecular Dynamics Simulations

Molecular dynamics simulation is a computational technique for studying the time evolution of position and velocity of a collection of molecules interacting with each other. The trajectory of the individual molecules is obtained by the numerical integration of the Newton's equations of motion at small intervals of time. Analysis of the trajectory can provide valuable insight about structural properties of the simulation system such as radial distribution functions, dynamic properties like diffusivity, viscocity, thermal conductivity etc. and molecular level description of processes such as phase transitions and protein folding [142]. Rapid increase in computer power and advancements in algorithms have made molecular dynamics simulations applicable in studying a variety of physical and chemical processes. Some of the recent applications of molecular dynamics simulations include the study of chemical reactions [143-151], structure and dynamics of aqueous solutions [152-163], ionic liquids [164-166], interfaces [115, 123-140, 167-171], electrochemical systems [172], biomolecular processes [173-183], nanomaterials [184-190] etc. In addition to these, physical processes such as ice nucleation [191-200] and gas hydrate formation [113, 114, 118-121, 201-212] have also been studied at a molecular level by applying molecular dynamics simulations.

In molecular dynamics simulations, the positions and velocities of the molecules are propagated at finite intervals of time. To perform this, it is necessary to know the force experienced by each atom due to its interaction with other atoms or molecules of the simulation system at every time step. Depending on the methods employed in calculating the force, molecular dynamics simulations are classified into *ab initio* molecular dynamics (AIMD) and classical molecular dynamics [213]. In AIMD, quantum mechanical methods are employed in calculating the forces at each time step of the simulation. The advantage of this method is that the forces calculated are highly accurate and hence provide accurate predictions of the nuclear motion. However, the high computational cost for electronic structure based calculations of intermolecular interactions limits the application of AIMD simulation to systems involving less number of atoms and small time scales. Classical molecular dynamics are applied as an alternative to AIMD in such cases. In classical molecular dynamics simulations, intermolecular

interactions are calculated from empirical potentials known as force fields which are parametrized to accurately reproduce experimental and quantum mechanical results. By using an appropriate force field, the dynamics of a system containing thousands of atoms can be accurately predicted over a time of several hundreds of nano seconds. The choice of the force field is one of the most crucial steps in performing a classical molecular dynamics simulation. The functional forms [214] of the various interaction terms in a force field is briefly disussed in the following section.

2. 1 Force Field

The interaction potential functions in the force field can be broadly divided into bonded and non bonded terms. The bonded interaction potentials include terms corresponding to the bond stretching, bending and torsional motion of covalently bonded atoms. The potential energy corresponding to bond stretching is represented as a harmonic potential given by,

$$V_b = \frac{1}{2} k_b (l - l_0)^2 \qquad (2.1)$$

where, k_b is the force constant for stretching and $(l - l_0)$ is the deviation from equilibrium bond length. The potential energy corresponding to angle bending is given by

$$V_\theta = \frac{1}{2} k_\theta (\theta - \theta_0)^2 \qquad (2.2)$$

where k_θ and $(\theta - \theta_0)$ are bending force constant and the deviation from eqilibrium bond angle, respectively. The other bonded interaction potentials in the force field are the dihedral angle and improper dihedral terms. The potential energy corresponding to dihedral angle deformation is given by

$$V_\Phi = \frac{1}{2} k_\Phi \cos(n\Phi - \Phi_0) \qquad (2.3)$$

where, k_Φ is the force constant for dihedral angle rotation, n , the periodicity of the potential and Φ_0 the optimal value of the dihedral angle.

The improper dihedral term in the force field is to ensure the planarity of moeities such as aromatic rings and to prevent the structure of certain molecules from transforming to their mirror images. The commonly employed potential energy function for improper dihedral is

$$V_{\xi}=\frac{1}{2}k_{\xi}(\xi-\xi_0)^2 \tag{2.4}$$

where, k_{ξ} and $(\xi-\xi_0)$ are the force constant and optimal value of the angle, respectively.

In addition to the bonded interactions, non covalent interactions also exist between molecules in the simulation system. These non bonded interactions include van der Waals and electrostatic interactions which are generally represented by pair interaction potential energy functions. The van der Waals interaction between atoms is described by the Lennard-Jones potential,

$$V=4\varepsilon[(\frac{\sigma}{r})^{12}-(\frac{\sigma}{r})^{6}] \tag{2.5}$$

where, ε and σ are the parameters representing the minimum potential energy and van der Waals diameter, respectively. The r^{-12} term in the potential arises from the repulsive interaction between atoms at short distances where the electron clouds overlap. The attractive r^{-6} term arises from the non bonded dispersive interactions between atoms and is predominant at larger distances. The other non bonded term is the electrostatic interaction potential which is given by

$$V=\frac{1}{4\pi\varepsilon_0}\frac{q_i q_j}{\varepsilon_r r_{ij}} \tag{2.6}$$

where, q_i and q_j are the partial charges and ε_0 , the permittivity of free space. The values of ε_r and r_{ij} represents the relative dielectric constant and the interatomic separation, respectively.

A force field such as AMBER [215, 216], CHARMM [217] or OPLS [218] in classical molecular dynamics specifies the functional form and the values of all the parameters appearing in the bonded and non bonded interaction potentials discussed above. These values of the parameters in the force field are determined through accurate quantum chemical calculations and by fitting to experimental thermophysical and phase coexistence data.

The present study involves the application of classical molecular dynamics simulations to study the dynamics of gas molecules in supersaturated solutions emulating hydrate melts and also at the interface of gas with water and aqueous solutions. Water forms a major component of the simulation systems studied and an accurate molecular model of water is necessary for the simulating these systems. A brief discussion of water models employed in molecular dynamics simulation is given below.

2.2 Water Models

To study the properties of aqueous systems, it is important to choose a water model that provides an accurate representation of the liquid and should be compatible with the solute models employed. The earliest interaction potential for water was proposed by Bernal and Fowler in the 1930's [219]. In this model, water molecule is represented as a four site model with the negative charge on oxygen atom shifted along the bisector of the HOH angle and dispersive interaction parameters assigned to oxygen. More recently introduced water models are SPC [220], TIP3P and TIP4P [221] models which still remain the most commonly applied potentials in molecular dynamics simulations. The SPC and TIP3P models represent water with three interaction sites, each centered on the nuclei, where partial charge is assigned on all sites and Lennard-Jones parameters only to the oxygen. The TIP4P model which resemble the one proposed by Bernal and Fowler [219] consists of four sites with the partial charge on oxygen shifted by 0.15 Å along the bisector of the HOH angle. The shift in the position of the negative charge provides a more accurate description of the electrostatics and gives better predictions for the liquid structure and properties [221]. The SPC, TIP3P and TIP4P water models were parametrized to reproduce the experimental density and radial distribution functions. In addition to these models, a five point interaction potential known as the TIP5P [222] model has also been developed which provided better prediction of the temperature at which water has maximum density. This five point water model contains partial charges on the hydrogen atoms as well as the lone pair sites near the oxygen atom with Lennard-Jones parameters assigned to oxygen. Several re-parametrizations of the SPC and TIP4P models have also been reported which resulted in new models such as the SPC/E [223], TIP4P-Ew [224], TIP4P/2005 [225] etc. Apart from the fixed charge water models discussed above, the incorporation of polarizability effects into these models has been gaining attention recently [226]. However, the inclusion of polarizability leads to a significant increase in the computational cost compared to the fixed charge models.

It has been reported that the TIP4P model provides a qualitatively accurate description of the phase diagram of water [227, 228]. Several simulations studies involving AMBER, CHARMM or OPLS force fields employed the TIP4P water model indicating the compatability of this model with these force fields [229]. Considering these factors, we have employed the

TIP4P water model in the moleclar dynamics simulation of processes such as dissolved gas evolution and the adsorption of gas molecules at liquid-gas interfaces. The OPLS and EPM2 [230] potentials used to model the other components of the simulation system such as CH_4, CH_3OH and CO_2 are known to be compatable with this water model.

2.3 Integrator Algorithms

As discussed above, the force field provides the total potential energy and the force acting on each particle in the simulation system. To obtain the time evolution of the simulation system, the Newtons's equation of motion must be solved for each atom of the system. As an atom interacts with many other atoms, the atomic motions are coupled to each other and an analytical solution to the equation of motion is not possible. Hence, in molecular dynamics the equation of motion for each atom is integrated numerically at definite time steps. Choosing a small time step provides accurate dynamics of the simulation system through this numerical integration procedure.

The most popular integrator algorithm employed in molecular dynamics is the Verlet algorithm. In this algorithm, the atomic positions are expanded in a Taylor series for a time step δt as,

$$r(t+\delta t)=r(t)+v(t)\delta t+\frac{1}{2}a(t)\delta t^2+\frac{1}{6}b(t)\delta t^3+... \tag{2.7}$$

where *a(t)* and *b(t)* are the second and third time derivatives, respectively of the position vector. Similarly, for a time step $-\delta t$ the expansion is given by,

$$r(t-\delta t)=r(t)-v(t)\delta t+\frac{1}{2}a(t)\delta t^2-\frac{1}{6}b(t)\delta t^3+... \tag{2.8}$$

The two expansions when added gives the position at $(t+\delta t)$ as

$$r(t+\delta t)=2r(t)-r(t-\delta t)+a(t)\delta t^2 \tag{2.9}$$

where, the higher order terms in the expansion are neglected.

The expression for velocity obtained through the central difference method by subtracting equation 2.8 from 2.7 is given by

$$v(t)=\frac{r(t+\delta t)-r(t-\delta t)}{2\delta t} \tag{2.10}$$

The above expression for velocity involves an error of the order of δt^2 which led to

modifications in the basic Verlet algorithm to reduce this error [142]. One of the most popular variant of the Verlet algorithm which provides more accurate velocities is the leap-frog algorithm. The expressions for position and velocity in the leap-frog integrator are given by

$$r(t+\delta t)=r(t)+v(t+\frac{\delta t}{2})\delta t \tag{2.11}$$

$$v(t+\frac{\delta t}{2})=v(t-\frac{\delta t}{2})+a(t)\delta t \tag{2.12}$$

In the leap-frog algorithm, the velocities at $t+\frac{\delta t}{2}$ are calculated from equation 2.12 which are applied in equation 2.11 to obtain the position at $t+\delta t$. Thus, the positions and velocities leap over each other by $\frac{\delta t}{2}$ during integration. In this algorithm velocities are explicitly calculated unlike in the basic Verlet algorithm. However, a disadvantage of the method is that the velocities and positions are not calculated simultaneously in the same integration step. Only an approximate value of velocity at δt is obtained from the following relation,

$$v(t)=\frac{1}{2}(v(t+\frac{\delta t}{2})+v(t-\frac{\delta t}{2})) \tag{2.13}$$

A further improvement to the Verlet algorithm is the Velocity-Verlet algorithm which explicitly calculates the value of position, velocity and acceleration at a given time t. In this method, the expressions for position and velocity are calculated simultaneously in the same time step according to the equations

$$r(t+\delta t)=r(t)+v(t)\delta t+\frac{1}{2}a(t)\delta t^2 \tag{2.14}$$

$$v(t+\delta t)=v(t)+\frac{1}{2}[a(t)+a(t+\delta t)]\delta t \tag{2.15}$$

The calculation of velocities in equation 2.15 is performed in two steps. In the first step, velocity at $t+\frac{\delta t}{2}$ is calculated according to

$$v(t+\frac{\delta t}{2})=v(t)+\frac{1}{2}a(t)\delta t \tag{2.16}$$

Following this, the forces are calculated at $t+\delta t$ from which the acceleration, $a(t+\delta t)$ is

deterimined. The velocity at $t+\delta t$ is then given by the equation

$$v(t+\delta t)=v(t+\frac{\delta t}{2})+\frac{1}{2}a(t+\delta t)\delta t \qquad (2.17)$$

The expression for velocity in equation 2.15, is obtained by combining equations 2.16 and 2.17.

2.4 Calculation of Thermodynamic Properties

Two important thermodynamic variables of the simulation system which are determined during molecular dynamics simulation are temperature and pressure. The value of temperature for an N-particle system [214] is obtained from the total kinetic energy (E_{kin}) according to

$$\frac{1}{2}N_{dof}k_B T = E_{kin} \qquad (2.18)$$

where, k_B is the Boltzmann constant and N_{dof}, the number of degrees of freedom. The number of degrees of freedom is given by

$$N_{dof}=3N-N_{constraints}-N_{com} \qquad (2.19)$$

where, the total number of constraints ($N_{constraints}$) imposed on the system and the three degrees of freedom (N_{com}) of the center of mass of the system are subtracted from the total number of degrees of freedom.

The value of pressure is obtained from the relation

$$PV = Nk_B T + \frac{1}{3}\sum_{i<j} r_{ij}.f_{ij} \qquad (2.20)$$

where the first term is associated with the kinetic energy and the second term related to the virial for a system considering pair interaction between particles.

2.5 Statistical Ensembles

The molecular dynamics simulations of physical and chemical processes are performed under thermodynamic conditions which match the experimental conditions at which these processes takes place. The most basic molecular dynamics simulation is performed in the microcanonical (NVE) ensemble in which the total energy of the system is conserved and there are no constraints over temperature and pressure. However, the numerical integration of the equations of motion introduces errors in the velocity and positions calculated as a result of which the total energy is not strictly conserved during the simulation. To minimize this error, a small

integration time step must be choosen to simulate the system in the NVE ensemble which makes such simulations computationally expensive.

Another important type of simulation is the one performed in the canonical (NVT) ensemble which is an extension of the NVE ensemble. This ensemble corresponds to a closed thermodynamic system with constant number of molecules which will interact with the surroundings only through heat transfer. The temperature of the simulation system is maintained in the NVT simulation by coupling it to a thermostat. Various thermostat algorithms have been developed such as the Berendsen [231], Nose-Hoover [232, 233] and Andersen thermostats [234] which when coupled to the simulation system generates the canonical ensemble.

A further extension to the NVT ensemble is the isothermal-isobaric (NPT) ensemble, where both the temperature and pressure of the simulation system are constrained. In NPT simulations, the system is coupled to a barostat in addition to the thermostat. The commonly applied barostats in molecular dynamics include the Berendson [231] and Parrinello-Rahman barostats [235].

In the present study, simulations are preformed in the canonical (NVT) as well as the isothermal-isobaric (NPT) ensembles. The various steps involved in a molecular dynamics simulation are explained briefly in the following section.

2.6 Simulation Procedure

A molecular dynamics simulation involves the preparation of the simulation system, energy minimization and equilibration steps followed by the production simulation. A brief description of these steps is given below.

(i) Simulation system

Choosing the correct size and composition of the simulation system is crucial to obtain accurate dynamics of the system. To minimize the effect of artefacts arising from the finite size of the simulation system, periodic boundary conditions are applied by which the system is surrounded by images of itself. The application of periodic boundary conditions enables the study of various processes through simulations of small systems by ensuring the continuity of these systems at their boundaries. However, when the simulation system is surrounded by copies

of itself, a particle in the system can interact with other particle as well as their periodic images. This problem is solved by introducing the 'minimum image criteria' according to which the cut off for non bonded interactions must be less than half of the shortest dimension of the simulation system.

(ii) Energy minimization

In this step, the initial configuration of the simulation system is relaxed by removing unfavorable interactions between atoms or molecules. During this step a criteria is set according to which the maximum force on an atom should be less than a critical value for the minimization to be considered successful. During the minimization process, the potential energy of the system converges to a low value. The energy minimization methods applied in moleclular dynamics include steepest descent, conjugate gradient etc.

(iii) Equilibration

Equilibration involves bringing the simulation system to the target temperature and pressure at which the production simulation is to be performed. The system is brought to equilibrium in two steps. In the first step it is simulated in the NVT ensemble by coupling to the Berendsen thermostat [231]. This is followed by a simulation in the NPT ensemble where the system is coupled to both thermostat and barostat. In this step, the Berendsen thermostat is replaced by the Nose-Hoover [232, 233] thermostat as the latter is known to generate a more accurate ensemble of kinetic energies. The pressure of the system is brought to the equilibrium value by coupling it to the Parrinello-Rahman Barostat [235].

(iv) Production simulation

In this step, the simulation from the previous step is continued for a sufficiently long time depending on the property studied. The average values of the thermodynamic properties and the time evolution of the simulation system is analyzed from the trajectory generated by the production simulation.

Chapter 3

Evolution of Dissolved Gas in the CH_4-CO_2-H_2O Mixture

3.1 Introduction

The discovery of large reserves of natural gas hydrates in the ocean bed and in the permafrost regions has provided an alternative to the rapidly diminishing conventional fossil fuel reserves [1, 3, 4]. The discovery of these reserves has kindled research to develop safe and efficient methods to recover natural gas from hydrate sediments.

One of the most attractive methods for extracting methane from its hydrates involves replacement with CO_2 leading to the recovery of CH_4 along with the sequesteration of CO_2. The replacement of CH_4 is achieved by the injection of gaseuos or liquid CO_2 into the porous hydrate sediments [58, 62]. In some cases, a micro emulsion of liquid CO_2 in water is also used [17, 58, 62]. The host cages of methane hydrates which encapsulate the gas molecules are made of five- and six- membered water rings. These rings are not large enough to allow the passage of most of the molecules. Therefore, it is anticipated that the replacement process would require the breaking of hydrate cages. Analysis of the replacement process using *in situ* Raman spectroscopy revealed the decomposition of methane hydrates during the process [59] which was later supported by results from molecular dynamics simulations [69]. Thus, it can be concluded that the dissociation of methane hydrate is an important step in the exchange process.

As mentioned in chapter 1, hydrate dissociation results in the formation of a liquid phase rich in dissolved gas. The evolution of dissolved gas molecules from this liquid phase referred to as the 'hydrate melt' is reported to have a significant effect on the rate of hydrate dissociation [80-86, 97-99]. Yagasaki *et al.* recently examined the effect of the formation of bubbles in the hydrate melt on the rate of hydrate dissociation [97, 98]. These studies showed that the formation of bubble accelerates the rate of dissociation and that a delay in bubble nucleation significantly slows down the dissociation process. Studies have also revealed the regeneration of the hydrate structure from the hydrate melt [80-83, 86, 97, 98]. Thus, the evolution of aqueous gas molecules from the hydrate melt is necessary for continuous dissociation of the hydrate structure.

Earlier reported simulation studies on the evolution of dissolved gas from hydrate melts were focussed on the case of melts containing CH_4 [80-86, 97, 98]. However, a similar study of

the evolution of dissolved gases from a hydrate melt containing both CH_4 and CO_2 has not been reported. Understanding dissolved gas evolution in a CH_4-CO_2-H_2O mixture is important as this mixture is formed during the early stages of the replacement of CH_4 in hydrate by CO_2. The structural and dynamical properties of this hydrate melt have an important role in the subsequent stages of replacement. Some of the recently reported experimental studies of the properties of CH_4-CO_2-H_2O mixture and their findings are discussed below.

Qin *et al.* examined the solubility of CH_4 and CO_2 in the CH_4-CO_2-H_2O ternary mixture at temperatures between 324 K and 375 K by varying the pressure from 10 MPa to 50 MPa [236]. They compared the solubility of CH_4 and CO_2 in the ternary mixture to the values predicted by Henry's law for the binary systems, CH_4-H_2O and CO_2-H_2O. The comparison revealed that higher CH_4 mole fraction in the CH_4-CO_2-H_2O system results in 6% to 20% enhancement in the solubility of CO_2, whereas a rise in the concentration of CO_2 leads to 10% to 40% increase in the solubility of CH_4. Recently, Al Ghafri *et al.* examined the two, three and four phase equilibria of the ternary system, in which the compositions of the coexisting phases were determined using gas and liquid chromatographic techniques [237]. The study reported that CH_4 and CO_2 act as co-solvents of each other in the ternary solution indicating that under identical conditions, the behavior of the CH_4-CO_2-H_2O ternary mixture is different from that of the individual CH_4-H_2O and CO_2-H_2O binary systems. Thus, it is important to investigate the ternary system in detail especially in the context of methane recovery from hydrate sediments by the replacement method. The experimental studies on the ternary mixture discussed above were focused on its phase behavior under different conditions of temperature and pressure. However, to the best of our knowledge, a molecular level investigation of the behavior of the ternary solution is lacking.

In this chapter, we present results from the application of classical molecular dynamics simulations to investigate the evolution of gas molecules in the three component (CH_4-CO_2-H_2O) hydrate melt formed during the replacement process. Different compositions of the ternary system are studied by varying the concentration of CO_2 for a fixed concentration of CH_4. The reason for changing the concentration of CO_2 is the fact that in the replacement process, its concentration can be easily controlled. In addition, the solubility of CO_2 is about ten times higher than that of CH_4 and hence the ternary mixture would have a higher concentration of CO_2 compared to that of CH_4. The results from the present work are expected to serve as useful input in the recovery of natural gas from hydrate sediments.

3.2 Models and Methods

The simulation system consists of three components, CH_4, CO_2 and H_2O enclosed in a cubic box similar to the CH_4-CO_2-H_2O ternary mixture formed by the decomposition of methane hydrates in the presence of CO_2. The system consists of 2000 H_2O and 80 CH_4, while the number of CO_2 molecules is varied from 100 to 240, with an increment of 20. Thus, we simulate eight systems, which differ in their concentration of CO_2. The compositions considered here are similar to that of the methane rich solution formed during the decomposition of hydrates in the presence of CO_2. In these simulations, the TIP4P model [221] was used to represent the water molecules. Methane and carbon dioxide molecules were represented by the single point [238] and EPM2 [230] models, respectively. This combination of potentials was reported to be suitable for studying the replacement of CH_4 by CO_2 in hydrate structures [69]. The EPM2 model used for CO_2 is a rigid linear three-site model. During the simulations using the three point model of CO_2 molecules, we observed a deviation of $\angle$OCO from 180°. This arises because the constraint algorithm is known to have difficulty in treating the linear angle. Therefore, the model used for CO_2 was modified by introducing additional point masses on either side of the carbon atom. The entire mass of CO_2 molecule was symmetrically distributed on the two point masses thereby removing the requirement of an angle constraint. The distance between the point masses is chosen to preserve the moment of inertia tensor of the original EPM2 model. The carbon and the oxygen atoms were rendered mass less (virtual interaction sites) and were assigned the respective charges and Lennard-Jones parameters originally used in the EPM2 model. Li *et al.* have used a similar protocol to model CO_2 molecules in their simulations [239]. The Lennard-Jones parameters for the interaction between CO_2 and H_2O molecules were obtained from the *ab initio* calculations reported by Duan *et al.* [240]. The remaining cross interaction parameters between unlike species were obtained using the Lorentz-Berthelot combination rule, which was reported to give an accurate description of the phase diagram of the CH_4-CO_2-H_2O system at a wide range of temperature and pressure [237].

The simulations were performed in the isothermal-isobaric ensemble using the program GROMACS-4.6.5 [241]. The initial configurations were relaxed by energy minimization followed by a 100 ps NVT simulation to bring the system to an average temperature of 270 K. Then, a 200 ps NPT simulation was performed, after which the system attained the equilibrium

with an average temperature and pressure of 270 K and 20 bar, respectively. These conditions were reported to favor the replacement reaction according to simulation studies, which used similar force fields [69]. After equilibration, NPT simulations were performed for a total simulation time of 10 ns with an integration time step of 1 fs. A Nose-Hoover thermostat [232, 233] and a Parrinello–Rahman barostat [235] were used with time constants 0.2 ps and 1.0 ps, respectively. Thermostats are known to affect the diffusivity of the molecular species in the system. However, recently Basconi *et al.* have reported that for the Nose-Hoover thermostat, the diffusivity of small solutes in water are unaffected provided the thermostat is coupled to the overall kinetic energy of the system [242]. The coulombic and Lennard-Jones interactions were calculated within a cutoff of 1.2 nm. The long range electrostatic interaction was treated using the particle mesh Ewald summation method. The molecular geometries were maintained stable using the LINCS algorithm and the water molecules were kept rigid by the SETTLE algorithm [243, 244]. Periodic boundary condition was applied in all three directions.

3. 3 Results and Discussion

3.3.1 Formation of Nanobubbles in the CH_4-CO_2-H_2O Ternary System

To investigate the change in distribution of CH_4 molecules with a change in concentration of CO_2, we consider the CH_4 molecule that has less than 15 neighboring H_2O molecules within a distance of 0.70 nm as part of a bubble. The conditions used here to recognize those CH_4 molecules, which belong to the bubble are appropriate, considering that the first hydration shell of the CH_4 molecule has a radius of ~0.55 nm with a hydration number of ~20 water molecules. Although a bubble may be better characterized by its radius, in the present study the nanobubble formed is described in terms of the number of molecules it contains. This is because of the fact that due to its small size, the nanobubble deviates from the spherical shape making it less convenient to determine its radius at every instant.

For solutions having various concentrations of CO_2, the change in the number of CH_4 molecules in the nanobubble as a function of time is shown in figure 3.1. The nucleation and growth of the bubble for the solution containing 140 CO_2 molecules is illustrated in figure 3.2. It is clear from the figure that no bubble formation takes place in the solution up to 3 ns. However, prior to 3 ns, several small short-lived clusters of dissolved methane are formed in the solution. A

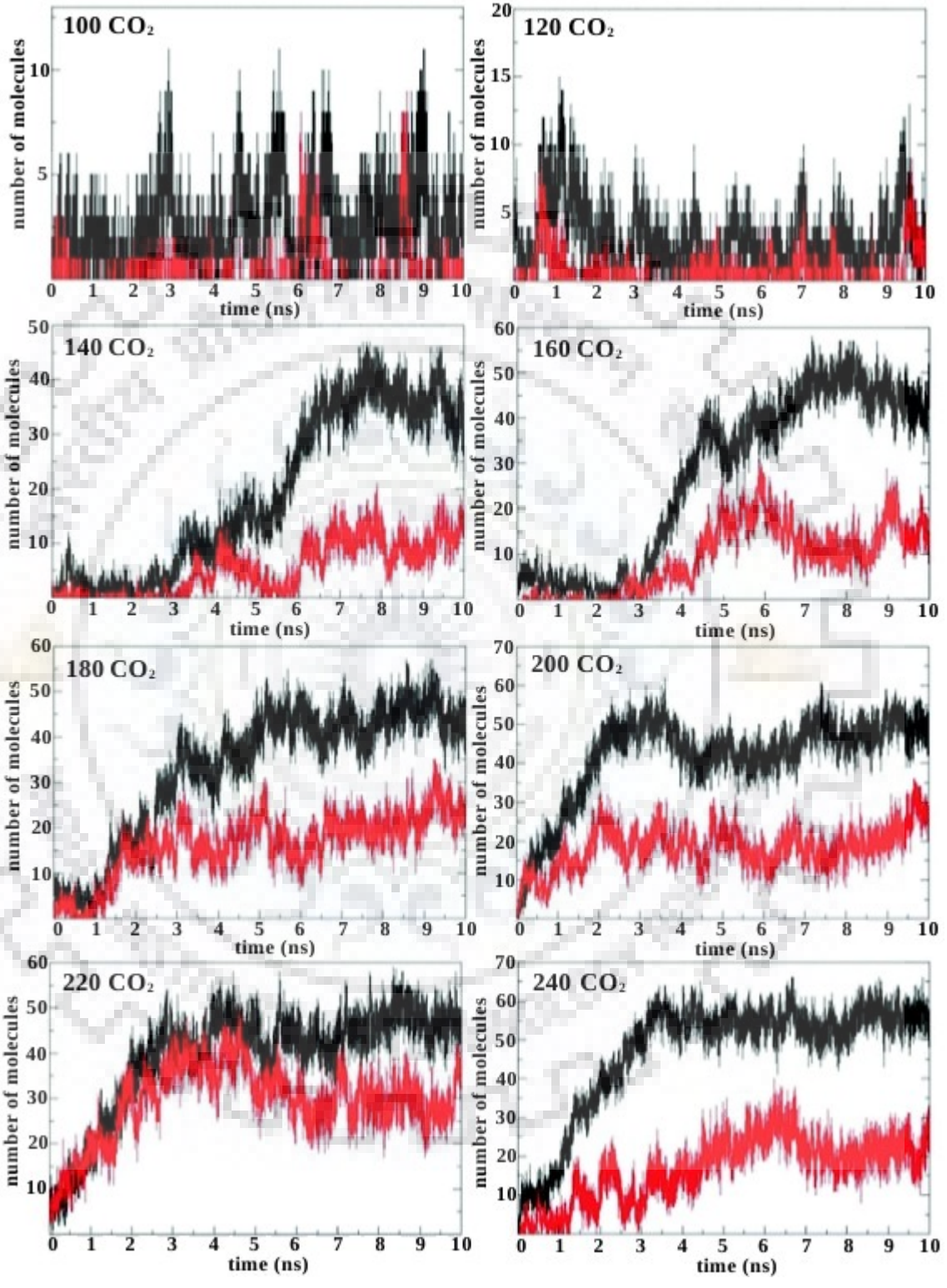

Figure. 3.1 Number of CH_4 molecules (black) in the gas bubble as a function of time for CH_4-CO_2-H_2O systems with different concentrations of CO_2. For each case the number of CO_2 molecules (red) associated with the bubble is also shown.

methane cluster thus formed can grow into a stable bubble only if its size exceeds that of the critical nuclei. At 3.5 ns, a small cluster of CH_4 molecules is formed, which grows rapidly in size and forms a bubble at ~7 ns. In all other cases studied, bubble formation is found to follow a similar procedure though the time at which the nucleation of the bubble commences depends on the concentration of CO_2 in the solution. In all cases, the formation of a single bubble is detected. This could be due to the limited size of the simulation system in which a bubble formed absorbs most of the dissolved gas molecules from the surrounding liquid thereby preventing the formation of a second bubble.

It was reported that gas bubbles formed in liquids may be unstable and dissolve in the surrounding liquid [245]. This is particularly true in the case of nanobubbles as they have very high excess pressure inside. The excess pressure inside a bubble is related to its size and the value of surface tension at the interface between the bubble and the liquid. The value of excess pressure inside a bubble, known as Laplace pressure, is given by

$$\Delta P = \frac{2\gamma}{R} \tag{3.1}$$

where, γ is the interfacial tension near the periphery of the bubble and R is the radius of the bubble. It is clear from the equation that excess pressure inside the bubble is higher for small bubbles. Experimental studies have shown that nanobubbles can remain stable when they are close to each other [246]. This observation suggested that in a cluster of bubbles, the diffusive efflux of gas molecules from a bubble may be shielded by the presence of neighboring bubbles. Using molecular dynamics methods, Weijs *et al.* [247] examined the role of diffusive efflux on the nucleation and stability of nanobubbles in their clusters and reported that for simulation systems of small size, the close proximity of nanobubbles and its periodic images prevents the diffusive efflux of gas molecules from the bubble thereby making it stable. However, with an increase in the size of the simulation system, the bubbles were found to dissociate due to diffusion of gas molecules of the bubble into the surrounding liquid.

In light of the above results, it is important to test whether the formation of nanobubbles in the present study is indeed a real physical phenomenon or is an artifact due to the limited size of the simulation system. To resolve this issue, we performed a simulation on a system of same size containing 80 CH_4 and 2000 H_2O molecules in the absence of CO_2. For this simulation, we

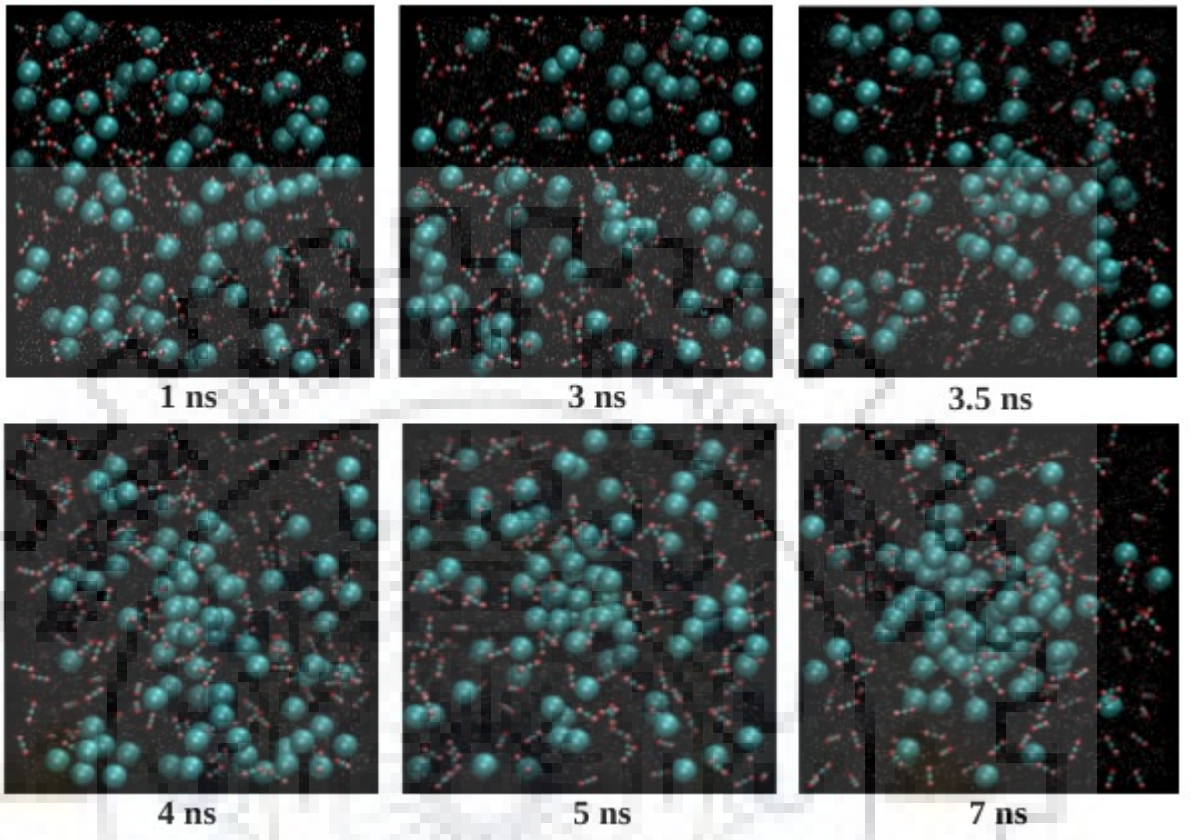

Figure. 3.2 Bubble formation in the CH_4-CO_2-H_2O system containing 140 CO_2 molecules. Methane molecules are represented as cyan spheres and carbon dioxide by ball and stick model.

used an initial conformation consisting of a preformed CH_4 bubble immersed in H_2O obtained by deleting the CO_2 molecules from the final conformation at 10 ns of the CH_4-CO_2-H_2O ternary system containing 140 CO_2 molecules. The analysis of the trajectory obtained from the simulation (figure 3.3) showed that the bubble is unstable and dissociates completely within a simulation time of 3.5 ns during which the gas molecules in the bubble diffuses into the surrounding liquid in contrast to the case of ternary CH_4-CO_2-H_2O solution. This shows that our observation of the nanobubbles in the CH_4-CO_2-H_2O ternary system is independent of the size of the simulation system rather the nucleation and stability of the bubble are due to the presence of CO_2 molecules in the system. The effect of concentration of CO_2 in the ternary system on the nucleation of the nanobubble is discussed in the following section.

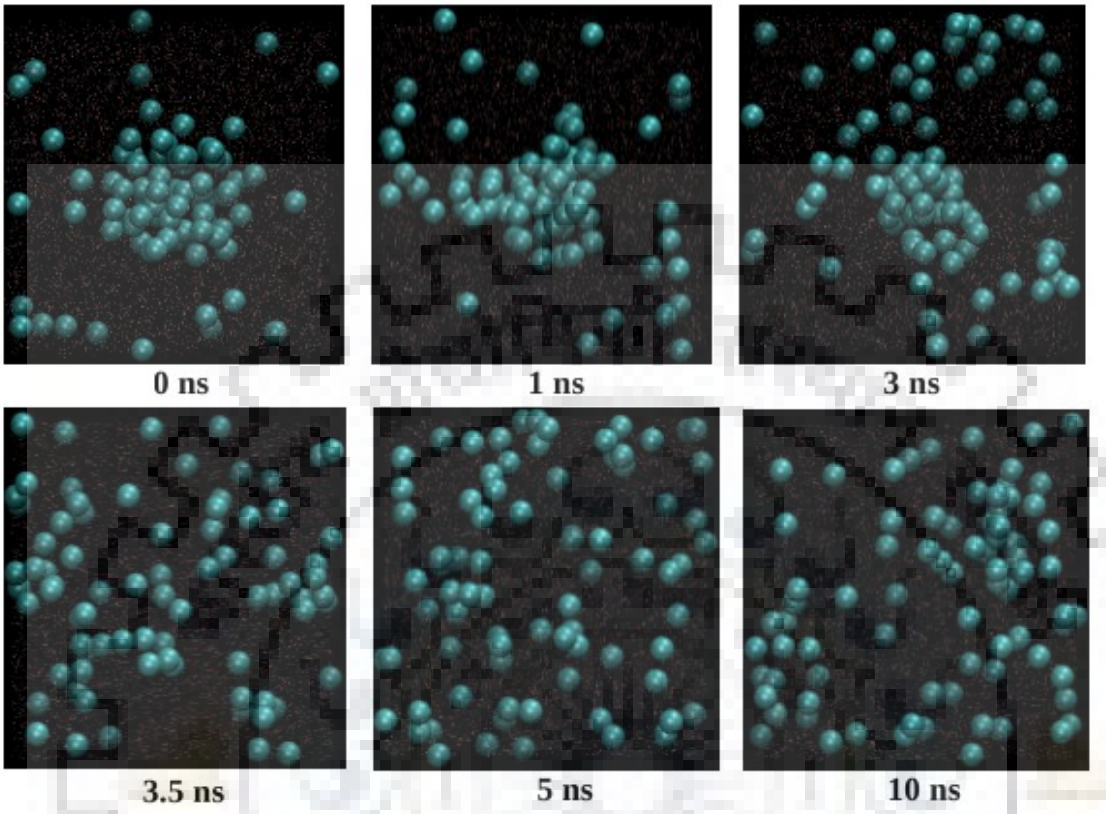

Figure 3.3 Decomposition of methane nanobubble in a CH_4-H_2O mixture containing 80 CH_4 and 2000 H_2O in the absence of CO_2 molecules.

3.3.2 Effect of CO_2 Concentration on Nanobubble Formation in the CH_4-CO_2-H_2O Mixture

A comparison of the nucleation and growth of nanobubbles in the CH_4-CO_2-H_2O ternary systems with varying concentrations of CO_2 is given in figure 3.1. From the figure, it is clear that with an increase in concentration of CO_2, early nucleation of the bubble occurs. Bubble formation was observed within 10 ns in all ternary systems except for the two mixtures with the lowest concentration of CO_2. However, on extending the simulations for longer time for these mixtures with 100 and 120 CO_2 molecules, nucleation of bubbles was observed within 15 ns (figure 3.4). Also, when the simulations were further extended to 60 ns, the bubbles were found to remain in the mixture confirming the stability of the nanobubbles formed. For solutions containing 140 and 160 CO_2 molecules, nucleation of the bubble is observed at ~3 ns. Whereas, for the system with 180 CO_2, nucleation happens at ~1 ns and with further rise in concentration

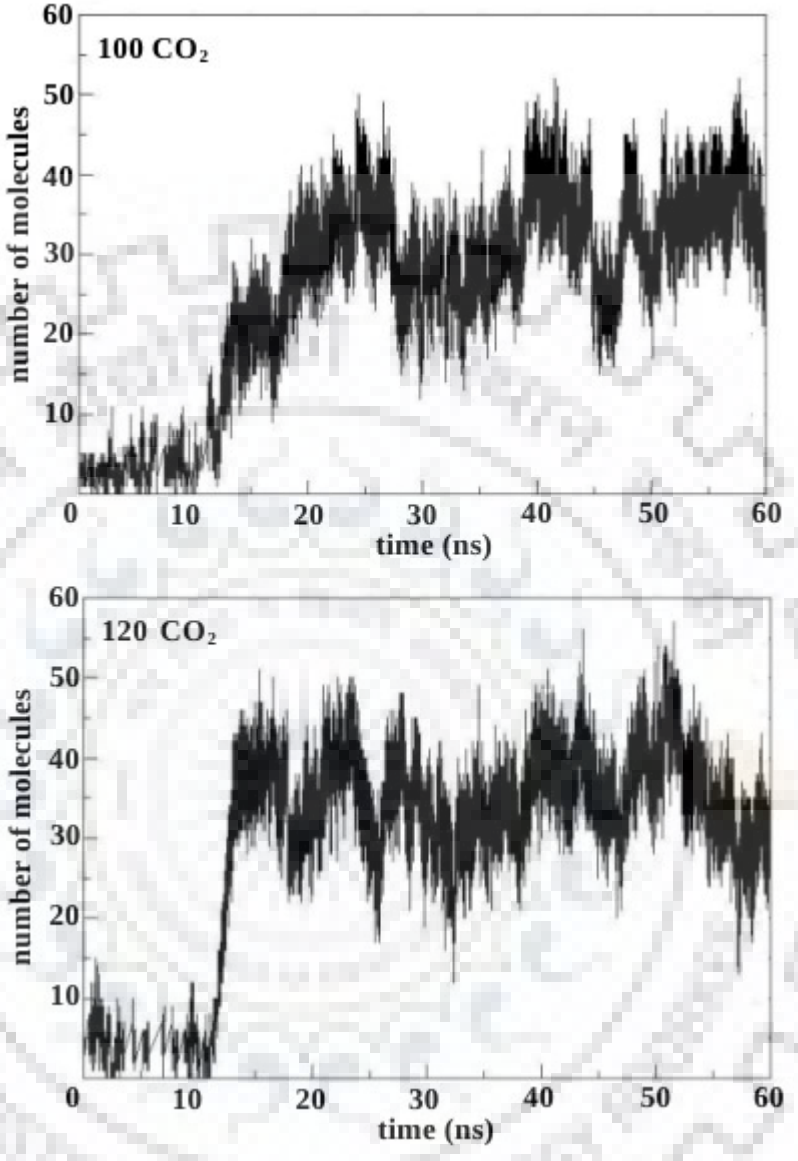

Figure 3.4 Number of CH_4 molecules in the gas bubble as a function of time for the CH_4-CO_2-H_2O ternary systems containing 100 and 120 CO_2 molecules.

of CO_2, the bubble forms immediately. Thus, the results suggest that CO_2 molecules have a role in stabilizing small clusters of dissolved gas molecules formed randomly in the ternary solution, thereby causing early nucleation of bubbles.

It can also be inferred from figure 3.1 that, in general the growth of the bubble is more steady in solutions with a high concentration of CO_2. This is clear if one compares the growth of the bubble in the system containing 140 CO_2 with that containing more than 200 CO_2 molecules.

It can also be noted that the bubble formed at a high concentration of CO_2 is more stable compared to that formed at a lower concentration. The difference in stability of the bubble is clear on comparing the number of CH_4 molecules in the bubble for the solutions containing 140 or 160 CO_2 molecules and that containing 240 CO_2 molecules. In the latter case, once the bubble was fully formed the number of CH_4 molecules in it is around 55 and remains nearly the same after that. Whereas, in the former the number of molecules in the bubble varies with time indicating that the molecules enter and leave the surface of the bubble. Thus, from the above results it can be concluded that the presence of CO_2 molecules assists the nucleation of nanobubble in the CH_4-CO_2-H_2O ternary solution.

3.3.3 Composition of the Nanobubble

In order to determine the composition of the nanobubbles formed in the ternary mixture, we performed the following analysis. A CO_2 molecule which has more than ten CH_4 molecules within a distance of 1 nm was considered as being associated with the bubble. The number of CO_2 molecules associated with the bubble as a function of time is given in figure 3.1. It is clear from the figure that in all the cases the bubble formed has CO_2 molecules associated with it during its nucleation and growth. However, it is not confirmed whether these CO_2 molecules are present within the bubble or at its surface. The exact distribution of CO_2 in the bubble formed is discussed in the following section.

3.3.4 Structure of the Bubble

In the above section, it was shown that the nanobubbles formed in the ternary solution have both CH_4 and CO_2 molecules associated with it. Based on this and also on the structure of the gas-water interface reported by Guo *et al.* [248], we divided the above ternary system into three regions as illustrated in figure 3.5, which include the bubble, the surrounding liquid and the interface between them. In order to obtain a more precise understanding of the structure of the bubble, in particular, the distribution of CO_2 molecules associated with the bubble, the following analysis was carried out.

It is noticed that in all systems where the bubble is formed within 10 ns, its formation is

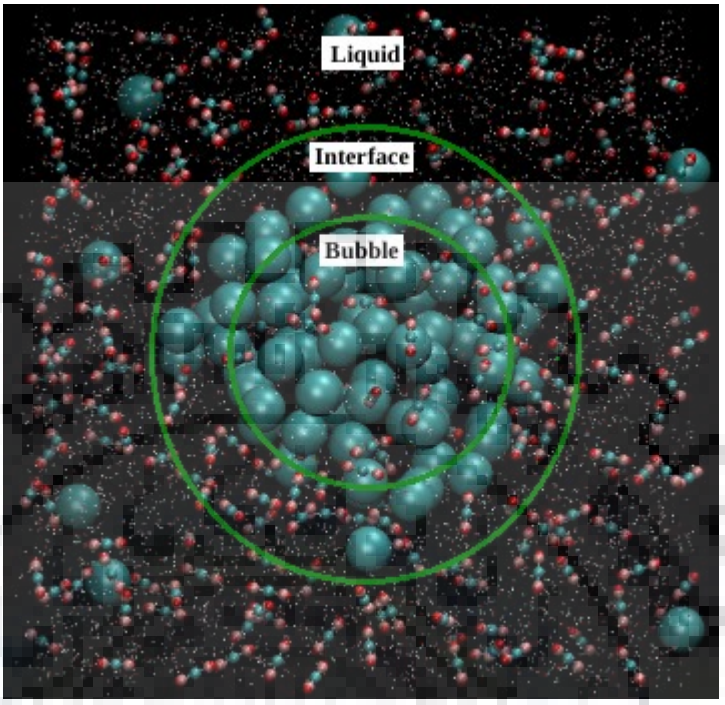

Figure 3.5 Figure illustrating the three regions: bubble, interface and the surrounding liquid of the CH_4-CO_2-H_2O ternary system.

complete before 7 ns. Thus, the solution in which the number of CO_2 molecules ranges from 140 to 240 is expected to contain a fully formed bubble during the time interval of 7-10 ns. From the trajectory within this time interval, the average number density of CH_4, CO_2 and H_2O molecules was determined as a function of distance from the center of the bubble. The center of the bubble was located by averaging the coordinates representing the position of CH_4 molecules belonging to it. During the simulation, the bubble moved within the system. Hence, the position of the center of the bubble was updated at each time step. Following this, we divided the simulation system into concentric spherical shells of thickness 0.1 nm about the center of the gas bubble. After every picosecond in the trajectory, the number of CH_4, CO_2 and H_2O molecules in each of the spherical shells was determined. The average of these values divided by the volume of the corresponding shell gave the number density of each type of molecule as a function of distance from the center of the bubble.

The number density of CH_4, CO_2 and H_2O molecules as a function of distance from the center of the bubble for the ternary systems containing varying number of molecules is given in

figure 3.6. From the figure, it is clear that in each solution where a bubble is formed there is a maximum in the concentration of CO_2 in the region where the bubble comes in contact with the liquid phase. It is also noticed that for systems with a high concentration of CO_2, there is nonzero number density of CO_2 inside the bubble, which means that the bubble formed has both CO_2 and CH_4 in it. This is more obvious in figure 3.7. Thus, it can be concluded that 'mixed' gas bubbles are formed in the CH_4-CO_2-H_2O ternary system containing a high concentration of CO_2.

Another observation about the bubble-water interface is that both the gas phase (bubble) and the surrounding liquid phase overlap and extend into each other as some of the methane molecules present in the bubble diffuse into water at the interface. Also, the concentration of the liquid and the gas phases extending into each other diminishes rapidly. The radial density profile of methane and water at the interface depicted in figure 3.6 is similar to that reported for a planar interface between gaseous methane and a water film [248].

3.3.5 Role of CO_2 in the Formation of Bubbles

In order to understand the role played by CO_2 in the formation of nanobubbles in the CH_4-CO_2-H_2O mixture, we examined the bubble-water interface in detail. From figures 3.6 and 3.7, it can be seen that CO_2 molecules accumulate at the bubble-water interface. The presence of CO_2 molecules at the interface is assumed to enhance the stability of the bubble in the ternary mixture. A detailed analysis of the interface was performed in order to elucidate the role of CO_2 in stabilization of the bubble. From the number density profiles, it can be noticed that on moving away from the center of the bubble, the pure gas (bubble) phase ends at a distance of $\sim$0.75 nm and the pure liquid phase starts near 1.5 nm. The region extending from 0.75 nm to 1.5 nm consisting of a mixture of CH_4, CO_2 and H_2O is defined as the bubble-water interface. It is clear from the number density profiles that there is an enhancement in the concentration of dissolved CO_2 molecules at the bubble-water interface, which is more obvious in figure 3.7. This rise in the concentration of CO_2 at the interface becomes more pronounced as the amount of CO_2 in the system increases.

To understand the nature of interaction between CH_4 and CO_2 molecules at the bubble-water interface, we performed a set of simulations on solutions in which mole fraction of

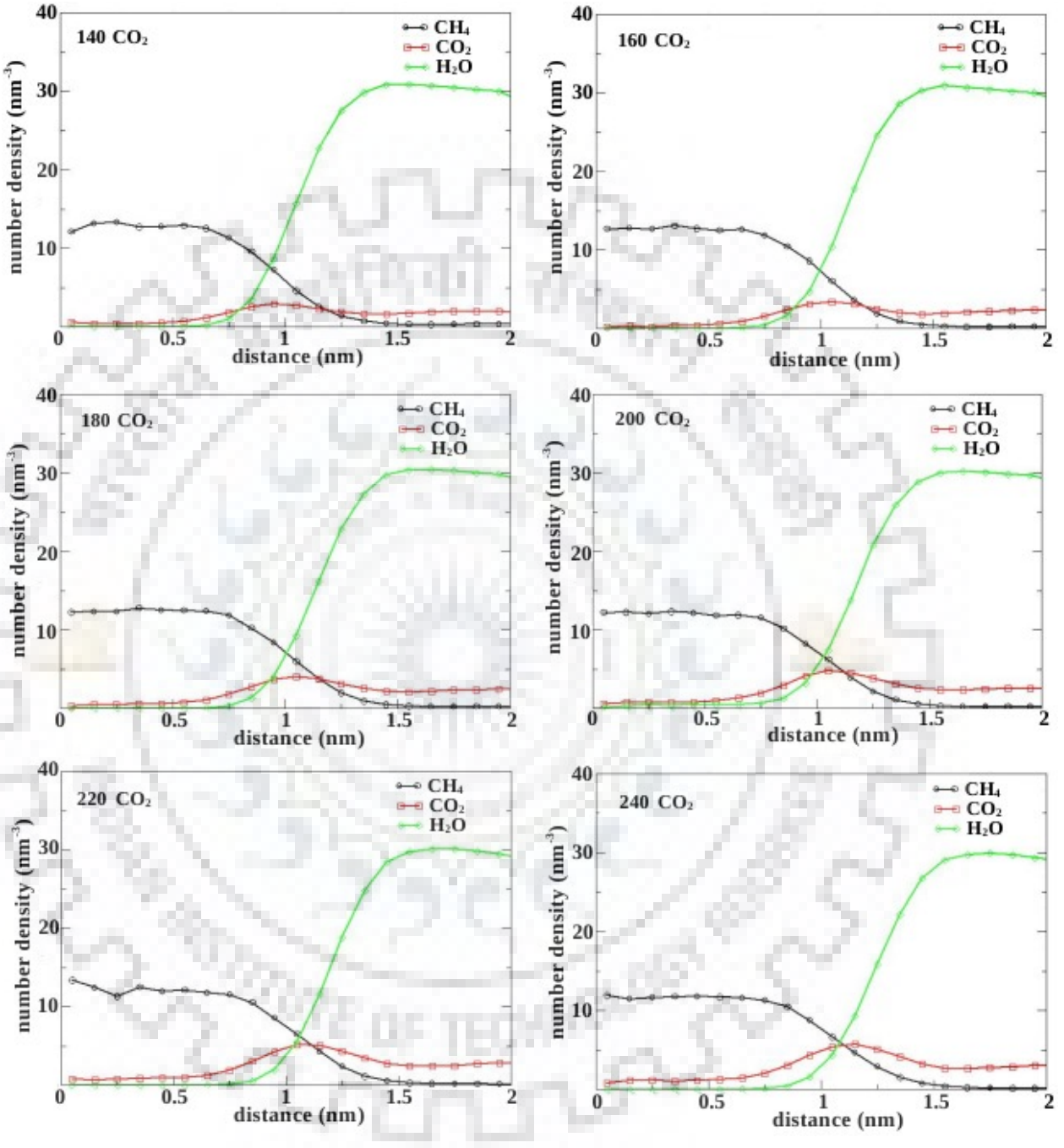

Figure 3.6 The number density of CH_4, CO_2 and H_2O molecules as a function of distance from the center of the gas bubble for the ternary systems containing different number of CO_2 molecules.

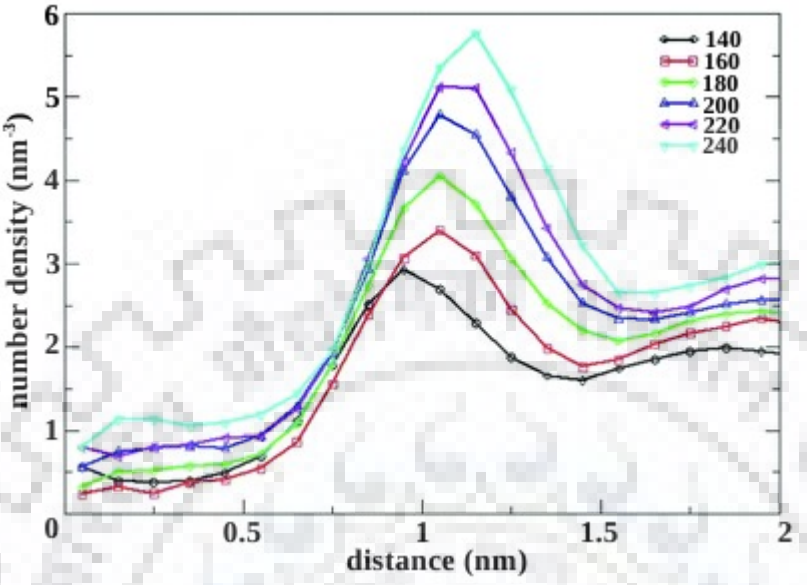

Figure 3.7 The number density of CO_2 molecules as a function of distance from the center of the gas bubble in the CH_4-CO_2-H_2O ternary solution for various numbers of CO_2 molecules.

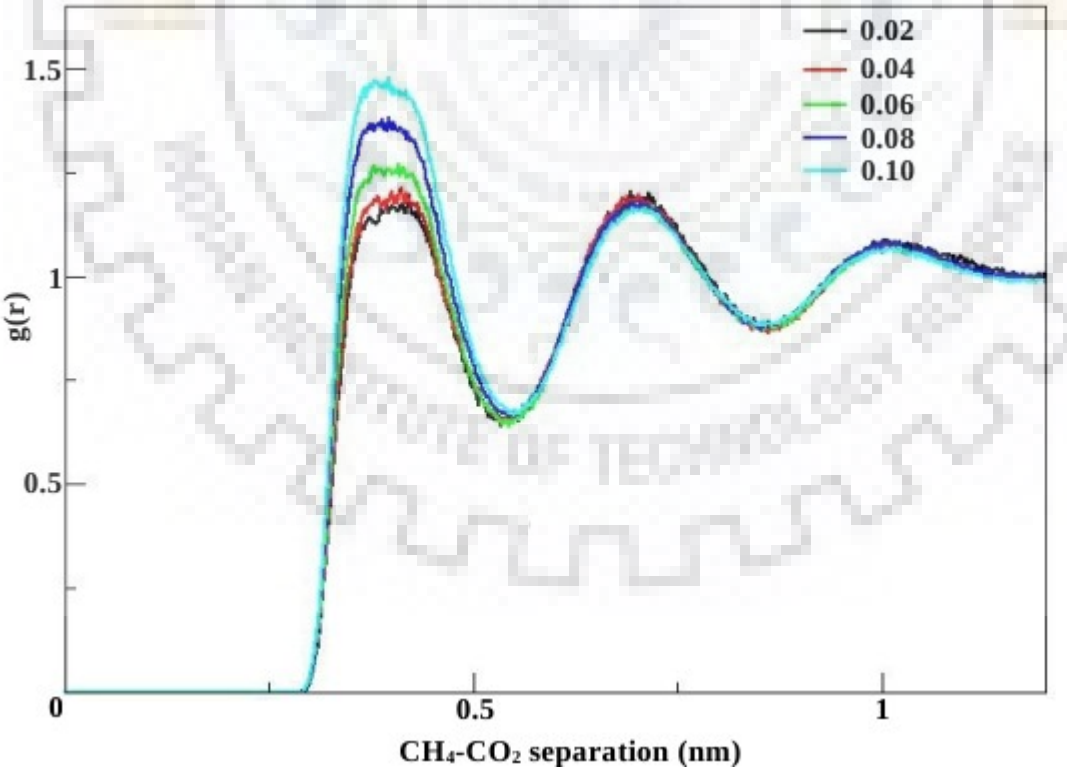

Figure 3.8 Radial distribution functions for the CH_4-CO_2 interaction pair in the CH_4-CO_2-H_2O mixture for various mole fractions of CO_2 keeping the CH_4 mole fraction at 0.02.

CH_4 is 0.02 with the concentration of CO_2 ranging from 0.02 to 0.1 mole fractions. The simulations were performed using the same models under the same conditions that were applied in the simulation of bubble formation. Each simulation was run for a total time of 10 ns and from the resulting trajectory, the CH_4-CO_2 radial distribution function for each case was plotted which is presented in figure 3.8. It is found that with increasing concentration of CO_2, the interaction via direct contact between a dissolved CH_4 and CO_2 molecule becomes more favorable. This indicates that the accumulation of dissolved CO_2 molecules at the interface between the bubble and water leads to a stable direct contact between the hydrophobic CH_4 and CO_2 molecules. This may be providing additional stability to the bubble-water interface compared to the case where there are no CO_2 molecules.

We also studied the effect of CO_2 present at the bubble-water interface on the surface tension at the interface. A decrease in surface tension can result in more stable and long-lived bubbles. The value of surface tension was determined by analyzing the number density profiles of gas molecules and water given in figure 3.6. It is observed that the core of the bubble extending up to a radius of 0.5 nm contains only gas molecules without the presence of water. For each ternary system studied, the average density of the gas in this region of the bubble was determined from the number density profiles. The pressure corresponding to this density was determined from a simulation in the NVT ensemble at 270 K and 20 bar. From the value of the pressure obtained and the radius of the bubble, the value of surface tension (γ) was calculated by using equation 3.1. We considered the radius of the bubble as the distance r at which the value of $\rho^{CH_4}(r)$ reaches 0.5, where $\rho^{CH_4}(r)$ is the number density of CH_4 at a distance r from the center of the bubble divided by the number density at the bulk of the bubble. The value of the surface tension (γ) at the bubble-water interface relative to its value for the ternary system with 140 CO_2 molecules (γ_0) is plotted against the mole fraction of CO_2 in the mixture in figure 3.9. The figure indicates that in general, there is a decrease in surface tension with increasing concentration of CO_2 in the ternary system.

Thus, in systems with a high concentration of CO_2 molecules, CO_2 accumulates at the bubble-water interface. This increases the stability of the interface leading to a decrease in the critical size of the bubble nuclei. Thus, at a high concentration of CO_2 the small clusters formed by dissolved CH_4 become more stable leading to early formation of the bubble.

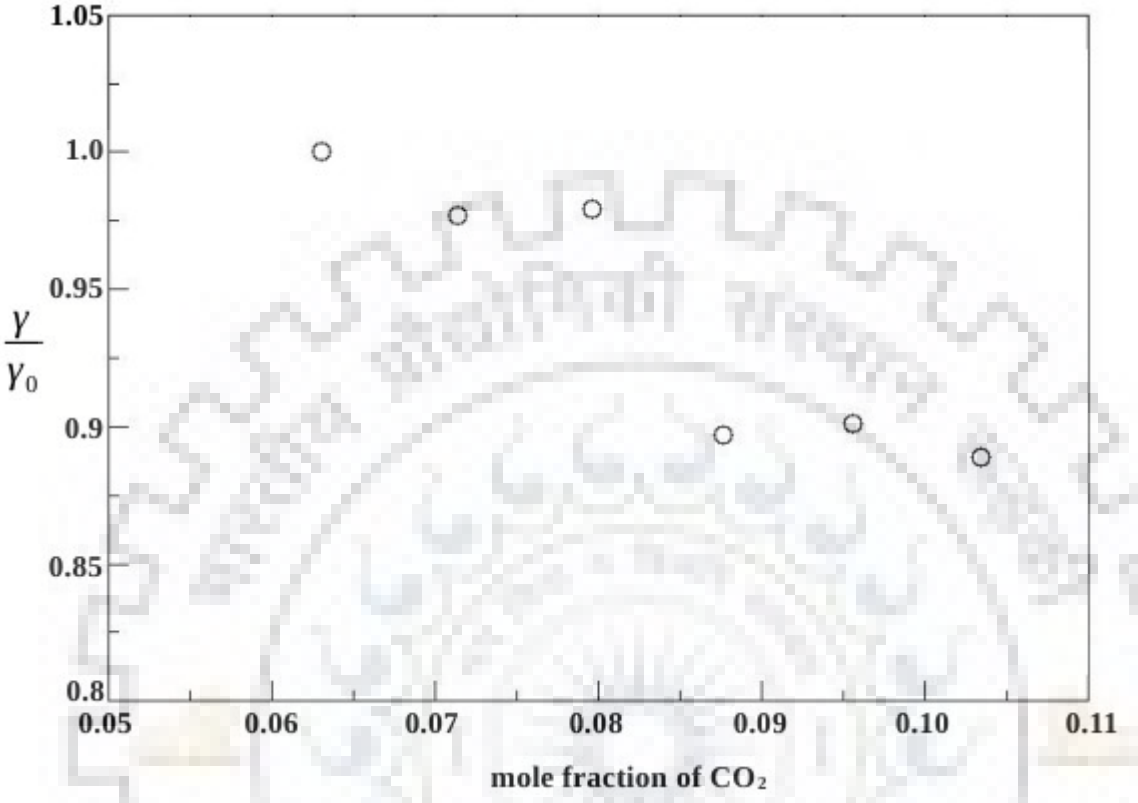

Figure 3.9 Effect of the concentration of CO_2 on surface tension at the bubble-water interface.

3.3.6 State of Methane inside the Nanobubble

In order to gain insight about the state of methane inside the nanobubbles discussed above, we determined the pressure at 270 K inside the bubble and studied the behavior of methane under identical conditions. The pressure inside the gas bubble was determined from the gas density by performing NVT simulations. The pressure was found to be the lowest for the system with the highest concentration of CO_2 due to a decrease in the bubble-water interfacial tension. The value of pressure obtained for this system was found to be 776.8 bar, which is much higher than the external pressure of 20 bar. The high excess pressure could be due to the small size of the bubble, which has a radius of ∼1.0 nm. For the single point model of methane used in the present study, the critical temperature and pressure of pure methane is 191.0 K and 45.0 bar respectively [249]. Thus, due to the high excess pressure inside the nanobubble, methane exists in a supercritical state.

As discussed above, particularly for CH_4-CO_2-H_2O ternary systems with high concentrations of CO_2, the bubbles formed are of mixed type containing both CH_4 and CO_2, the former being the dominant species. In order to study the effect of supercritical conditions on the distribution of CH_4 and CO_2 molecules inside the bubble, we performed an independent 10 ns NPT simulation on a system with 0.1 mole fraction of CO_2 dissolved in super critical methane. The simulation was carried out at a temperature of 270 K and a pressure of 700 bar, which correspond to super critical conditions of methane. From the resulting trajectory, the radial distribution function (RDF) for the interaction pairs, CH_4-CH_4, CH_4-CO_2 and CO_2-CO_2, were plotted. It is evident from the RDF plots (figure 3.10) that the first peak for the CH_4-CO_2 pair interaction is weaker than that for the other two pair interactions. Thus, the solute-solute (CO_2-CO_2) and solvent-solvent (CH_4-CH_4) interactions are stronger than the solute-solvent (CH_4-CO_2) interaction, indicating that the binary mixture under super critical conditions is a repulsive one. However, separation of the components in the binary mixture was not observed in

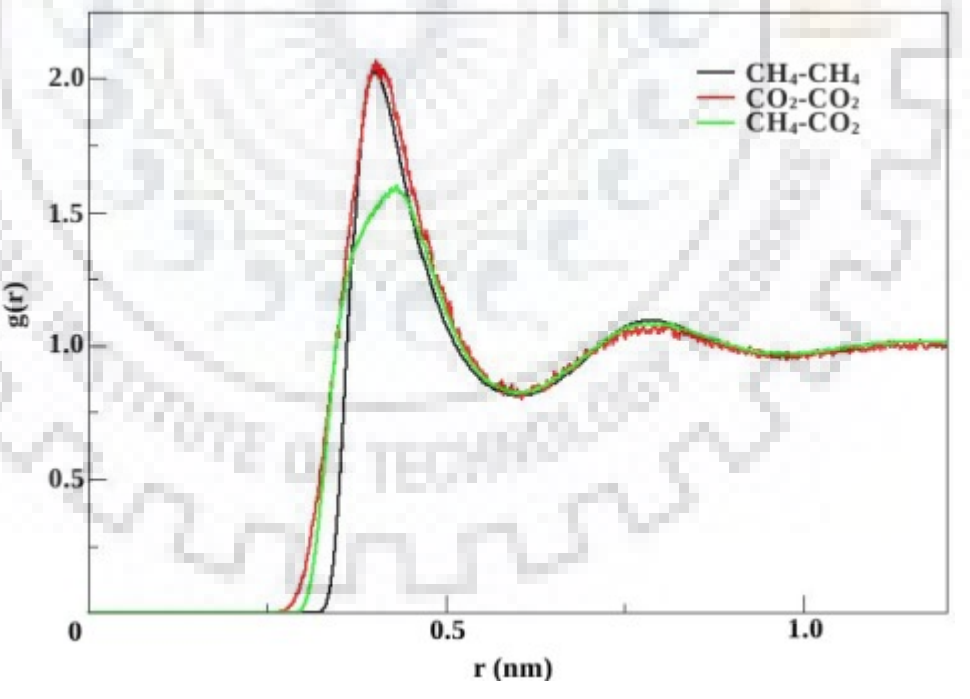

Figure 3.10 Radial distribution function for the solvent-solvent, solute-solute and solvent-solute pair interactions in a dilute binary solution of CO_2 in super critical CH_4.

the solution. The repulsive nature of the binary mixture of super critical CH_4 and CO_2 indicates that CO_2 molecules which accumulate at the bubble-water interface, will not readily diffuse into the bulk of the bubble.

3.3.7 Effect of CO_2 Concentration on the Replacement of Methane in CH_4 Hydrates

It is known that the initial stage of the replacement process involves hydrate dissociation leading to the formation of a CH_4-CO_2-H_2O mixture [59, 69]. Previous studies on the decomposition of CH_4 hydrates revealed that supersaturation of the surrounding liquid by dissloved gas molecules slows down the dissociation process [97]. The formation of bubbles in the supersaturated CH_4 solution was found to be preceded by an induction time before the nucleation of the bubbles occur. The rate of decomposition of methane hydrates increases once the bubbles starts to form [97, 98].

Our results suggest that due to the presence of CO_2, bubble formation occur at an early stage in the CH_4-CO_2-H_2O mixture generated during hydrate decomposition. The bubbles thus formed will lead to more effective removal of aqueous CH_4 from the solution which assists the decomposition of CH_4 hydrates. Therefore, an increase in the concentration of CO_2 ensures more efficient decomposition of methane hydrates thereby improving the rate of replacement of CH_4 by CO_2.

3.4 Conclusion

Classical molecular dynamics simulations were performed to study the evolution of dissolved gas in the CH_4-CO_2-H_2O ternary solution containing various concentrations of CO_2. It was observed that nucleation of nanobubbles occur rapidly in solutions with a high concentration of CO_2, compared to those with lower concentrations. It was also revealed that for solutions with a high concentration of CO_2, dissolved CO_2 molecules enter the bubble leading to the formation of a ‘mixed’ gas bubble.

Due to the formation of the bubble, an interface between the bubble and the surrounding liquid was created. Analysis of the structure of this interface showed that it is similar to the planar interface formed between methane gas and a water film. An accumulation of CO_2 molecules was observed at the bubble-water interface with a rise in concentration of CO_2 in the

solution. Radial distribution function showed that as the concentration of CO_2 at the bubble-water interface rises, the interactions between CH_4 and CO_2 molecules through direct contact become more prominent. The values of surface tension at the bubble-water interface indicated that the accumulation of CO_2 at the interface resulted in a decrease in surface tension. Thus, at higher concentrations of CO_2 in the ternary system, the bubble-water interface becomes more stable thereby assisting the early nucleation of the gas bubbles. The present study also showed that the small size of the bubbles formed lead to high Laplace pressure inside the bubble and that the CH_4 gas present in the bubble exists in its super critical state. Simulations of a binary solution of CO_2 in super critical CH_4 at dilute concentrations revealed that the two gas species form a repulsive mixture, indicating that CO_2 molecules accumulated at the bubble-water interface will not readily enter the bubble in a large quantity.

The observed effect of the concentration of CO_2 on bubble formation in the CH_4-CO_2-H_2O ternary solution is related to the replacement of CH_4 in methane hydrates by CO_2 molecules. The fact that CO_2 concentration causes early nucleation of bubbles suggests that by increasing CO_2 concentration, more efficient decomposition of CH_4 hydrates can be attained by preventing the accumulation of gas molecules in the surrounding liquid.

Chapter 4

Natural Gas Evolution in a Gas Hydrate Melt: Effect of Thermodynamic Hydrate Inhibitors

4.1 Introduction

As discussed in the previous chapters, most of the studies on gas hydrates in the past were related to the safe and efficient recovery of natural gas encapsulated within the hydrate structure. Various natural gas extraction techniques such as thermal stimulation, depressurization and injection of thermodynamic hydrate inhibitors like alcohols and salts were discussed in chapter 1. In all these extraction techniques, dissociation of hydrate structure is induced by making the hydrate thermodynamically unstable. Dissociation of gas hydrates is an important step during the recovery of natural gas from hydrates. Several molecular dynamics simulation studies have been reported which provided significant understanding of the hydrate dissociation mechanism [80-89, 94-99, 141]. These studies showed that several factors such as guest occupancy, heat transfer and the presence of hydrate inhibitors significantly influence the rate of hydrate dissociation. In addition to these, the role of mass transfer on the rate of hydrate dissociation has also been investigated [80-83, 97-99, 141]. These studies indicated that the diffusion of dissolved gas molecules from the melting hydrate into the surrounding liquid significantly affects the rate of dissociation. The dissociation leads to the formation of a solution supersaturated with gas molecules, from which nanobubbles are formed. The bubbles thus formed rapidly absorb dissolved gas molecules from the surrounding liquid, thereby increasing the rate of dissociation of the hydrate. The effect of thermodynamic hydrate inhibitors dissolved in the surrounding liquid on the dissociation process was also reported [98, 141]. It was found that thermodynamic inhibitors such as NaCl and CH_3OH aid the formation of bubbles, thereby helping the dissociation of hydrates. Formation of nanobubbles has also been reported in several other simulation studies of hydrate dissociation [80-83, 97, 99, 141]. However, a quantitative study of the effect of inhibitor concentration on the formation and stability of the bubbles is lacking.

A common observation of all the above-mentioned studies on hydrate dissociation is the

formation of a supersaturated gas solution during the dissociation process. The phase changes, such as bubble formation, occurring in this liquid phase have significant influence on the mass transfer of gas molecules released by the melting hydrate thereby affecting the dissociation kinetics. The presence of thermodynamic hydrate inhibitors makes the properties of the liquid phase more subtle, as indicated by Yagasaki *et al* [98, 141]. On the basis of the reported studies, the process of gas extraction from hydrates can be considered to occur in different stages, as discussed below. In the first stage, dissociation of the hydrates takes place forming a liquid composed of gas molecules dissolved in water. In the second stage, the dissolved gas molecules, upon reaching a critical concentration, aggregate to form bubbles, which further grow in size and eventually migrate out of the liquid phase. Although the first stage has been well studied, the evolution of dissolved gas molecules from the hydrate melt is not well understood. A very recent experimental study of methane hydrate dissociation by Uchida *et al.* [100] indicated the importance of evolution of dissolved gas molecules from the hydrate melt in the dissociation process. They applied tunneling electron microscopic techniques for the characterization of bubbles formed during the dissociation of methane hydrate. Their study confirmed the formation of bubbles of radius in the range of nanometers and micrometers in the hydrate melt. They also reported that the rate at which these bubbles rise in water is low, allowing them to stay in the solution for a long time. Surprisingly, such bubbles in the hydrate melt continued to form for several hours even after dissociation of methane hydrate was complete. Due to the fact that these bubbles can lead to the regeneration of hydrate structures, their long lifetime in the hydrate melt has significant consequences [83, 101].

Previous studies [80-83, 97-99, 141] on the formation of nanobubbles during gas hydrate dissociation were focused on the impact of bubbles on the rate of dissociation. Bubble formation in the presence of thermodynamic inhibitors such as NaCl and CH_3OH was also reported, which indicated the role of inhibitors in enhancing bubble formation [98, 141]. However, an exclusive molecular level study of the formation, stability, and composition of nanobubbles formed is not yet available. The experimental studies on the observation and characterization of nanobubbles in the hydrate melt produced results with significant uncertainties [100]. This necessitates the need for computational methods to gain insight into the molecular level understanding of nanobubbles in the hydrate melt. In this chapter, we present the results from classical molecular dynamics simulation study of the formation, stability, and composition of methane nanobubbles in the

presence of two thermodynamic hydrate inhibitors, NaCl and CH_3OH. Through this study, we compare the stability and properties of nanobubbles formed in the presence of the two different hydrate inhibitors at various concentrations. It is known that the CH_4-CO_2 binary hydrate is formed during the extraction of CH_4 from its hydrate by replacement with CO_2 [69]. Considering this, we also study the effect of the inhibitor molecules on bubble formation in a CH_4-CO_2-H_2O solution. Our study on the formation and dynamic properties of the nanobubbles is expected to provide greater understanding of the evolution of dissolved gas from the gas hydrate melt.

4.2 Computational Methods

The initial conformation of the simulation system consists of CH_4 and CO_2 molecules dissolved in water contained in a cubic box. For all simulations, the number of water molecules is fixed to be 3000. We studied the CH_4-H_2O system with two different CH_4 concentrations; 100 and 125 CH_4 molecules in 3000 water molecules corresponding to 0.032 and 0.040 mole fractions, respectively. For the force fields employed, the saturation concentration of CH_4 under the thermodynamic conditions applied is 0.0004 mole fraction. We determined the limit of supersaturation as 0.042 mole fraction, above which spontaneous nucleation of CH_4 bubbles occurs. Thus, the CH_4 concentrations considered in the present study correspond to highly supersaturated solutions. However, because these concentrations lie below the limit of supersaturation, spontaneous bubble formation is absent in the CH_4-H_2O system, as it fails to overcome the energy barrier for bubble nucleation. To study the effect of CO_2 on bubble formation, 100 CO_2 corresponding to a mole fraction of 0.032 molecules are introduced into the CH_4-H_2O systems mentioned above. To study the effect of the concentration of NaCl and CH_3OH on dissolved gas evolution, the number of inhibitor molecules introduced into the CH_4-H_2O and CH_4-CO_2-H_2O systems was varied from 40 to 240, with an increment of 40. The composition of the simulation systems considered is assumed to emulate the liquid state formed during the dissociation of gas hydrates.

To model CH_4 and CO_2 molecules, the single-point Lennard-Jones [238] and EPM2 [230] models, respectively, were used. Water molecules are represented by the TIP4P model [221]. This combination of force fields was previously employed in the study of the CH_4-CO_2-H_2O ternary system [69, 250]. For Na^+ and Cl^- ions, the parameters reported by Smith *et al.* were

employed, and CH_3OH molecules were modeled by the OPLS-UA force field [251, 252]. The parameters chosen to model the inhibitor molecules have recently been applied in the study of the dissociation of methane hydrate in the presence of inhibitors, NaCl and CH_3OH [141]. To model the interaction between CO_2 and H_2O molecules, parameters obtained from *ab initio* calculations reported by Duan *et al.* [240] were applied and the remaining cross-interaction parameters were obtained using the Lorentz-Berthelot combination rule. The EPM2 model used for CO_2 is a rigid three-site model in which deviation of the angle O-C-O from 180° arises due to the known problems in the constraint algorithm in treating a linear angle. To solve this, we introduced two additional point masses as explained in section 3.2 of chapter 3 on either side of the carbon atom in the original EPM2 model. Details of the modified model are discussed elsewhere [239].

The simulations were performed in the isothermal-isobaric ensemble at a temperature of 270 K and pressure of 20 bar using the program GROMACS-4.6.5 [241]. The initial conformation was relaxed by an energy minimization, followed by a 100 ps NVT simulation by which the system was brought to an average temperature of 270 K. Then, an NPT simulation was performed for a simulation time of 250 ps during which the system attained the equilibrium state with an average temperature and pressure of 270 K and 20 bar, respectively. Thereafter, the production simulation was performed in the NPT ensemble for a total simulation time of 40 ns with a time step of 2 fs. The simulation system was coupled to a Nosé-Hoover [232, 233] thermostat and a Parrinello-Rahman [235] barostat with time constants 0.5 and 1 ps, respectively. Although thermostat coupling is known to affect the diffusivity of molecules in the system, diffusivity of small solute molecules in water was reported to be unaffected by the Nosé-Hoover thermostat if it is coupled to the overall kinetic energy of the system [242]. During the simulations, the molecular geometries were constrained using the LINCS [243] algorithm and the H_2O molecules were maintained rigid using the SETTLE algorithm [244]. Long-range electrostatic interactions were treated by the particle-mesh Ewald summation method, and periodic boundary conditions were applied in all three dimensions. Visual analysis of the simulation results was performed using the visualization program, VMD (Visual Molecular Dynamics) [253].

4.3 Results and Discussion

4.3.1 Effect of Hydrate Inhibitors on the Formation of Nanobubble in the CH_4-H_2O System

To study the effect of NaCl and CH_3OH on the formation of nanobubbles in the CH_4-H_2O mixtures containing 100 and 125 CH_4 molecules, simulations were performed on the CH_4-NaCl-H_2O and CH_4-CH_3OH-H_2O systems. The number of inhibitor molecules was varied from 40 to 240, with an increment of 40. Simulations indicated that in both mixtures, which differ in CH_4 concentration, nanobubbles form at higher concentrations of the inhibitors. To characterize the formation of a nanobubble, we define each CH_4 molecule in the system as either belonging to the bubble or as a solute dissolved in liquid. The two types of CH_4 molecules are differentiated based on the number of water molecules in their first hydration shell. For a methane molecule dissolved in water, the radius of the first hydration shell was determined to be ~0.55 nm, and the hydration number was ~20. However, a methane molecule belonging to the bubble would have hydration number significantly lower than that of aqueous methane. In the present study, we define CH_4 molecules that have less than 10 H_2O molecules within the first hydration shell to be part of the bubble. The remaining CH_4 molecules are considered to be dissolved in water.

On the basis of the above definition, we determined the number of CH_4 molecules in the bubble as a function of time for CH_4-NaCl-H_2O and CH_4-CH_3OH-H_2O systems for varying number of NaCl and CH_3OH molecules. For the mixture containing 100 CH_4 molecules, the results are shown in figure 4.1. The corresponding results for the mixture containing 125 CH_4 molecules are given in figure 4.2. It is clear from the figures that in both cases an increase in the concentration of NaCl and CH_3OH promotes the nucleation of the nanobubble. As expected, for a given concentration of the inhibitor, bubble nucleation occurs earlier in the mixtures containing a higher concentration of CH_4. When the concentration of the inhibitor molecules is very low, the induction time preceding the nucleation is long, so that bubble formation is not observed within the 40 ns simulation. For the CH_4-NaCl-H_2O mixture containing a lower concentration of CH_4, the bubble is not formed when the number of NaCl present is 40. For the corresponding CH_4-CH_3OH-H_2O mixture, the bubble is not formed in the systems in which up to 120 CH_3OH molecules were present. However, with an increase in the concentration of the inhibitor, induction time for nucleation of the nanobubble is reduced and the bubble is formed thereafter.

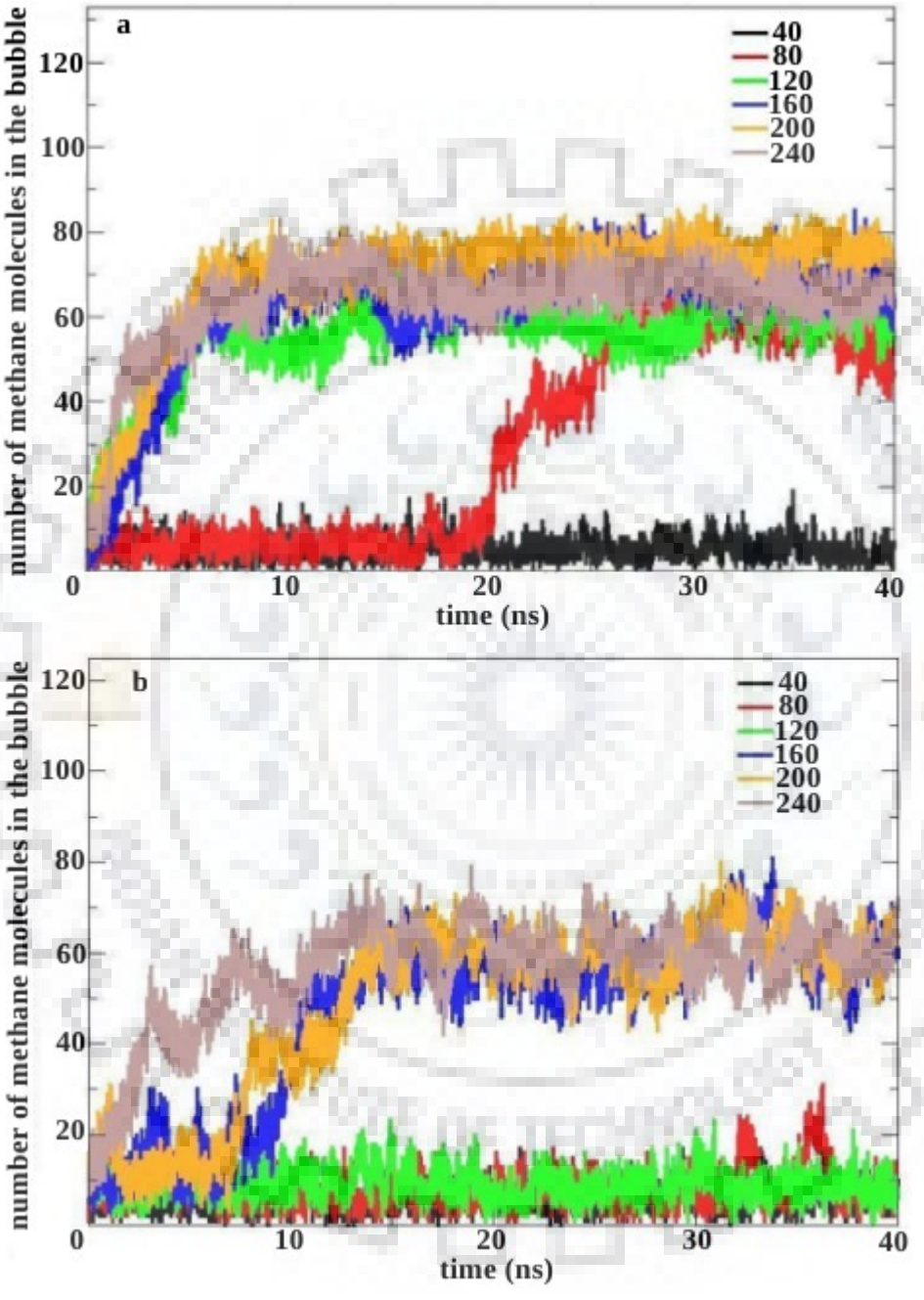

Figure 4.1 Number of CH_4 molecules in the bubble as a function of time for the (a) CH_4-NaCl-H_2O and (b) CH_4-CH_3OH-H_2O systems containing 100 CH_4 with varying number of thermodynamic inhibitor (NaCl and CH_3OH) molecules.

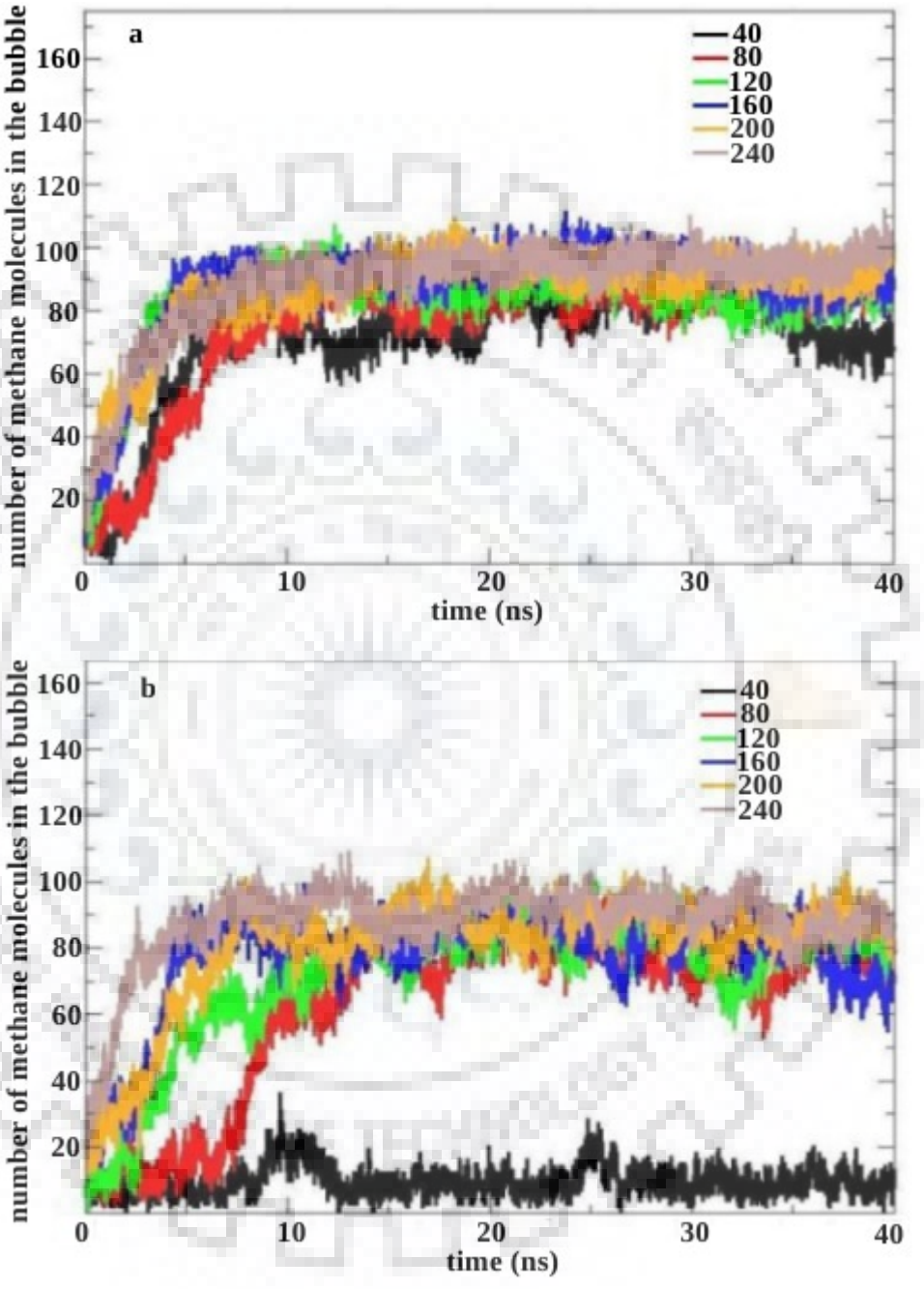

Figure 4.2 Number of CH_4 molecules in the bubble as a function of time for the (a) CH_4-NaCl-H_2O and (b) CH_4-CH_3OH-H_2O systems containing 125 CH_4 with varying number of thermodynamic inhibitor (NaCl and CH_3OH) molecules.

Another observation from figures 4.1 and 4.2 is that the bubble formed in the CH_4-NaCl-H_2O or CH_4-CH_3OH-H_2O ternary mixture with varying concentrations of the inhibitor reaches nearly the same size in terms of the number of CH_4 molecules. This may be due to the fact that once a stable bubble nucleus is formed, further growth of the bubble by absorption of dissolved CH_4 molecules is driven by the difference in free energy of CH_4 molecules present in the bubble and in the dissolved state. This free energy difference is expected to be much larger than the difference in free energy of hydration of CH_4 caused by changes in the concentration of the inhibitor. Thus, although the inhibitor plays a key role in the formation of the bubble nuclei, further growth of the bubble is independent of the inhibitor concentration. This is also supported by the fact that the rate at which the bubble grows is almost the same for different concentrations of the inhibitor in the mixtures.

Figure 4.1a gives the number of CH_4 molecules present in the bubble as a function of time for CH_4-NaCl-H_2O system containing lower concentration of CH_4 and varying number of NaCl molecules. In the system containing 80 NaCl molecules, nucleation of the nanobubble occurred at 19 ns and bubble formation was complete within 30 ns. The bubble so formed remained stable till the end of the simulation. The nucleation and growth of the bubble in the CH_4-NaCl-H_2O system is illustrated in figure 4.3. For the systems containing 120-240 NaCl molecules, nucleation of the nanobubble takes place immediately at the start of the simulation. In all cases, the bubble so formed remained till the end of the simulation. Bubbles formed in the mixtures with higher CH_4 concentrations also remained stable as shown in figure 4.2.

In the CH_4-CH_3OH-H_2O ternary system containing 100 CH_4 molecules, nanobubble formation was observed when the number of CH_3OH was 160 or higher. From figure 4.1b, it can be observed that the time at which formation of the bubble starts is ~8 ns in the system containing 160 CH_3OH and is further decreased for the system containing 200 CH_3OH. When the number of CH_3OH molecules was increased to 240, the nucleation of the bubble occurs immediately in the beginning of the simulation. For the system containing 125 CH_4 molecules, nanobubble nucleation was observed when the number of CH_3OH molecules was 80 or higher (figure 4.2).

An important factor that has to be considered to explain the stability of nanobubbles is the size of the simulation system. The influence of the size of the simulation system on the stability of the bubble was studied in detail by Weijis *et al.* [247]. Through molecular dynamics

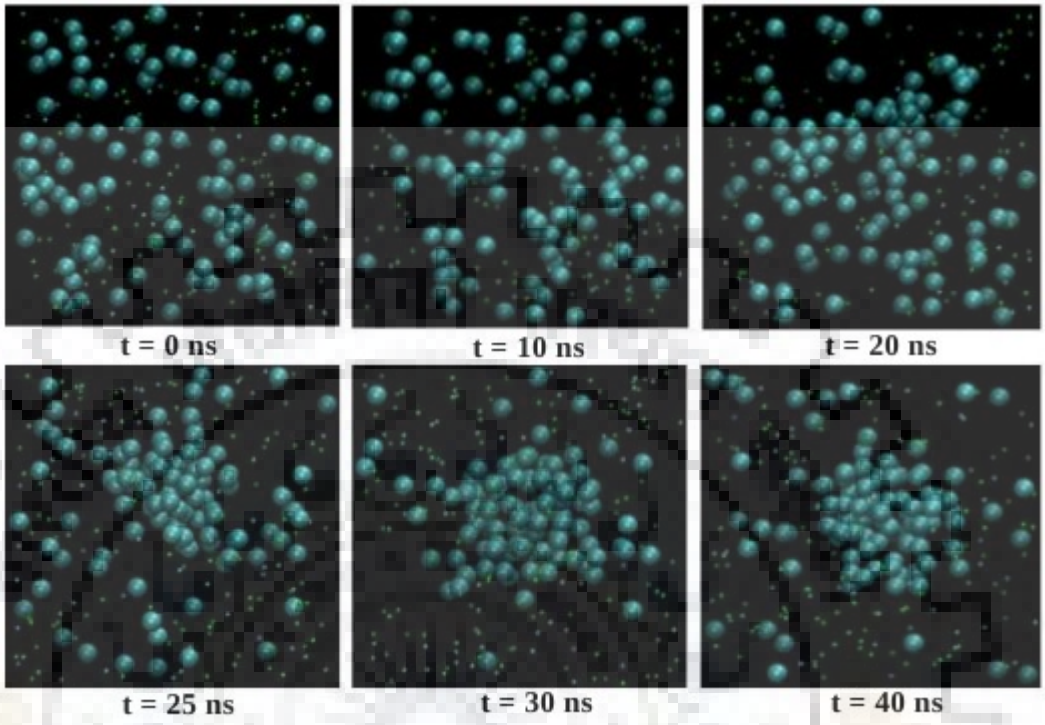

Figure 4.3 Nucleation and growth of the methane nanobubble in a CH_4-NaCl-H_2O system containing 100 CH_4, 80 NaCl, and 3000 H_2O molecules. CH_4 molecules are represented as large cyan spheres, Cl^- and Na^+ ions are shown as small spheres. H_2O molecules are not shown for clarity.

simulations, they studied the role of diffusive efflux of molecules from the bubble to the surrounding liquid on the stability of nanobubbles in their clusters. The stability of nanobubbles was found to be sensitive to the size of the simulation system, as the close proximity of nanobubbles in a small simulation system and its periodic images shield the diffusive efflux of gas molecules. Thus, a nanobubble that decomposes through diffusive efflux in a large simulation system remains stable when the size of the system is small. Thus, in the present study, it is necessary to ensure that the stability of the bubble is not an artefact arising from the limited size of the simulation system. For this, we performed a simulation on a CH_4-H_2O system containing 100 CH_4 and 3000 H_2O molecules starting from an initial conformation with a methane nanobubble in the system. The result of the simulation is illustrated in figure 4.4. From

the figure, it can be observed that in the absence of inhibitor molecules, the nanobubble dissociates through diffusive efflux of CH_4 molecules from the bubble to the surrounding liquid. The bubble dissociates completely within 20 ns and is absent during the rest of the simulation. Thus, it can be concluded that, in the present study, the size of the simulation system does not have any role in shielding the diffusive efflux of CH_4 molecules from the bubble. The formation and stability of methane nanobubbles observed in the CH_4-NaCl-H_2O and CH_4-CH_3OH-H_2O systems are entirely due to the presence of NaCl and CH_3OH molecules.

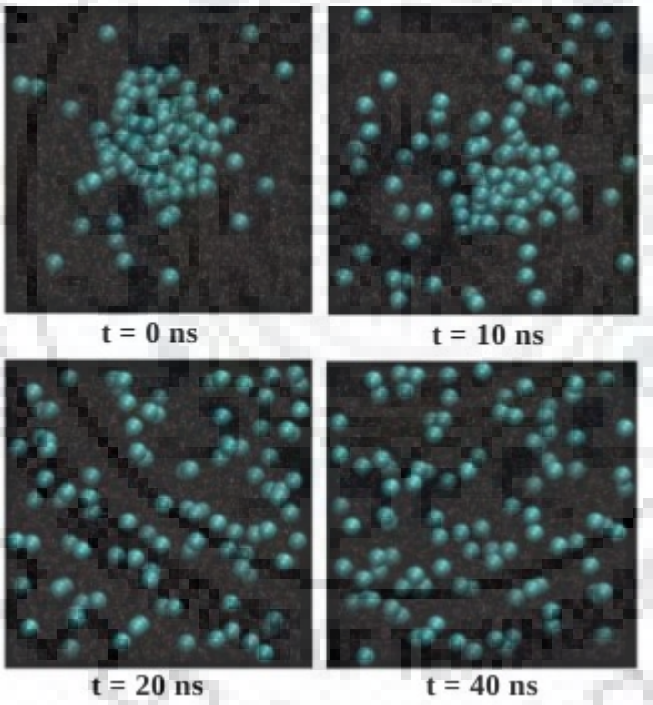

Figure 4.4 Decomposition of the methane nanobubble in the CH_4-H_2O system in the absence of inhibitor molecules. CH_4 molecules are shown as large cyan spheres.

The increase in the probability of nucleation of methane nanobubble with increasing concentration of NaCl is attributed to the fact that the presence of NaCl enhances the hydrophobic interaction between the dissolved CH_4 molecules [141, 254]. As a result, larger clusters of CH_4 molecules are formed in the system containing NaCl. Once the size of a cluster reaches the critical size of the bubble nuclei, it grows in size by absorbing dissolved CH_4 molecules from the surrounding liquid to form a nanobubble. Higher probability of nanobubble nucleation with an increase in the concentration of CH_3OH can be attributed to its amphiphilic character. This was recently demonstrated by Yagasaki *et al.* [141] in their studies of methane hydrate dissociation in presence of thermodynamic hydrate inhibitors. We analyzed the effect of concentration of CH_3OH on the nucleation of the nanobubble in more detail. To understand the role of CH_3OH in the early nucleation of the bubble, we examined the structure of the nanobubble formed in the CH_4-CH_3OH-H_2O system for various numbers of CH_3OH molecules. The structure of the bubble was analyzed as explained in section 3.3.4 of chapter 3, by splitting the simulation system into concentric spherical shells with respect to the center of the methane nanobubble. At a given instant of time, the number of CH_4, CH_3OH, and H_2O in each shell was determined. This provided the number density distribution of the respective molecular species as a function of distance from the center of the bubble at a particular instant of time. The nanobubble formed in the solution is a highly dynamic entity, and hence, the shape and the number density distributions of molecules in the bubble are subject to fluctuations. Thus, for an accurate analysis, we determined the time average of the number density distribution over a time interval of 10 ns at a frequency of 10 ps. The average number distribution thus obtained for the CH_4-CH_3OH-H_2O system containing 100 CH_4 and 160 CH_3OH molecules, is given in figure 4.5. It is clear from the figure that CH_3OH molecules accumulate near the surface of the methane nanobubble. A similar accumulation of CH_3OH molecules was also observed in the CH_4-CH_3OH-H_2O systems containing 125 CH_4 molecules (figure 4.5b). It can also be inferred from the number density distribution that the hydrophobic methyl (-CH_3) group of the CH_3OH molecule is directed toward the surface of the bubble, whereas the hydrophilic -OH group is oriented toward the surrounding liquid. Figure 4.5 also compares the number density distribution of CH_3OH molecules in the CH_4-CH_3OH-H_2O systems with varying number of inhibitor molecules. It is observed that with an increase in the concentration of CH_3OH in the system, more number of CH_3OH molecules accumulate at the surface of the bubble.

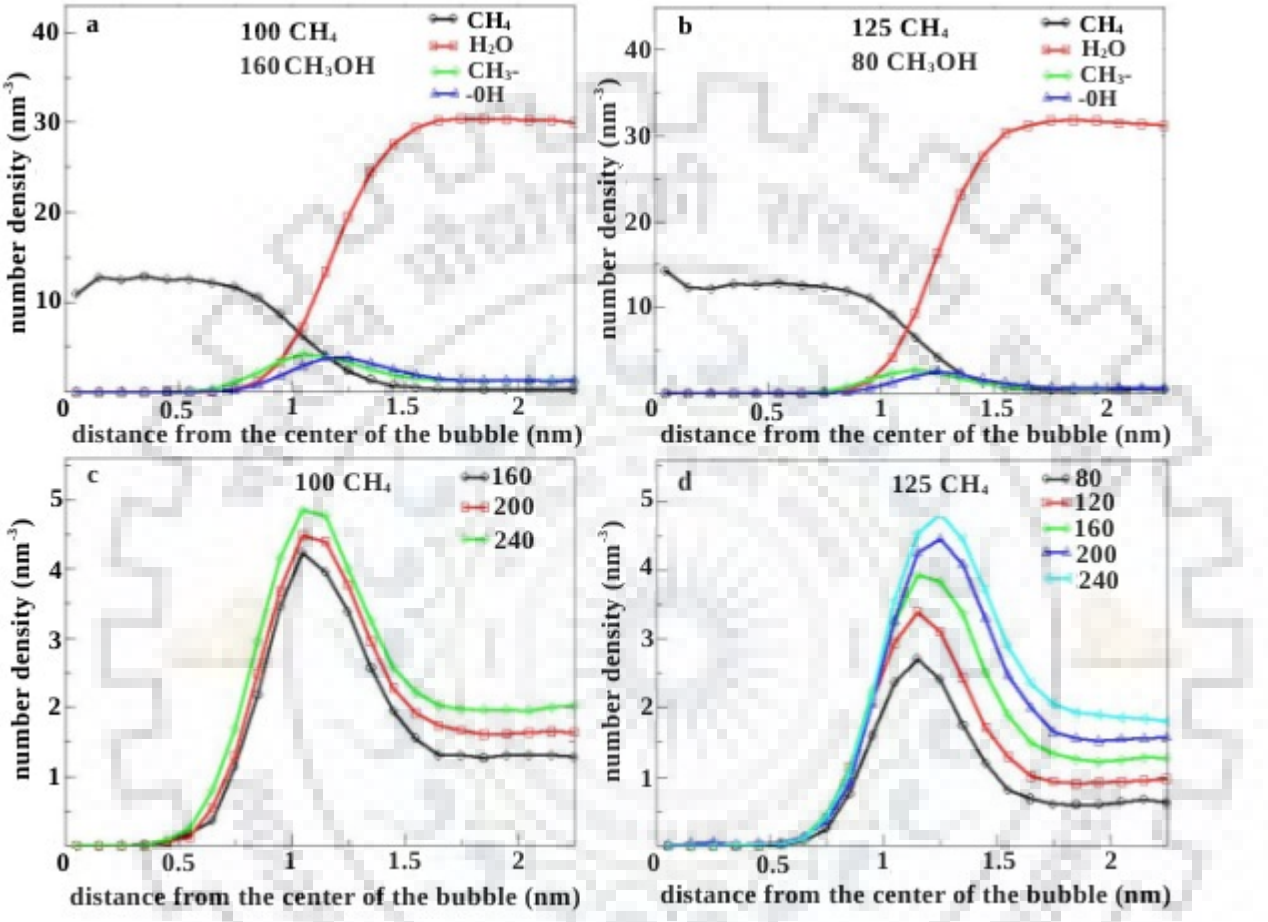

Figure 4.5 Time averaged number density distribution of molecules as a function of distance from the center of the CH_4 bubble for the CH_4-CH_3OH-H_2O mixture containing (a) 100 CH_4 and 160 CH_3OH, (b) 125 CH_4 and 80 CH_3OH molecules. The number densities of -CH_3 and -OH groups of the CH_3OH molecule are shown separately. Time averaged number density of the -CH_3 group of methanol in the CH_4-CH_3OH-H_2O system containing (c) 100 CH_4 and varying number of CH_3OH (d) 125 CH_4 and varying number of CH_3OH.

To understand the reason behind the rapid nucleation of bubble in the presence of CH_3OH, we examined the effect of CH_3OH accumulated at the surface of the bubble on its stability. The presence of CH_3OH could be reducing the surface energy of the bubble nuclei thereby making it more stable. To confirm this, the value of surface tension at the bubble-water interface was determined at different concentrations of CH_3OH considered using the Young-Laplace equation. The Young-Laplace equation is given by,

$$P_g = P_l + \frac{2\gamma}{R} \tag{4.1}$$

where P_g and P_l are the pressure inside the nanobubble and in the surrounding liquid, respectively. R is the radius of the bubble and γ is the surface tension. Equation 4.1 relates the excess pressure inside a spherical bubble to the value of surface tension at the periphery of the bubble.

From the number density distribution of CH_4 molecules, the density of methane inside the bubble was determined. The pressure, P_g, corresponding to the density was determined through an NVT simulation at 270 K. The number densities of CH_4 and H_2O become equal on moving away from the center of the bubble (figure 4.5), and the corresponding distance from the bubble center is defined as the radius, R, of the bubble. Substituting the value obtained for P_g in equation 4.1, and considering the value of P_l to be 20 bar, the value of surface tension γ was estimated. The surface tension at the bubble-liquid interface determined for nanobubbles formed in the CH_4-CH_3OH-H_2O ternary systems containing 0.032 and 0.04 mole fractions of CH_4, at different inhibitor concentrations, is given in table 4.1. The table shows that the excess pressure inside the bubble is significantly higher than the pressure of 20 bar in the surrounding liquid. The high excess pressure inside nano and microbubbles is expected and is in agreement with the recent findings of Uchida *et al.*, [100] in which they reported the excess pressure inside methane nanobubbles having an average radii of 300 nm in pure water as 70 ± 50 bar. The nanobubbles considered in the present study are much smaller, with radii approximately equal to 1 nm (figure 4.5). From table 4.1, it can be observed that in both CH_4-CH_3OH-H_2O systems, which differ in the concentration of CH_4, the value of surface tension at the bubble-liquid interface decreases with an increase in the accumulation of CH_3OH near the bubble (figure 4.5). It is also observed that for the same concentration of CH_3OH, the methane bubbles formed in the ternary system with 0.04 mole fraction of methane have a higher value of surface tension. This can be explained

Table 4.1 Value of excess (Laplace) pressure inside the nanobubble and surface tension at the bubble-liquid interface for the CH_4-CH_3OH-H_2O systems with CH_4 concentrations of 0.032 and 0.04 mole fractions.

number of CH_3OH	χ_{CH_4} = 0.032		χ_{CH_4} = 0.04	
	Laplace pressure ($P_g - P_l$) (bar)	surface tension(γ) (mN m^{-1})	Laplace pressure ($P_g - P_l$) (bar)	surface tension(γ) (mN m^{-1})
40	nb[a]	nb	nb	nb
80	nb	nb	720.88	40.23
120	nb	nb	686.23	38.17
160	735.44	38.09	674.76	38.14
200	678.16	34.95	606.76	35.42
240	667.07	33.81	595.92	34.90

[a] No bubble formation

Table 4.2 Average radius of the CH_4 nanobubbles formed in the CH_4-CH_3OH-H_2O systems containing 0.032 and 0.04 CH_4 mole fractions.

number of CH_3OH	χ_{CH_4} = 0.032	χ_{CH_4} = 0.04
	radius (nm)	radius (nm)
40	nb[a]	nb
80	nb	1.116
120	nb	1.113
160	1.039	1.131
200	1.031	1.168
240	1.017	1.171

[a] No bubble formation

based on the difference in size of the bubbles formed in each case. For the ternary system containing higher concentration of CH_4, more CH_4 molecules are available for bubble formation, thereby leading to larger bubbles. The average radius of the methane nanobubble formed in CH_4-CH_3OH-H_2O systems with 0.032 and 0.04 mole fractions of CH_4 is given in table 4.2. The larger bubble, which has a larger surface area, will have a slightly lower number density of CH_3OH molecules which accumulate at the bubble surface. Thus, the effect of CH_3OH on reducing the surface tension at the bubble-liquid interface is slightly lower in the ternary system with a higher concentration of CH_4. The calculated value of surface tension depends on the radii of the bubble and hence depends on how the latter is defined. Zakharov *et al.* [255] performed molecular dynamics simulations to determine the value of surface tension of pure water droplets using the TIP4P water model. The calculated value of surface tension at 300 K was found to be 54 mN/m. It has also been reported by experimental and theoretical studies that surface tension of the methanol-water mixture decreases with an increase in the concentration of methanol [256, 257]. This suggests that the values of surface tension obtained in the present work for the CH_4-CH_3OH-H_2O system are reasonable. The decrease in surface tension leads to a decrease in surface energy associated with the formation of the nanobubble, making the process energetically more favorable. Moreover, a decrease in surface tension at the bubble-liquid interface reduces critical size of the bubble nuclei leading to early nucleation of the nanobubble.

4.3.2 Effect of Hydrate Inhibitors on Gas Evolution in the CH_4-CO_2-H_2O System

The CH_4-CO_2 binary gas hydrate is formed during CH_4 extraction through guest gas replacement in CH_4 hydrates with CO_2 [69]. The dissociation of CH_4-CO_2 binary gas hydrate leads to the formation of CH_4-CO_2-H_2O ternary mixture [250]. Formation of the ternary system is also observed during the initial stages of the replacement process during which CH_4 hydrates undergo dissociation in presence of CO_2 injected into the hydrate sediment [69]. Thus, it is important to understand the role of hydrate inhibitors on the evolution of dissolved gas from CH_4-CO_2-H_2O ternary system. To study the effect of thermodynamic hydrate inhibitors, NaCl and CH_3OH on the formation of nanobubbles in CH_4-CO_2-H_2O system, we performed molecular dynamics simulations on CH_4-CO_2-NaCl-H_2O and CH_4-CO_2-CH_3OH-H_2O systems. These systems contained 3000 H_2O molecules and 100 CO_2 molecules, respectively. As mentioned in the case of pure methane hydrate melt, two different CH_4 concentrations, 0.032 and 0.04 mole

fraction in water, were considered. The concentration of the thermodynamic inhibitor was varied as was done for CH_4-NaCl-H_2O and CH_4-CH_3OH-H_2O systems.

The nucleation and growth of nanobubbles in the CH_4-CO_2-NaCl-H_2O and CH_4-CO_2-CH_3OH-H_2O mixtures were examined by determining the number of CH_4 molecules belonging to the bubble as a function of time. Such CH_4 molecules were identified based on the hydration number, as explained above for the CH_4-H_2O mixture. For mixtures containing 0.032 mole fraction of methane, the number of methane molecules in the nanobubble as a function of time is plotted in figure 4.6. For the mixture with 0.04 mole fraction of CH_4, the results are shown in figure 4.7. The most important observation from the figures is that the formation of nanobubbles in the CH_4-CO_2-NaCl-H_2O and CH_4-CO_2-CH_3OH-H_2O systems is promoted by the presence of carbon dioxide. For example, nucleation of the nanobubble was absent in the CH_4-NaCl-H_2O ternary system containing 100 CH_4, with 40 molecules of NaCl and occurred at ~19 ns with 80 molecules of NaCl (figure 4.1a). Whereas in the CH_4-CO_2-NaCl-H_2O system with 40 and 80 NaCl molecules, nucleation of the bubble was observed as early as ~3 and ~2 ns, respectively, as illustrated in figure 4.6a.

The role of CO_2 as a promoter for the formation of nanobubbles is also observed in the case of CH_4-CO_2-CH_3OH-H_2O mixture (figure 4.6b). In this case, the presence of CO_2 caused bubble nucleation in systems with 80 and 120 CH_3OH molecules compared to the case of the CH_4-CH_3OH-H_2O system with the same number of CH_3OH molecules, in which bubble did not form (figure 4.1b). Also, in the case of CH_4-CO_2-CH_3OH-H_2O systems containing 160 and 240 CH_3OH molecules, the presence of CO_2 molecules induced the formation of the bubble at an earlier stage. Similar to the case of the quarternary mixtures containing 0.032 mole fraction of CH_4, the enhancement of bubble nucleation by CO_2 is observed in the case of mixtures containing higher concentration of CH_4 (0.04 mole fraction). This is clear from the comparison between figures 4.2 and 4.7 which shows that the induction time for bubble nucleation is reduced due to the presence of CO_2.

As in the case of bubbles formed in the CH_4-H_2O system with varying concentration of the inhibitors considered, the bubbles formed in both types of quarternary systems at various concentrations of the inhibitors are of nearly the same size in terms of the number of gas molecules in them. This is due to the fact that the growth of the bubble is independent of the concentration of the inhibitor, as explained in the case of the CH_4-H_2O system. The role of CO_2 in

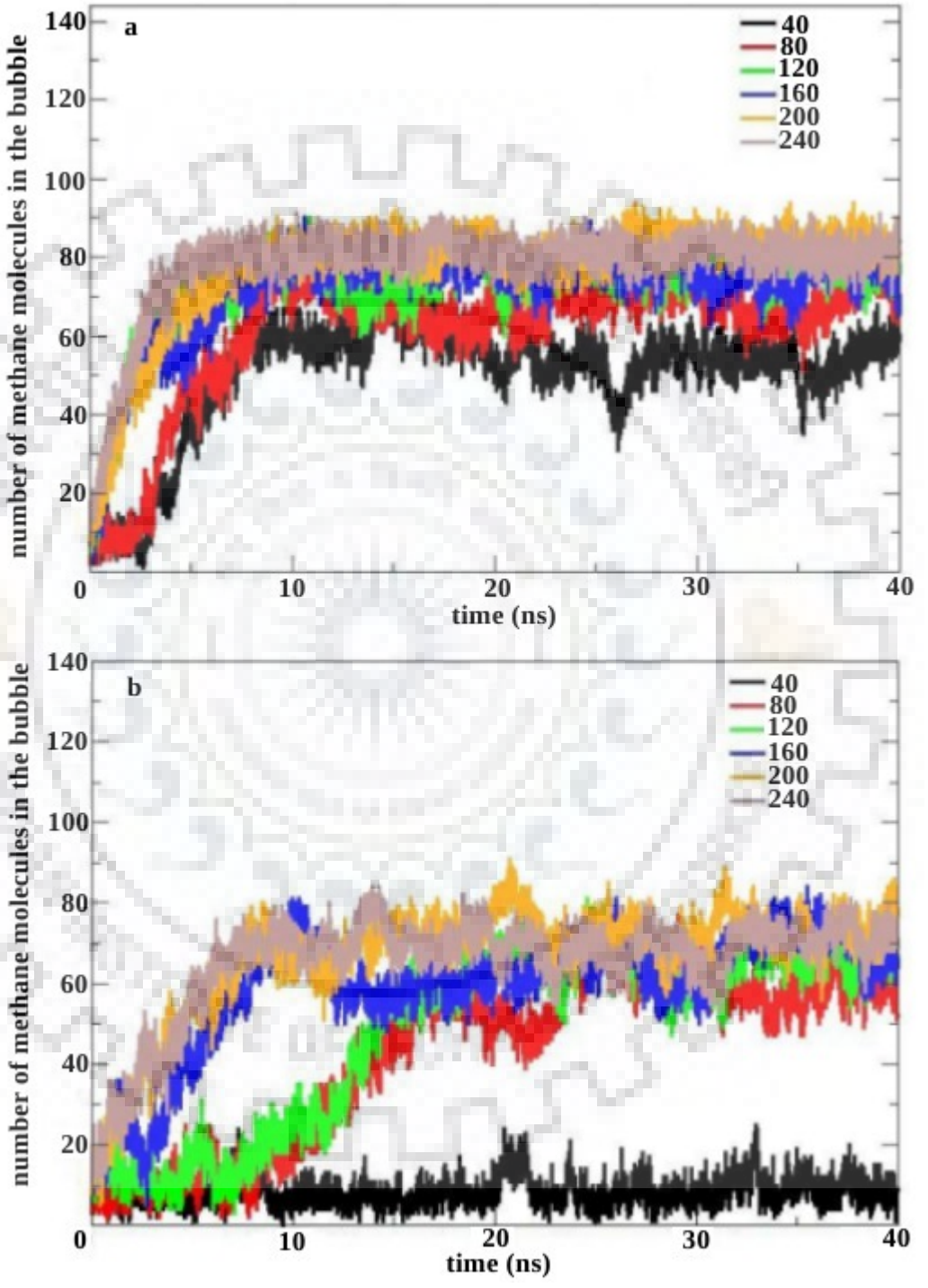

Figure 4.6 Number of CH_4 molecules in the bubble as a function of time for the (a) CH_4-CO_2-NaCl-H_2O and (b) CH_4-CO_2-CH_3OH-H_2O systems containing 100 CH_4 (0.032 mole fraction) with varying number of NaCl and CH_3OH molecules.

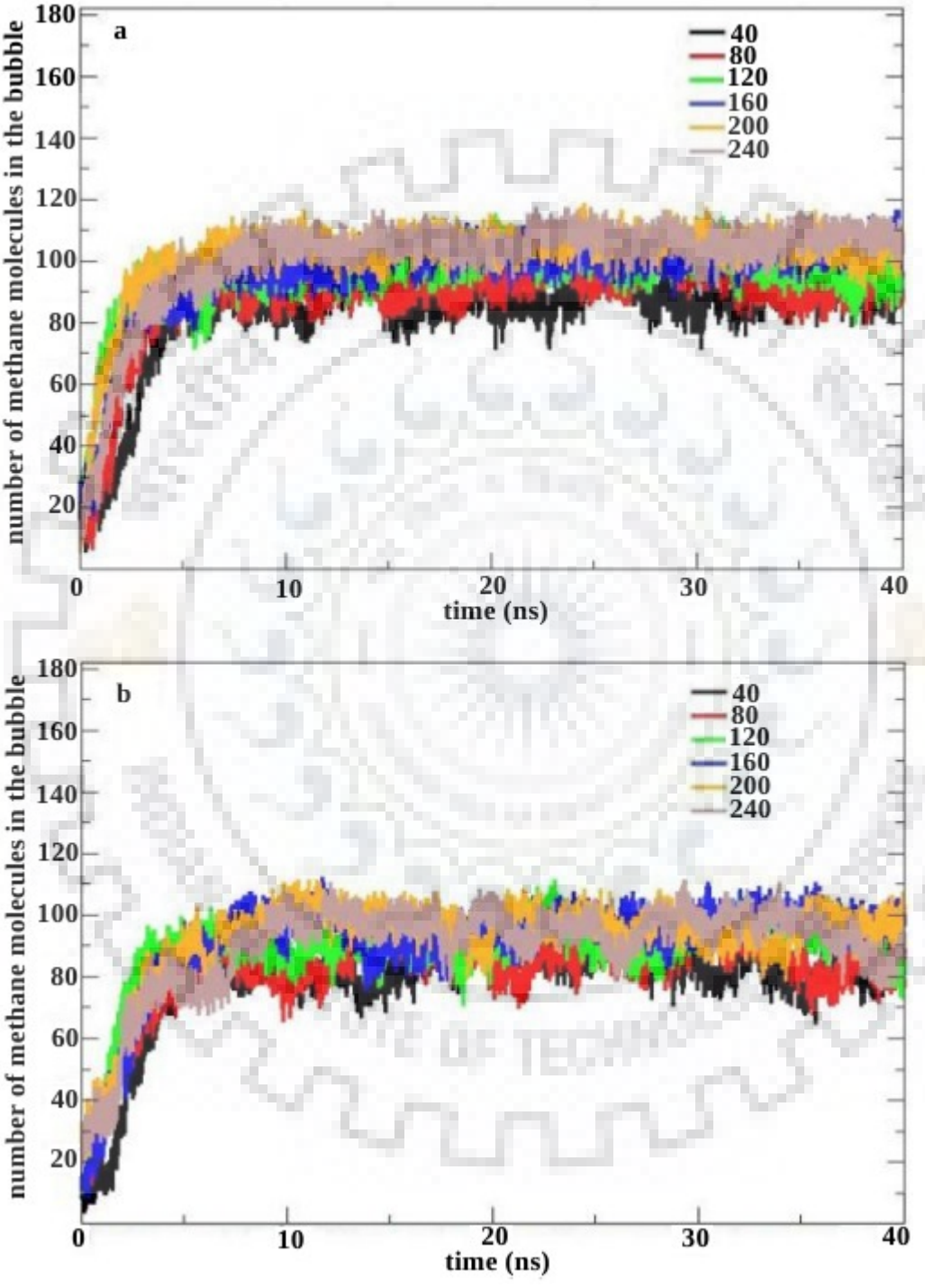

Figure 4.7 Number of CH_4 molecules in the bubble as a function of time for (a) CH_4-CO_2-NaCl-H_2O and (b) CH_4-CO_2-CH_3OH-H_2O systems containing 125 CH_4 (0.04 mole fraction) with varying number of NaCl and CH_3OH molecules.

assisting the nucleation of nanobubbles in the CH_4-CO_2-NaCl-H_2O and CH_4-CO_2-CH_3OH-H_2O systems can be explained based on the interaction of the bubble with CO_2 molecules present in the surrounding liquid. The average number density of CH_4, CO_2, and H_2O molecules as a function of the distance from the center of the bubble for some of the quarternary systems is shown in figure 4.8. The figure indicates that CO_2 molecules accumulate at the interface between the nanobubble and the surrounding liquid. The induction of bubble formation by CO_2 in the CH_4-CO_2-H_2O ternary system was discussed in Chapter 3 where it was shown that the presence of CO_2 molecules near the bubble-water interface enhance the stability of the bubble.

The present study indicates that, in the CH_4-CO_2-NaCl-H_2O mixture, an increase in the concentration of NaCl enhances the formation of small clusters of gas molecules. Once formed, these clusters are stabilized by the accumulation of CO_2 molecules at the interface of the cluster with the surrounding liquid phase. These stable clusters then grow in size by absorbing dissolved gas molecules from the surrounding liquid. In CH_4-CO_2-CH_3OH-H_2O also, CO_2 molecules accumulate around the cluster of gas molecules formed in the mixture. In this mixture, the accumulation of CO_2 in addition to that of the amphiphilic CH_3OH molecules around the cluster provides additional stability to the cluster thereby enhancing the formation of nanobubbles.

The composition of the nanobubbles formed in CH_4-CO_2-NaCl-H_2O and CH_4-CO_2-CH_3OH-H_2O mixtures was examined in further detail by determining the time-averaged number density of CO_2 within the bubble. A distance of up to $\sim$0.75 nm from the center of the bubble consists of the pure gas phase, beyond which the mixing of the bubble and liquid phase at the bubble-liquid interface begins. The time-averaged number density of CO_2 within 0.75 nm for the CH_4-CO_2-NaCl-H_2O and CH_4-CO_2-CH_3OH-H_2O mixtures containing 0.032 and 0.04 mole fractions of CH_4 is given in figures 4.9 and 4.10. It can be observed that in all cases, the nanobubble contains CO_2 inside it in addition to CH_4. The results also suggest that the composition of the nanobubble is influenced by the concentration and type of the hydrate inhibitor present in the mixture. The amount of CO_2 inside the bubble formed in CH_4-CO_2-NaCl-H_2O is found to be higher than that in CH_4-CO_2-CH_3OH-H_2O. The density of CO_2 in the bubble for systems with the highest number of inhibitor molecules shows that the concentration of CO_2 in the bubble formed in the CH_4-CO_2-NaCl-H_2O system is about twice of that observed for the CH_4-CO_2-CH_3OH-H_2O system. Thus, the results indicate that during the dissociation of CH_4-CO_2 binary gas hydrate in the presence of a thermodynamic hydrate inhibitor

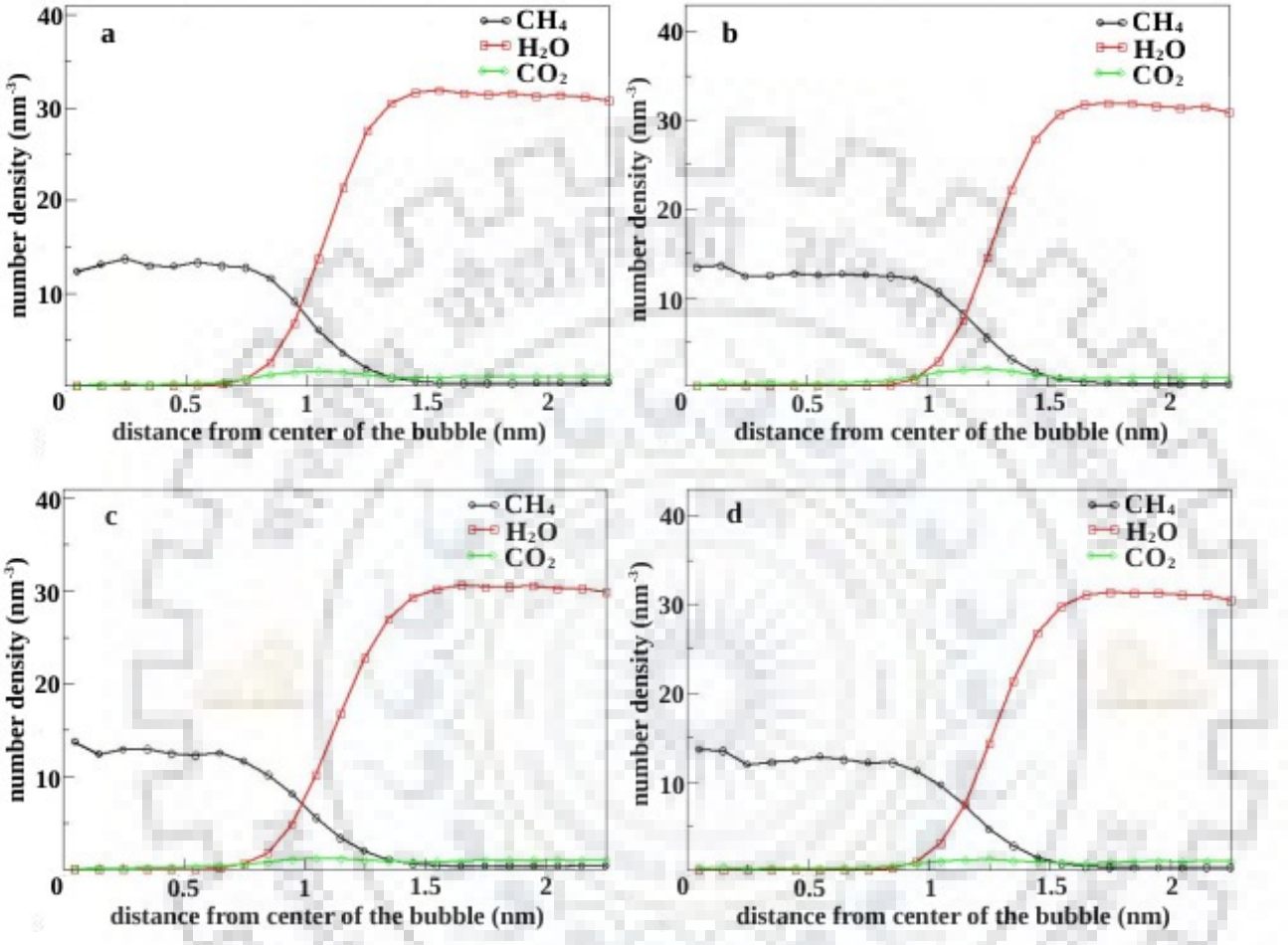

Figure 4.8 Time-averaged number density distribution of molecules as a function of distance from the center of the CH_4 bubble in the (a) CH_4-CO_2-NaCl-H_2O system containing 100CH_4 and 40 NaCl (b) CH_4-CO_2-NaCl-H_2O system containing 125 CH_4 and 40 NaCl (c) CH_4-CO_2-CH_3OH-H_2O system containing 100 CH_4 and 80 CH_3OH and (d) CH_4-CO_2-CH_3OH-H_2O system containing 125 CH_4 and 40 CH_3OH molecules. All the systems contain 100 CO_2 and 3000 H_2O molecules.

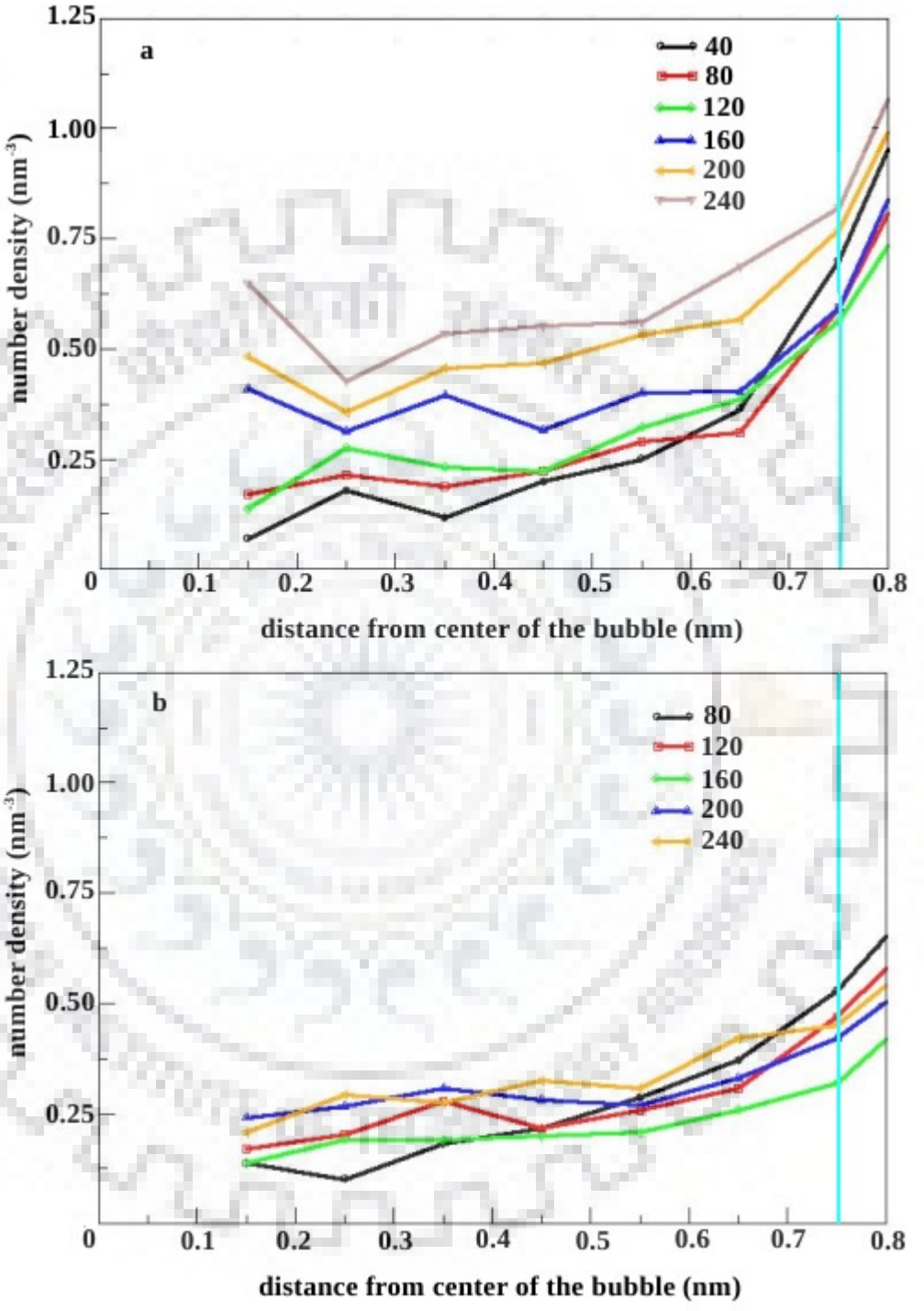

Figure 4.9 Time averaged number density distribution of CO_2 molecules inside the nanobubble formed in (a) CH_4-CO_2-NaCl-H_2O and (b) CH_4-CO_2-CH_3OH-H_2O systems containing varying number of NaCl and CH_3OH molecules. The mole fraction of CH_4 in water is 0.032. The vertical line at 0.75 nm indicates the approximate distance at which the mixing of the bubble(gas) and the liquid phase begins.

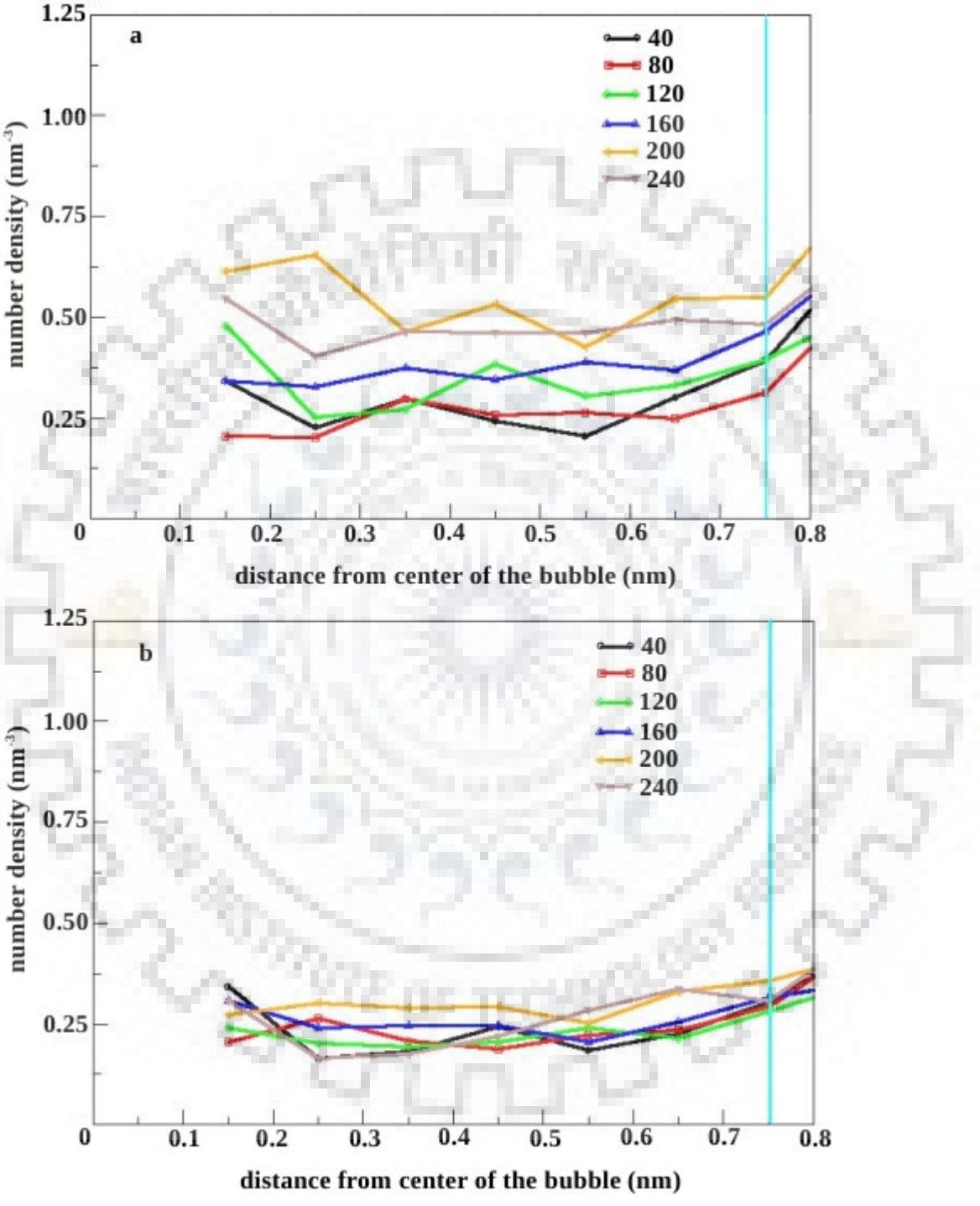

Figure 4.10 Time averaged number density distribution of CO_2 molecules inside the nanobubble formed in (a) CH_4-CO_2-NaCl-H_2O and (b) CH_4-CO_2-CH_3OH-H_2O systems containing varying number of NaCl and CH_3OH molecules. The mole fraction of CH_4 in water is 0.04. The vertical line at 0.75 nm indicates the approximate distance at which the mixing of the bubble(gas) and the liquid phase begins.

mixed gas nanobubbles are formed whose composition depends on the type and concentration of the inhibitor.

4.3.3 Interaction of Nanobubbles with the Surrounding Liquid

Following the formation of the nanobubble, the stability and lifetime of the bubble would depend on its interaction with the surrounding liquid phase. An important process affecting the stability and lifetime of nanobubbles in a solution is disproportionation or Ostwald ripening [258]. This process involves the growth of a bubble in the presence of a neighboring smaller bubble through diffusion of gas molecules from smaller to the larger one. The driving force behind this process is the difference in the Laplace pressure inside the bubbles. The higher Laplace pressure inside the smaller bubble creates a gradient in the concentration of gas molecules in the liquid between two bubbles, leading to the diffusion of molecules from the smaller to the larger bubble. Thus, Ostwald ripening leads to further growth of large bubbles at the expense of the smaller ones. The phenomenon of Ostwald ripening is therefore related to the interaction of the bubbles with the surrounding liquid region. From number of gas molecules in the nanobubble as a function of time (figures 4.1, 4.2, 4.6 and 4.7), it can be observed that the number of molecules in the bubbles fluctuate with time. This indicates that a continuous exchange of gas molecules takes place between the bubble and the surrounding liquid during which gas molecules enter and leave the bubble.

To determine the effect of the concentration of thermodynamic inhibitors on the dynamic behavior of the nanobubbles, we performed a quantitative analysis of the exchange of gas molecules between the bubble and the liquid in CH_4-NaCl-H_2O and CH_4-CH_3OH-H_2O mixtures. Corresponding to each ith gas molecule in the system, a unit step function $f(i)$ is defined such that $f(i) = 0$, when the molecule belongs to the bubble, and $f(i) = 1$, when the molecule is dissolved in the liquid. Thus, when the value of $f(i)$ changes during a time step in the simulation, it indicates that the gas molecule passed from the nanobubble into the surrounding liquid or vice versa. By keeping track of variations in the value of $f(i)$ over a sufficiently long time, the number of times a gas molecule is exchanged between the bubble and the surrounding liquid can be determined. We determined the average number of such exchanges, N_{exc} per nanosecond between the bubble and liquid phase by calculating $f(i)$ for all gas molecules over a simulation time of 10 ns at a frequency of every 10 ps. A schematic representation of the above analysis of gas

exchange between the bubble and the surrounding liquid is given in figure 4.11.

The values of N_{exc} for CH_4-NaCl-H_2O and CH_4-CH_3OH-H_2O ternary mixtures containing CH_4 at 0.032 and 0.04 mole fractions are given in table 4.3. It is observed that in all cases, an increase in the concentration of the inhibitor reduces the exchange of CH_4 molecules between the bubble and the surrounding liquid, thereby making the bubble less dynamic. It is also observed that for a given concentration of the inhibitor, the bubble formed in the ternary mixture containing a higher concentration of CH_4 is less dynamic compared to that formed in the mixture containing a lower CH_4 concentration. The observed dependence of the dynamic behavior of the bubble on the concentration of the inhibitor and the size of the bubble can be explained based on on the Laplace pressure and the solubility of CH_4 in the liquid phase surrounding the bubble. These two factors are the driving forces behind the exchange of gas molecules between the bubble and the surrounding liquid. For a methane nanobubble in the pure CH_4-H_2O system, a high Laplace pressure inside the bubble pushes the CH_4 molecules across the bubble-liquid interface into the surrounding liquid. However, once the CH_4 molecule enters the liquid phase, its

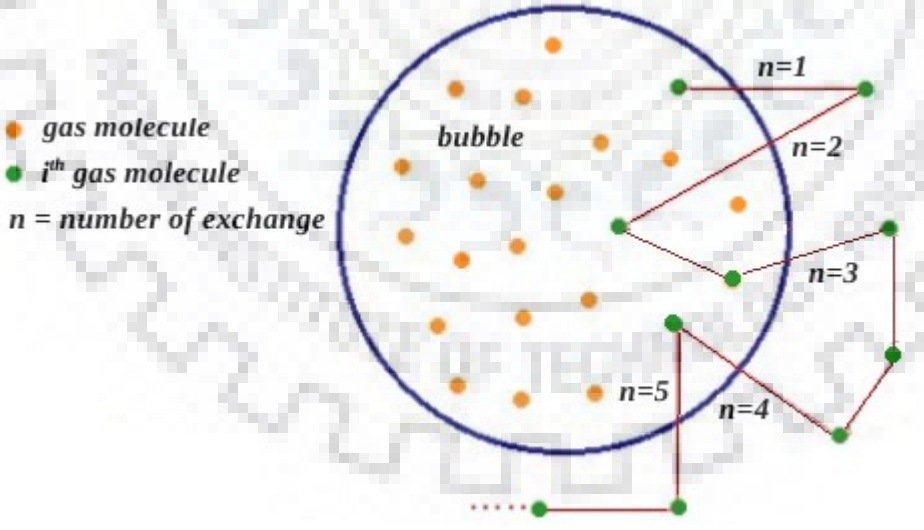

Figure 4.11 Schematic representation of the analysis of exchange of gas molecules between a bubble and its surrounding liquid phase.

low solubility in water drives the molecule back into the nanobubble. For a given concentration of CH_4, a decrease in the dynamic nature of the methane nanobubble in the CH_4-NaCl-H_2O ternary mixture with increasing concentration of NaCl is attributed to the effect of NaCl on the solubility of CH_4. It is known that the presence of NaCl leads to a decrease in the solubility of CH_4 in water [141]. This hinders the transfer of CH_4 molecules from the bubble to the liquid, thereby reducing the exchange of CH_4 molecules. For the CH_4-NaCl-H_2O ternary mixture containing a given concentration of CH_4, the lack of any apparent trend in the Laplace pressure with increase in concentration of NaCl **(**table 4.4**)** confirms that, it is the solubility of CH_4 which

Table 4.3 Average number of CH_4 exchanges between the bubble and the surrounding liquid in the CH_4-CH_3OH-H_2O (top) and CH_4-NaCl-H_2O (bottom) mixtures containing 0.032 and 0.04 mole fractions of CH_4.

Number of CH_3OH	χ_{CH_4} = 0.032	χ_{CH_4} = 0.04
	N_{exc} (ns^{-1})	N_{exc} (ns^{-1})
40	nb[a]	nb
80	nb	14.00
120	nb	13.52
160	12.97	12.01
200	12.95	9.88
240	12.57	9.79

Number of NaCl	χ_{CH_4} = 0.032	χ_{CH_4} = 0.04
	N_{exc} (ns^{-1})	N_{exc} (ns^{-1})
40	nb[a]	17.40
80	19.75	14.15
120	15.18	13.57
160	13.68	10.60
200	11.57	8.70
240	11.37	8.70

[a] No bubble formation

Table 4.4 Laplace pressure inside methane nanobubble formed in the CH_4-NaCl-H_2O mixtures containing 0.032 and 0.04 mole fractions of CH_4.

number of NaCl	χ_{CH_4} = 0.032	χ_{CH_4} = 0.04
	Laplace pressure (P_g-P_l) (bar)	Laplace pressure (P_g-P_l) (bar)
40	nb[a]	836.17
80	908.90	825.93
120	974.18	885.74
160	886.57	864.65
200	1010.63	925.10
240	983.47	930.00

[a] No bubble formation

decides the dynamic behavior of the bubble. Thus, at a high concentration of NaCl, the exchange of CH_4 molecules between the bubble and the liquid is hindered by the low solubility of CH_4 in the presence of NaCl. The increase in the dynamic nature of the nanobubble with decreasing bubble size can be explained based on the difference in the Laplace pressure. Table 4.4 indicates that, for a given concentration of NaCl in the CH_4-NaCl-H_2O system, the Laplace pressure is higher for smaller bubble in the ternary system with a low concentration of CH_4 (table 4.2). Thus, for similar CH_4 solubility, the exchange of CH_4 molecules between the bubble and the surrounding liquid is more predominant for small bubbles.

In the case of CH_4-CH_3OH-H_2O mixtures, the decrease in dynamic nature of the nanobubble with increasing concentration of CH_3OH can be correlated to the decrease in Laplace pressure inside the bubble. It was reported that aqueous CH_3OH acts as a cosolvent for CH_4 molecules in water [141] thereby favoring the transfer of CH_4 from the bubble into the surrounding liquid. However, as shown in table 4.1, Laplace pressure decreases with an increase in the concentration of CH_3OH making the bubble less dynamic in spite of the increase in solubility of CH_4. As in the case of CH_4-NaCl-H_2O mixture, increase in the dynamic behavior of smaller bubbles in CH_4-CH_3OH-H_2O mixture compared to larger ones for a given concentration of CH_3OH is due to the higher Laplace pressure inside the former (table 4.1).

4.4 Conclusion

Classical molecular dynamics simulations were employed to study the role of thermodynamic hydrate inhibitors, NaCl and CH_3OH in the evolution of dissolved gas from a liquid mixture resembling the gas hydrate melt. The simulations showed that an increase in the concentration of hydrate inhibitors promotes the clustering of dissolved gas molecules leading to the formation of nanobubbles in the methane hydrate melt. Whereas NaCl enhances the hydrophobic interaction between dissolved CH_4 molecules, CH_3OH due to its amphiphilic character assists the formation of bubble by accumulating at the bubble-liquid interface. An increase in the concentration of CH_3OH molecules leads to greater accumulation of CH_3OH at the interface. The calculated values of surface tension at the bubble-liquid interface suggest that the presence of CH_3OH at the interface leads to a decrease in the surface tension, thereby making the bubble more stable.

The evolution of dissolved gas in the CH_4-CO_2-H_2O system containing hydrate inhibitors was also examined. The simulations indicated that for a given concentration of the hydrate inhibitor, the induction time for bubble nucleation was significantly reduced in CH_4-CO_2-H_2O system compared to that in the CH_4-H_2O system. The role of CO_2 in assisting the nucleation of the nanobubble was explained based on the accumulation of CO_2 at the bubble-liquid interface. The type of hydrate inhibitor was also found to influence the composition of the bubbles formed. The bubbles formed were found to contain a mixture of CH_4 and CO_2 molecules. The concentration of CO_2 in the bubble formed in the presence of NaCl was found to be more in comparison with that formed in the presence of CH_3OH.

The interaction of the nanobubbles with the surrounding liquid phase containing NaCl and CH_3OH at various concentrations was analyzed, and it was found that bubbles are highly dynamic with frequent exchange of gas molecules between the bubble and the surrounding liquid. The effect of size of the nanobubbles on their dynamic nature was also examined. It is observed that an increase in the concentration of the hydrate inhibitor reduces the exchange of gas molecules between the bubble and the surrounding liquid, thereby making the bubble less dynamic. At a given concentration of the hydrate inhibitor, an increase in the size of the nanobubble also reduces the dynamic behavior of the bubble. The observed dependence of the dynamic nature of nanobubbles on the concentration of the inhibitor and bubble size is explained

in terms of the solubility of gas molecules in the liquid phase surrounding the bubble and the Laplace pressure inside the bubble.

Chapter 5
Effect of Surface Roughness on Adsorption and Distribution of Methane at the Water-Methane Interface

5.1 Introduction

In chapters 3 and 4, the evolution of dissolved gas during the extraction of natural gas from hydrate sediments was discussed. Dissolved gas evolution in hydrate melts involves the formation of bubbles whose stability is influenced by the properties of the interface between the bubble (gas) and the surrounding liquid. Besides its role in natural gas evolution, the interface between liquid and gas is important in several other areas such as gas hydrate nucleation and atmospheric chemistry.

One of the most studied liquid-gas interface is the one between water and gas molecules. The significance of this interface in hydrate formation and atmospheric chemistry was discussed in chapter 1. The importance of water-gas interface has inspired several molecular dynamics simulation studies aimed on understanding the structure and dynamics of this interface at a molecular level [115, 123-128]. An important characteristic of the interface revealed by these studies is that solute molecules get readily adsorbed on the water surface leading to the formation of a thin film [123-127]. The observation of a minimum in the free energy when a gas molecule is close to the surface of water confirmed the thermodynamic feasibility of the adsorption of gas molecules on the water surface. However, when the gas molecules moves closer and comes in contact with the liquid surface, the value of free energy increases from its minimum to reach a maximum value [123, 126, 127]. A molecule must overcome this free energy barrier in order to cross the water-gas interface and dissolve into the bulk liquid region. Based on the analysis of free energy profiles for water-gas interaction, it was suggested that the dissolution of gas molecule is a two step process [126]. In the first step, the gas molecule gets adsorbed on the surface of water followed by the incorporation of adsorbed molecule into the bulk liquid. Recent studies of water-methane interface proposed two contrasting descriptions of methane dissolution at the interface [125, 127]. Ghoufi *et al.* suggested that water molecules play an active role in the dissolution of methane molecules adsorbed on the water-methane interface through the

progressive hydration of methane molecules [125]. In this process, the structure of water surface is affected by methane molecules adsorbed on it. Murina *et al.* proposed a different mechanism for the dissolution of methane molecules in which the molecular level configuration of water surface is unaffected by the presence of adsorbed methane [127]. Here, water molecules do not have an active role in the dissolution of methane. Instead, methane molecules dissolve by occupying the cavities formed due to the spontaneous fluctuations in water density. The uncertainties in the mechanism of important interfacial phenomena such as methane dissolution arises from the lack of proper understanding of the structure of water-gas interface. One of the crucial properties of this interface which has been neglected by earlier studies is its inherent molecular level roughness. The importance of surface roughness in the study of water-gas interfaces is discussed below.

In earlier molecular dynamics simulation studies [115, 127, 259] of water-methane interface, the interface was considered as a slab of definite width bound by smooth parallel surfaces whose positions are defined based on the average densities of water and methane phases. However, at any instant the surface of water at the interface is significantly different from a perfectly planar surface. The surface is rough at a molecular level with several humps and wells arising from the presence of capillary waves [129, 260]. Thus, when the water-methane interface is approximated as a slab, an interfacial molecule may lie on either side of the slab due to inherent roughness of the surface (figure 5.1). At a given instant, some of the molecules present within the slab may belong to the bulk phase instead of the interface. Similarly, all the molecules belonging to the interface may not always be included within the slab representing the interface. Hence, the representation of interface as a slab will introduce an error in the results obtained from such analysis. Recent molecular dynamics simulation studies on the dissolution of methane at the methane-water interface did not take into account the influence of molecular level surface roughness on the interaction of gas molecules with the water surface [125-127]. The influence of thermodynamic conditions and other factors like water-gas interaction on the adsorption of methane at the water-methane interface are also not well studied.

In this chapter, we present results from a classical molecular dynamics simulation study of the structure of water-methane interface. The distribution of methane molecules adsorbed at the interface is examined and the influence of surface roughness on this distribution is analyzed. The effect of pressure and water-gas interaction on the properties of the interface is also studied.

5.2 Models and Methods

5.2.1 Simulation System and Simulation Method

The initial configuration of the simulation system considered in the present study consists of a spherical water cluster containing 4000 molecules surrounded by methane molecules enclosed in a cubic box with a dimension of 12 nm (figure 5.2). The water cluster present in the system was prepared through an independent simulation starting with molecules dispersed in the simulation box. During the course of the simulation, the molecules aggregate leading to the formation of a stable spherical cluster. The spherical water cluster contains a large fraction of its molecules near the surface making it suitable for studying the surface properties in presence of methane. The choice of a similar spherical geometry for the molecular dynamics simulation study of surface phenomena such as water evaporation has been reported earlier [261]. To study the effect of pressure on the structure of water-methane interface, three different compositions of the simulation system were considered in which the number of methane molecules is 475, 2050 and 4540, respectively. These compositions correspond to pressures of 10, 40 and 80 bar, respectively, at a temperature of 270 K considered in the simulations. The large number of CH_4 molecules in the system ensures adequate sampling for studying the adsorption and ditribution of methane on the water surface. At the temperature applied in the simulations, water remains in the liquid state for the model considered in the present study. Hence, the cluster of water molecules remain stable throughout the simulation and the probability for a molecule to desorb from the surface of the cluster is less. To ensure that a change in the curvature of the water surface does not affect the trends in the surface properties observed in the present study, all the simulations were repeated for a water cluster of larger radius containing 6000 molecules surrounded by methane at densities corresponding to 10, 40 and 80 bar, respectively, at 270 K.

The water and methane molecules were modeled using the TIP4P [221] and the OPLS-UA [238] forcefields, respectively. The Lennard-Jones parameters for interaction between water and methane was obtained from a modified Lorentz-Bethelot combination rule [248] given by

$$\sigma_{OM} = \frac{\sigma_O + \sigma_M}{2} \tag{5.1}$$

$$\varepsilon_{OM} = \chi \left(\varepsilon_O \varepsilon_M \right)^{\frac{1}{2}} \tag{5.2}$$

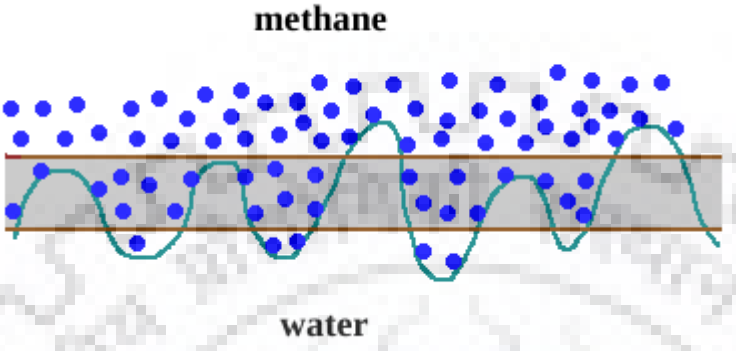

Figure 5.1 Schematic representation of the rough water-methane interface. The shaded region bound by brown lines indicate the interface approximated as a slab.

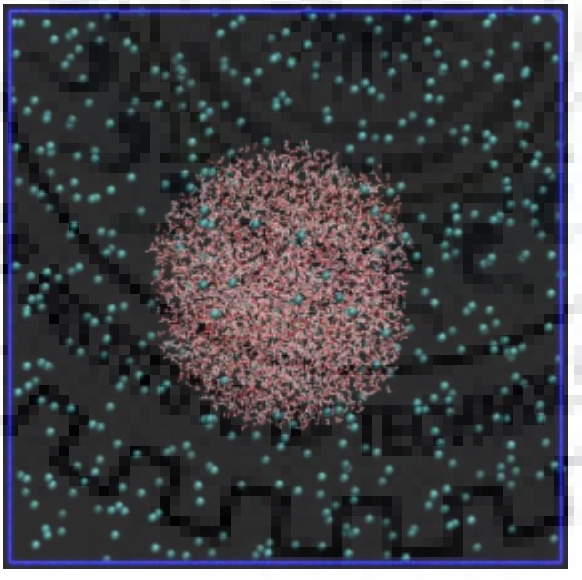

Figure 5.2 The initial conformation of the simulation system containing a water cluster (H-white, O-red) surrounded by methane molecules (cyan spheres).

A scaling factor, χ was introduced in the expression for ε_{OM} between water and the gas molecule to examine the effect of water-gas interaction on the properties of the interface. Four values of χ (1.0, 1.1, 1.2 and 1.3) were considered corresponding to various strengths of interaction between the gas and water molecules. The value of χ=1.0 corresponds to the interaction between water and methane. An increase in the value of χ means an increase in the strength of water-gas interaction and hence an enhancement in the solubility of the gas molecule. The short range interactions were truncated at 1.2 nm and long range electrostatic interactions were calculated with the particle-mesh Ewald summation method. Periodic boundary conditions were applied in all three directions. In addition to the simulations at different values of pressure, the effect of the strength of water-gas interaction on the properties of the interface was examined by performing a set of four simulations at 40 bar for different values of χ.

The simulations were performed in the canonical (NVT) ensemble at a temperature of 270K using the program GROMACS-4.6.5 [241]. The simulations started with an energy minimization followed by a 200 ps simulation which brought the system to an equilibrium at 270 K. This was followed by a production run for a total simulation time of 10 ns with a time step of 2 fs. The simulation time was sufficient for the methane molecules to come in equilibrium with the surface of water. The temperature of the system was maintained by coupling it to a Nosé-Hoover thermostat with a time constant of 0.5 ps [232, 233]. The geometry of water molecule was maintained stable by applying the SETTLE algorithm [244]. The structural features of the water-methane interface were studied by analyzing the last 3 ns of the 10 ns simulations. Various properties of the interface were calculated by analyzing 3000 equally spaced trajectory points lying within this 3 ns time window.

5.2.2 Identification of Molecules at the Surface of Water Cluster

It was mentioned in the introduction that the interface between water and a gas is rough at a molecular level with several humps and wells present. Thus, it is incorrect to consider the water cluster to be a sphere with a smooth surface. Due to the roughness at the surface of the cluster, the molecules present at the surface are found at various distances from the geometric center of the cluster. Therefore, the definition of an interfacial region based on the value of average density is insufficient. For an accurate analysis of the interface, it is important to identify the water molecules present at the outermost molecular layer of the water cluster. This was achieved by

implementing an algorithm described below which is similar to the one proposed by Pártay *et al.* [129, 260] who reported the identification of truly interfacial molecules (ITIM) at the interface of aqueous mixtures.

For a given conformation of the simulation system, the algorithm for identifying water molecules present at the surface of the cluster starts by discarding those molecules which are isolated and far away from the surface of the cluster. Water molecule that does not have any neighbouring molecule within its first hydration shell of radius 0.33 nm is considered as isolated and is not considered to be associated with the cluster. Following this step, a water molecule associated with the cluster is examined to test whether it belongs to the outermost layer of the cluster. This is done by considering a vector directed from the geometric center of cluster to the oxygen atom of the water molecule. Then, a spherical probe is moved from the center of the cluster along the direction of the vector. The diameter of the probe is equal to the Lennard-Jones distance parameter (σ_O) of the water molecule. If the water molecule considered belongs to the outermost molecular layer of the cluster, it will be the last molecule with which the moving probe will come in contact with. The analysis when applied to all the water molecules associated with the cluster led to the identification of all molecules present in the outermost molecular layer of the cluster for a given conformation. These water molecules will be referred to as 'surface water molecules' in the following sections.

5.3 Results and Discussion

5.3.1 Effect of Methane Molecules on the Surface of the Water Cluster

Earlier reported studies about the entry of methane molecules into the water phase across the water-methane interface were not conclusive in understanding the role of water surface in the process [125, 127, 128]. Some of these works [125, 128] suggested that the water surface plays an active role in the entry of methane molecules into water with the dissolution process involving changes in the configuration of the water surface. Whereas, a more recent study [127] on the dissolution of methane indicated that the moelcular level configuration of the water surface is unaffected by the presence of methane molecules at the water-methane interface. Therefore, a detailed analysis of the effect of the methane molecules on the surface of water is necessary. Recently reported experimental studies confirmed that the presence of hydrophobic solutes

enhance the hydrogen bonding interaction between water molecules [262, 263]. A change in hydrogen bonding interaction between water molecules present close to a hydrophobic surface has also been investigated [264-266]. However, the effect of hydrophobic solutes on the molecular level roughness arising from capillary waves at the surface of water has not been studied. To understand this, we examined the surface of the cluster in presence of methane at various pressures around the cluster. The method applied for this analysis and the resulting observations are explained below.

To understand the effect of pressure on the roughness of water surface, a quantitative description of surface roughness is necessary. For this, the roughness of the spherical water cluster surface was characterized in terms of two parameters; the frequency and amplitude [129, 260]. The frequency of roughness refers to the frequency at which the humps and wells on the surface are present while moving on the surface. The amplitude refers to the height or depth of these humps or wells. The values of the frequency and amplitude parameters for the rough surface of the water cluster were determined as follows.

For a given conformation of the simulation system, the 'surface water molecules' of the cluster were identified. Following this, the average radius (r_{avg}) of the cluster was calculated as the mean of the distances from the geometric center of the cluster to the oxygen atoms of the surface water molecules. Then, for a given pair of these water molecules, the following analysis was performed. The separation (R) between oxygen atoms in the radial direction was calculated. Then, a sphere of radius r_{avg} was constructed with its center at the geometric center of the water cluster. The positions of the pair of water molecules were projected to the surface of this sphere and the minimum distance (S) between them on the spherical surface was calculated. Repeating this for all pairs of surface water molecules gave the value of R as a function of S. The analysis was performed over 3000 different conformations of the simulation system obtained from the last 3 ns of the simulation and the results were averaged. A schematic representation of the analysis is given in figure 5.3.

The above analysis was carried out for the simulation systems containing the water cluster consisting of 4000 molecules surrounded by methane molecules at various pressures. The resulting plot of R as a function of S is shown in figure 5.4. The value of R rises steeply at low values of S and becomes steady at larger values of S. As reported by Pártay *et al.* [129] and later

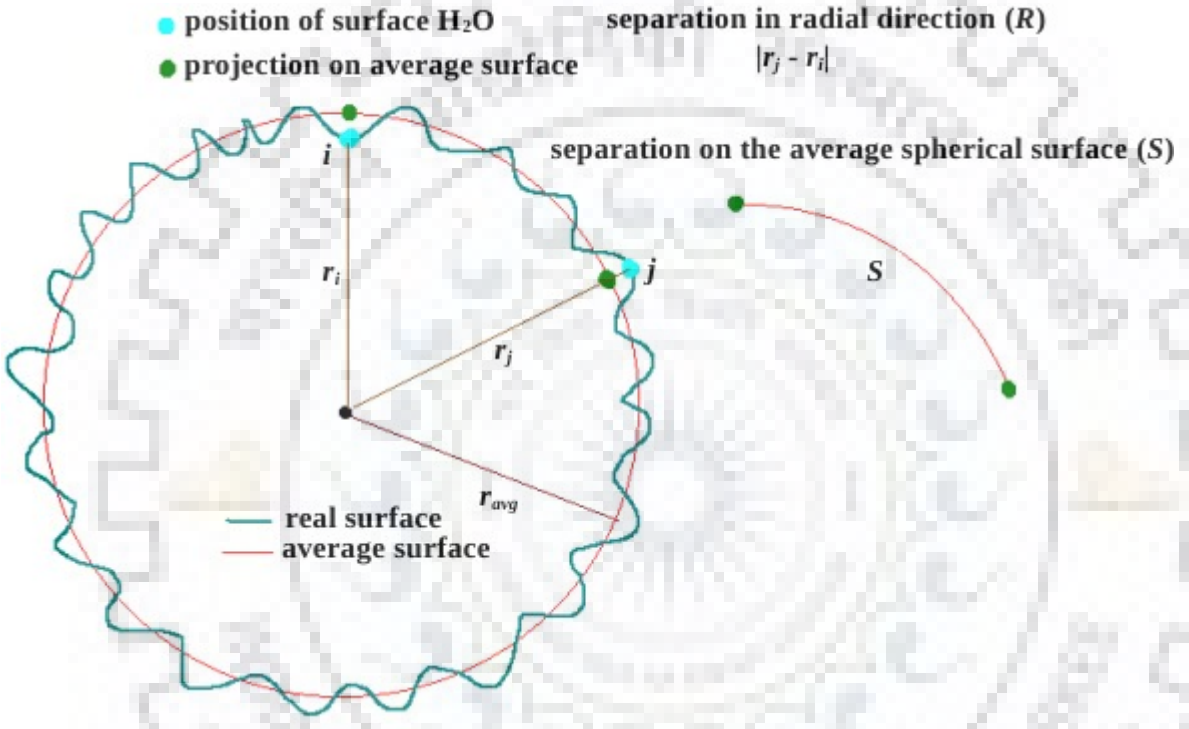

Figure 5.3 Scheme of analysis of the surface roughness of the water cluster

by Darvas *et al.* [140] the slope of *R* vs *S* at the steep portion of the graph indicates the frequency of surface roughness, and the steady value attained by *R* at large values of *S* gives the amplitude of roughness. For a more accurate determination of the roughness parameters, the *R* vs *S* plots at different pressures (figure 5.4) was fitted with the function [140, 267]

$$R = \frac{\alpha \gamma S}{\alpha + \gamma S} \tag{5.3}$$

where, the values of α and γ represents the amplitude and frequency parameters of surface roughness of the spherical water cluster. The values of α and γ for the surface of the smaller water cluster surrounded by methane molecules at different pressures are given in table 5.1. The corresponding data obtained from a similar analysis of surface roughness of the larger water cluster containing 6000 molecules is also given in table 5.1.

From figure 5.4 and table 5.1, it is clear that the presence of methane molecules around the water cluster influences the roughness of the water surface. With an increase in pressure of gas around the water cluster, the amplitude of roughness is found to increase with a simultaneous decrease in the value of the frequency parameter. This indicates that the presence of methane molecules makes the surface of the water cluster more uneven in terms of the height and depth of the humps and wells on the surface. However, the frequency at which these humps/wells appear on the surface decreases with increase in the pressure of methane around the cluster. Thus, it can be concluded from the above analysis that the presence of methane molecules around the water cluster affects the surface roughness of the cluster and that the roughness parameters vary as a function of pressure.

Following the roughness of the water surface, we also examined the adsorption of methane molecules on the surface of the water cluster at various pressures. Earlier studies [115] on the water-methane interface examined gas adsorption at the interface by dividing the system into several slabs or slices parallel to the interface followed by determining the average number density of methane molecules within each of these slabs. However, as explained earlier, the interface is rough at a molecular level and hence cannot be contained within a slab of definite width. Therefore, we examined the adsorption of methane on the surface of the water cluster by identifying the gas molecules that are in direct contact with the 'surface water molecules' of the cluster. The effect of hydrophobicity of a gas molecule on its adsorption on the surface was also investigated. The analysis and the results obtained are described in the following section.

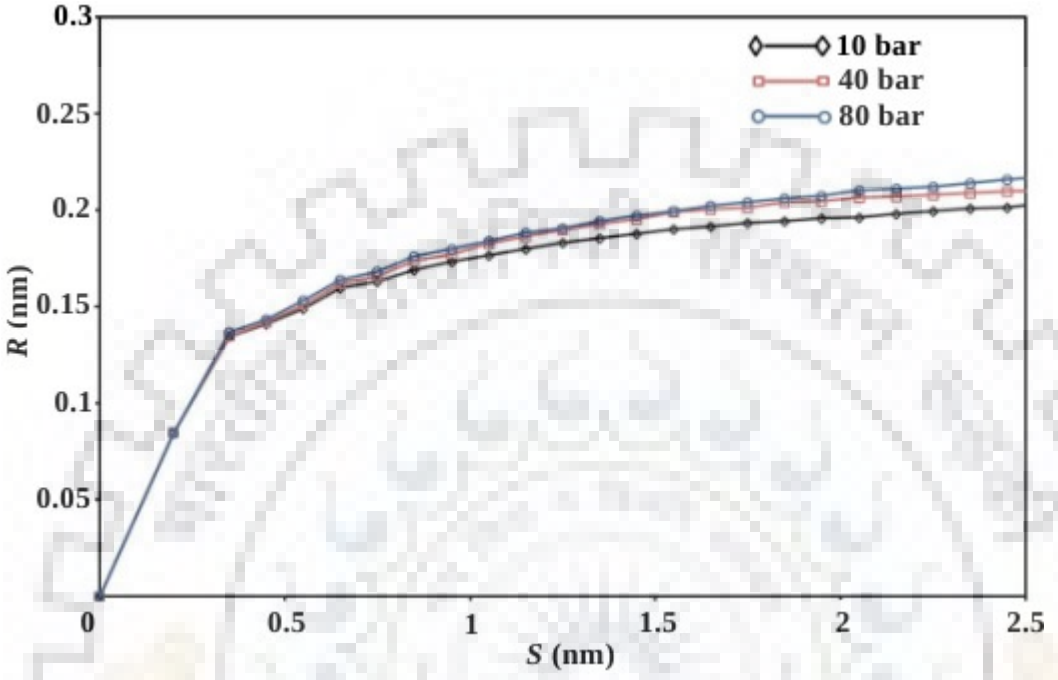

Figure 5.4 The separation (R) between surface water molecules in the radial direction as a function of the minimum distance (S) between them on the surface of the spherical water cluster containing 4000 molecules at different pressures.

Table 5.1 Values of roughness parameters, α (amplitude) and γ (frequency) for the surface of spherical water cluster containing 4000 and 6000 molecules surrounded by methane at different pressure.

pressure (bar)	smaller cluster		larger cluster	
	α (nm)	γ	α (nm)	γ
10	0.224	0.813	0.236	0.775
40	0.236	0.771	0.238	0.771
80	0.241	0.755	0.241	0.754

5.3.2 Adsorption of Methane Molecules on the Water Surface

Earlier studies [125, 268] reported that hydrophobic forces [269] result in an enhancement in the density of methane molecules at the water surface leading to the formation of a thin film of methane at the surface. We studied the adsorption of methane on water surface in detail and examined the effect of pressure and water-gas interaction on adsorption. At a given instant of simulation, the gas molecules which are adsorbed on the surface of water cluster were identified as follows.

To identify methane molecules adsorbed on water cluster at a given instant, all methane molecules away from the cluster were discarded and only those molecules which have more than one water molecule within a distance of 0.5 nm were considered. The methane molecules which are adsorbed on the surface of the cluster were identified by a method similar to the one applied to identify the 'surface water molecules' as explained in section 5.2.2. In this method, for a given methane molecule, a spherical probe is moved along the vector pointing from the geometric center of the spherical water cluster to the position of methane. If methane molecule considered is adsorbed on the surface of the cluster, the probe will not come in contact with any water molecule once it has passed through this methane. By performing this analysis for all methane molecules near the cluster, those methane molecules which are adsorbed on the water surface were determined. Such molecules will be referred to as 'surface methane molecules' in rest of the discussion.

To examine the effect of pressure on methane adsorption, the surface density of methane molecules adsorbed on the water cluster was examined. For a given conformation of the system, the surface density of methane was obtained by dividing the number of 'surface methane molecules' by the surface area of the water cluster. The surface area was estimated as the area of the sphere of radius, r_{avg} ,which is the average radius of the water cluster as defined in section 5.3.1. The value of surface density ($<\rho>$) at various pressures determined by averaging over 3000 conformations of the simulation systems containing the smaller and larger water clusters is given in table 5.2. The results indicate that the surface density of methane molecules increases with an increase in pressure as expected.

In addition to the effect of pressure on methane adsorption, we also examined the effect of hydrophobicity of the gas molecule on its adsorption on the water surface. To study this, we performed simulations at 270 K and 40 bar on four systems which differ in the hydrophobicity of

Table 5.2 Surface density (<ρ>) of methane molecules adsorbed on the surface of water cluster at different pressure.

pressure (bar)	smaller cluster	larger cluster
	<ρ> (nm^{-2})	<ρ> (nm^{-2})
10	0.254	0.254
40	0.958	0.949
80	1.730	1.703

Table 5.3 Surface density (<ρ>) of gas molecules adsorbed on the surface of water cluster for different hydrophobicity of the gas at 40 bar.

χ	smaller cluster	larger cluster
	<ρ> (nm^{-2})	<ρ> (nm^{-2})
1.0	0.958	0.949
1.1	1.104	1.097
1.2	1.267	1.249
1.3	1.442	1.417

gas molecules surrounding the water cluster. The hydrophobicity of the gas molecule was tuned by varying the parameter χ in equation 5.2. Lower values of χ lead to weak water-gas interaction making the gas molecule more hydrophobic. With an increase in the value of χ, the gas molecule becomes less hydrophobic. The average surface density (<ρ>) of molecules adsorbed on the surface of the water clusters was determined for the systems with different values of χ and are listed in table 5.3. As expected, the results show that a less hydrophobic gas molecule will be more readily adsorbed on the surface of water.

The method for determining 'surface methane molecules' as explained above identifies a single layer of methane molecules in direct contact with the outer most layer of the water cluster. However, the layer of methane adsorbed on the water surface is thicker and extends beyond the

single molecular layer of 'surface methane molecules'. Thus, the film of methane adsorbed at the water surface includes molecules which are in direct contact with the surface as well as other methane molecules which are held near the surface by attractive water-methane non bonded interactions. For a complete analysis of methane adsorption on the surface, both the surface density of methane molecules in direct contact with water as well as the density of methane molecules in a region of finite thickness above the surface must be considered.

In the following section, we present the analysis of the distribution of methane molecules adsorbed on the surface of the cluster by considering both the 'surface methane molecules' as well as the molecules which lie above this surface layer. The influence of molecular level roughness of water surface on this distribution is examined in detail.

5.3.3 Distribution of Methane Molecules on the Water Surface

At molecular level, the surface of the water is rough with several humps and wells as explained in section 5.3.1. To understand the effect of roughness on the distribution of 'surface methane molecules', the 'surface water molecules' which form the humps and wells were identified. For a given conformation of the simulation system, the 'surface water molecules' which lie at a distance greater than r_{avg} from the geometric center of the cluster were considered to form the humps. Whereas, the 'surface water molecules' at a distance less than r_{avg} from the center were considered to form wells on the surface. The distribution of 'surface methane molecules' was examined by determining the fraction of these molecules adsorbed on the humps and wells of the water surface. A 'surface methane molecule' is considered to be on the hump, if it has more 'surface water molecules' of the humps within 0.5 nm than those of the wells within the same distance. Whereas, the 'surface methane molecules' which has more 'surface water molecules' of the wells within this distance are considered to be adsorbed on the wells. A small fraction of these methane molecules has equal number of 'surface water molecules' of the humps and wells around them. Such molecules are not considered as either belonging to the hump or the well. The average fraction of surface methane adsorbed on the humps and wells of the rough surface of the water clusters at different pressure is given in table 5.4.

It is clear from the table that irrespective of the size of the cluster, the methane molecules in direct contact with the water surface prefer to be adsorbed at the humps rather than the wells.

Table 5.4 Fraction of surface methane molecules directly adsorbed on humps and wells at the surface of water at different pressure.

Pressure (bar)	smaller cluster		larger cluster	
	humps	wells	humps	wells
10	0.489	0.390	0.494	0.393
40	0.506	0.378	0.508	0.379
80	0.521	0.365	0.523	0.367

Table 5.5 Fraction of gas molecules directly adsorbed on humps and wells at the surface of water for different hydrophobicity of the gas at 40 bar.

χ	smaller cluster		larger cluster	
	humps	wells	humps	wells
1.0	0.506	0.378	0.508	0.379
1.1	0.500	0.385	0.504	0.383
1.2	0.496	0.386	0.502	0.385
1.3	0.493	0.394	0.495	0.398

Thus, the distribution of these moleclues on the water cluster is not uniform and has a greater presence at the humps compared to that at the wells. It is also observed that with an increase in pressure the fraction of 'surface methane molecules' near the humps increases indicating an increasingly non uniform distribution of methane on the surface. A similar analysis was performed for the simulation systems which contain the water cluster surrounded by gas molecules of varying hydrophobicity. The results of the analysis given in table 5.5 indicate that at different values of χ corresponding to different hydrophobicities, the distribution of gas molecules which are in direct contact with the water surface is non uniform with greater presence

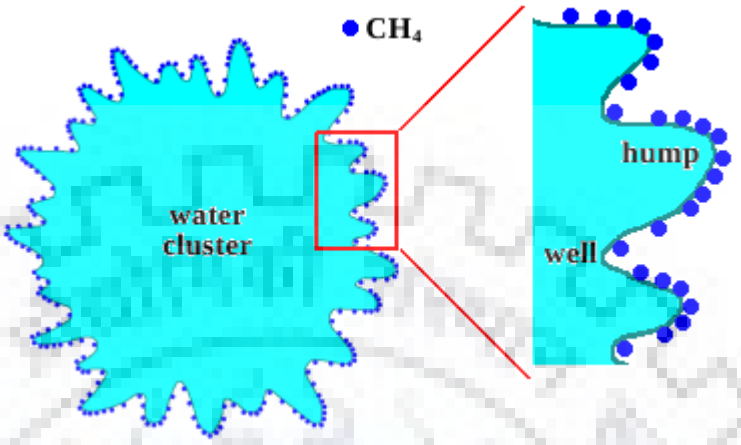

Figure 5.5 Schematic representation of the non uniform distribution of methane molecules adsorbed on the rough surface of the water cluster.

at the humps as observed in the above case. The results also suggest that with an increase in the value of χ (decreasing hydrophobicity), the distribution becomes slightly more uniform. A schematic representation of the non uniform distribution of gas molecules on the rough water surface is given in figure 5.5.

As explained above, methane molecules adsorbed on the surface of the water cluster extend beyond the first layer, which is in direct contact with the water surface due to attractive water-methane non bonded interactions. To understand the distribution of the adsorbed methane molecules present beyond the first layer of methane, the following analysis was carried out.

For a given 'surface water molecule', a vector is constructed which originates from the geometric center of the water cluster and points towards the oxygen atom of the water molecule. Starting from a distance of 0.5 nm above the surface water oxygen, a spherical probe is moved away from the center of the cluster along the direction of the vector. The probe which has a radius equal to the Lennard-Jones distance parameter of methane is allowed to move until it has covered a distance of 0.5 nm from its initial position. At a given instant of time the number of methane molecules with which the probe comes in contact was determined. This when divided by the volume of the region covered by the probe gives the number density of methane in the region above the 'surface water molecule' at that instant. The number density of methane above

the water surface thus obtained will be referred to as the 'local density' of methane in the following discussion. The value of the 'local density' of methane was calculated by averaging over all the 'surface water molecules' and over 3000 points in the trajectory within 7 to 10 ns of the simulation. From this analysis, the 'local density' of methane near the humps and wells of the rough surface of the water cluster was determined. The results obtained for the small and large water clusters at different pressures of methane are given in table 5.6. Results from a similar analysis for the systems at 40 bar with varying hydrophobicity of the gas are given in table 5.7.

Table 5.6 Local density of methane molecules near humps and wells at the water surface at different pressure.

Pressure (bar)	local density of CH_4 (smaller cluster)		local density of CH_4 (larger cluster)	
	humps	wells	humps	wells
10	0.306	0.352	0.293	0.333
40	1.344	1.527	1.294	1.456
80	2.995	3.333	2.883	3.154

Table 5.7 Local density of gas molecules near humps and wells at the water surface for different hydrophobicity of the gas at 40 bar.

χ	local density of gas (smaller cluster)		local density of gas (larger cluster)	
	humps	wells	humps	wells
1.0	1.344	1.527	1.294	1.456
1.1	1.352	1.563	1.304	1.489
1.2	1.365	1.609	1.308	1.525
1.3	1.369	1.638	1.309	1.554

The results indicate that the 'local density' of methane molecules near the water surface is influenced by the molecular level roughness of the surface. In all the simulation systems considered, the average density of methane beyond the first layer of methane molecules that in direct contact with the surface is higher at the region above the wells on the surface compared to that above the humps in contrast to distribution of density observed for the surface layer. This indicates that inspite of more availability of methane molecules above the wells of the rough water surface, methane prefer to come in direct contact with the humps on the surface as indicated by tables 5.4 and 5.5. Thus, it is clear that there is a preference for methane molecules to be adsorbed directly on the humps of the water surface rather than on the wells. The reason behind the non uniform distribution of methane near the water surface can be related to the nature of interaction between the gas moleclue and the water surface as explained below.

5.3.4 Interaction between Methane and Water Surface

The interaction of a methane molecule with the water surface involves contributions from both attractive and repulsive components [103]. The attractive component arises from the non-bonded interactions between methane and the water molecules of the surface. This attractive interaction is prominent when methane molecule is close to the water surface but not in direct contact with it. The repulsive component of the interaction is due to the excluded volume effect which refers to the free energy cost for the formation of a cavity in water to host a methane molecule. The repulsive component dominates when methane molecule comes in contact with water surface and tries to enter into the bulk water region. The 'surface methane molecules' identified in the present study are in direct contact with the water cluster. Hence, repulsive interaction due to the excluded volume effects will be more predominant in this case. Whereas, the molecules near the water surface above the layer of 'surface methane molecules' are not in direct contact with the surface and their interaction with water is dominated by the non-bonded attractive component.

Based on the above arguments, we examined the characteristics of the 'surface water molecules' that come in contact with a methane molecule approaching the cluster. The density of these water molecules was analyzed in terms of the number of molecules within a given distance around a water molecule of the surface layer. For regions of high density, each of these molecules will have more number of neighbouring molecules within a given distance. The

average number (<*nw*>) of 'surface water molecules' within a distance of 0.5 nm around a molecule of the surface layer was determined. The values of <*nw*> for the molecules belonging to the humps and wells of the rough surface of the water clusters surrounded by methane at various pressures are given in table 5.8. The results of a similar analysis performed for the cluster surrounded by gas molecules of varying hydrophobicity at 40 bar are shown in table 5.9.

Table 5.8 Number of surface water molecules (<*nw*>) within 0.5 nm around a water molecule at humps and wells on the water surface at different pressure.

Pressure (bar)	<*nw*> (smaller cluster)		<*nw*> (larger cluster)	
	humps	wells	humps	wells
10	4.370	4.553	4.220	4.367
40	4.355	4.543	4.206	4.343
80	4.371	4.479	4.187	4.325

Table 5.9 Number of surface water molecules (<*nw*>) within 0.5 nm around a water molecule at humps and wells on the water surface for different hydrophobicity of the gas at 40 bar.

χ	<*nw*> (smaller cluster)		<*nw*> (larger cluster)	
	humps	wells	humps	wells
1.0	4.355	4.543	4.206	4.343
1.1	4.175	4.331	4.186	4.329
1.2	4.142	4.322	4.164	4.296
1.3	4.136	4.293	4.141	4.252

The results indicate that the 'surface water molecules' are closer to each other at the wells than at the humps of the water surface. Thus, these molecules when present at the humps are more free to move making a cavity in which the 'surface methane molecule' can occupy when in contact with the water surface. Therefore, the repulsive contribution to the interaction between methane and water surface due to the excluded volume effect will be less prominent at the humps than at the wells. This explains the preferential adsorption of 'surface methane molecule' at the humps of the water surface. The earlier analysis of the distribution of adsorbed gas molecules also showed that the 'local density' of gas molecules present beyond the layer of 'surface methane molecules' is more above the wells of the surface than that above the humps. This can be explained based on the predominant attractive interaction of these gas molecules with the water surface. A methane molecule above the hump of the water surface is at a greater distance from the average surface of the water cluster compared to a methane molecule above the well. Thus, above the wells, the gas molecule interacts with more number of water molecules of the cluster. This leads to a higher 'local density' of methane in a region above the wells compared to that above the humps.

5.4 Conclusion

The structure of the water-methane interface was studied at a molecular level by applying classical molecular dynamics simulations. Simulations were performed on systems consisting of a water cluster surrounded by methane molecules at different pressures. To understand the effect of methane molecules on the structure of the water surface, molecules forming the outermost layer of the cluster were identified. Analysis of the molecular level roughness of the surface showed that an increase in the pressure of methane made the water surface more rough in terms of the amplitude of humps and wells of the surface.

The adsorption of methane molecules and their distribution on the surface of water cluster was examined. The results indicated that the methane molecules those are in direct contact with the surface prefer to be adsorbed at the humps of the surface. However, the density of adsorbed methane molecules above the layer in direct contact was found to be more near the wells rather than that near the humps. The nonuniformity in the distribution of adsorbed methane molecules in direct contact with the water surface and those above this layer is explained in

terms of the interaction between water and methane. The interaction between the water surface and methane molecules in direct contact is dominated by the repulsive component arising from excluded volume effect. However, the interaction of adsorbed methane molecules above the surface layer of methane is dominated by attractive non-bonded terms. The humps of the surface have less density of water making excluded volume effect less prominent at these sites. This causes the methane molecules which are in direct contact with the surface to be preferentially adsorbed on the humps. However, the adsorbed methane molecules above this layer will be closer to the average surface of the cluster when above the wells rather than on the humps. This leads to stronger attractive non-bonded interactions between these methane molecules and water at the wells, resulting their higher density in the region above the wells than the humps.

The results of the present study indicate a clear preference for adsorbed methane molecules to come in contact with water surface at the humps. The methane molecules which are in direct contact with the surface can be considered to be in an intermediate state during their passage from the gaseous phase into the bulk liquid region. The preferential binding of these molecules on the humps suggests that the roughness of the water surface has an important role in the process of methane dissolution. The humps formed at the surface can act as regions of low water density where a cavity can easily form to accommodate the methane molecule.

Chapter 6
Adsorption and Dissolution of Methane at the Surface of the Methanol-Water Mixture

6.1 Introduction

In chapter 5, adsorption and distribution of methane on the surface of water was studied. Several previous experimental studies about water-methane interaction examined the solubility of methane in water and various factors affecting the solubility [270-279]. Molecular dynamics simulation studies on the factors affecting the solubility of methane in water have also been reported [248, 280-283]. These studies showed that thermodynamic conditions as well as the presence of different chemical species has a significant effect on the solubility of methane. Among the chemical species which influence the solubility of methane, the effect of methanol on methane dissolution is of particular significance to the natural gas industry. Methanol, which is a widely used thermodynamic inhibitor of gas hydrate formation is reported to act as a cosolvent for methane [141, 279]. Therefore, it is important to understand the effect of methanol on the dissolution of methane. The dissolution of methane is a process that occurs at the interface between gaseuos methane and the liquid phase. Earlier reported simulation studies of this important interface were mainly focussed on the interaction between methane and pure water at their interface [115, 125, 127]. Some of the recent studies of water-methane interface and the insights they provide about methane dissolution are discussed below.

The most important characteristic of the methane-water interface is the formation of a thin film of methane adsorbed on the surface of water [125, 127]. This was supported by the observation of a minimum in the free energy of interaction when a methane molecule approaches the water surface from the gas phase [125, 127]. Somasundaram *et al.* reported that adsorption of gas molecules on the liquid surface is the first step in gas dissolution which is followed by the entry of the adsorbed molecule into the bulk liquid [126]. As explained in chapter 5, two different mechanisms for the entry of methane into water across the water-methane interface have been reported [125, 127]. One of the mechanisms involves progressive hydration of the methane by water molecules at the interface [125]. According to the other mechanism, CH_4

enters the liquid phase by occupying the cavities formed due to spontaneous fluctuations in water density [127]. The latter mechanism does not involve any change in the molecular level configuration of interfacial water.

The above mentioned studies did not consider the effect of an aqueous solute on the dissolution of methane at water surface. As explained above, understanding the effect of aqueous methanol on methane dissolution at the surface of methanol-water mixture is of great relevance to the natural gas industry. Earlier reported studies on the liquid-vapor interface of the methanol-water mixture provided molecular level insight into the structure and properties of this interface [129-131, 133, 134, 136-140]. Experiments [133, 134, 136]] indicated an enhancement in the concentration of methanol molecules at the surface of the mixutre which was later supported by simulation studies [129-131, 137, 138, 140]. Simulations also showed that interfacial methanol molecules have a strong orientational preference with its methyl group pointing towards the vapor side of the interface [129, 131, 137, 138, 140]. Pártay *et al.* and Darvas *et al.* studied the molecular level roughness of the methanol-water liquid surface and examined the residence time of molecules at the surface layer [129, 140]. In addition to the structural characteristics of the liquid-vapor interface of the methanol-water mixture, studies of its dynamic properties have also been reported. Studies of the hydrogen bond dynamics at this interface by Paul *et al.* and Choudhuri *et al.* revealed that the relaxation of hydrogen bonds in the interfacial region is slower than that in the bulk region of the mixture [138, 139]. It was also showed that both water and methanol molecules at the interface have higher diffusivity compared to that in the bulk.

The studies of the liquid-vapor interface of methanol-water mixture discussed above did not consider the interaction of gas molecules with the interface. In this chapter, we report the results of classical molecular dynamics simulation study on the interaction of methane with the surface of methanol-water mixture. The effect of the structural characteristics of the interface on adsorption and dissolution of methane is examined in detail for different compositions of the mixture. The influence of methane on the molecular level orientation of interfacial methanol molecules is also studied.

6.2 Computational Methods

6.2.1 Simulations

To study the interaction of methane with the surface of methanol-water mixture, the interface between liquid mixture and methane gas was simulated for various concentrations of aqueous methanol. The simulation system consists of a slab of liquid mixture in contact with the gas phase containing methane at the interface (figure 6.1). The equilibrium conformation of the liquid slab which contains 4000 molecules was prepared by an independent simulation. The slab which has a dimension of 4 nm along X and Y directions is then placed in an expanded rectangular box of dimensions 4 nm x 4 nm x 20 nm. The liquid slab occupies a portion of the simulation box along the z-axis and the remaining volume is filled with methane. Thus, the simulation system contains a planar interface between the liquid and methane whose plane is perpendicular to the z-axis. Three different compositions of the liquid mixture were considered in which mole fraction of CH_3OH is 0.1, 0.3 and 0.5 (table 6.1). In addition to the interface of methane with methanol-water mixture, its interface with pure water was also studied. The number of methane molecules in each system corresponds to a pressure of 40 bar at the simulation temperature of 270 K. The high pressure of methane enhances its dissolution into the liquid thereby decreasing the simulation time required to study dissolution. The number of gas molecules varies since the volume occupied by the liquid slab increases with increasing concentration of methanol. The initial conformation of the simulation system (figure 6.1) was energy minimized followed by a 200 ps simulation in the NVT ensemble during which the system attained an equilibrium temperature of 270 K. After equilibration, a production simulation was performed for a total simulation time of 100 ns in the NVT ensemble with an integration time step of 2 fs. During the simulation, the system was coupled to the Nose-Hoover thermostat [232, 233] with a time constant of 0.5 ps.

The CH_3OH and CH_4 molecules were modeled using the OPLS-UA force field [238, 252] and water molecules were represented by the TIP4P model [221]. The cross interaction Lennard-Jones parameters were obtained using the Lorentz-Berthelot combination rule. The short range non-bonded interactions were truncated at 1.2 nm and particle mesh Ewald summation method was applied to treat the long electrostatic interactions. LINCS algorithm [243] was applied to constrain the molecular geometries and water molecules were maintained

stable using the SETTLE algorithm [244]. Periodic boundary conditions were applied in all three directions.

Table 6.1 Composition of the simulation systems consisting of the liquid slab and CH_4 molecules.

number of CH_3OH	number of H_2O	number of CH_4
0	4000	240
400	3600	225
1200	2800	207
2000	2000	192

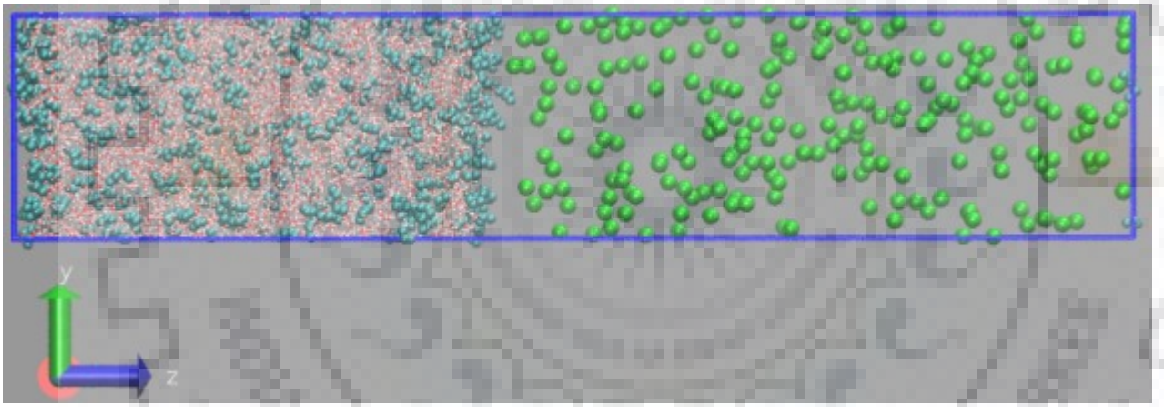

Figure 6.1 Initial conformation of the simulation system containing CH_3OH (cyan), H_2O (red-O, white-H) and CH_4 (green) molecules.

6.2.2 Identification of Interfacial Solvent Molecules

The conventional method in molecular dynamics to identify the interface between two phases is to consider it as a region of finite thickness within which the average density of the system undergo a transition from its value in one phase to that in the other. As discussed in section 5.2.2 of chapter 5, this method is unsuccessful in the accurate determination of interfacial molecules due to the inherent roughness of the interface. A region of definite thickness may not contain all the molecules which are present at the rough interface between the two phases.

Similarly, some molecules in the bulk phase may be misidentified as belonging to the interface. Thus, a more accurate study of the interface requires the identification of the layer of molecules of methanol-water mixture present at the boundary of the liquid phase. The method for identifying molecules present at a curved interface between methane and water was discussed in section 5.2.2 of chapter 5. We followed a similar approach in identifying the solvent molecules at the planar interface between methanol-water liquid mixture and methane which is perpendicular to the z-axis as shown in figure 6.1. The details of this method are explained below.

The origin of z-coordinate was placed at the center of the liquid slab along the z-axis such that the interface between methanol-water mixture and methane lie along the positive z-direction. Following this, all the molecules of the liquid mixture with a positive z-coordinate were identified. For a given such molecule of the liquid, a vector parallel to the z-axis was constructed which originate from the XY plane at the center of the slab and points to the molecule considered. The position of the water or methanol molecules were considered to be the respective positions of their oxygen atoms. Then a spherical probe was moved along this vector whose diameter is equal to the Lennard-Jones distance parameter of the oxygen atom of CH_3OH or H_2O considered. If the molecule considered belongs to the layer at the boundary of the liquid phase, the probe after passing through it will not come in contact with any other molecule of the liquid. Through this procedure, all the water and methanol molecules which belong to the surface layer of the methanol-water liquid slab at an instant were identified. The molecules thus identified will be referred to as 'surface solvent molecules' in the following sections.

6.3 Result and Discussion

6.3.1 Role of Surface Roughness in Methane Dissolution

Earlier studies reported that, at molecular level, the surface of a liquid is rough with several humps and wells due to the presence of capillary waves [129, 140, 260]. We examine in detail the effect of surface roughness on the adsorption and dissolution of methane at its interface with methanol-water liquid mixture. The distribution of methane at the interface was analyzed by determining its number density profile along the z-direction perpendicular to the interface. The effect of interfacial roughness on the distribution of methane was examined by performing the following analysis on the conformations of the systems between 90 and 100 ns of the simulation.

For each 'surface solvent molecule', a vector parallel to the z-axis was considered which originate from the bulk liquid region and pass through the solvent molecule considered. Along this vector, a spherical probe was moved whose diameter is equal to the Lennard-Jones distance parameter of CH_4. The probe when moved from within the methanol-water liquid mixture to the gas phase across the interface between the liquid and methane cover a cylindrical volume as shown in figure 6.2. The number of CH_4 molecules with which the probe comes in contact when moving through the cylindrical region was determined. For a given conformation of the simulation system, this analysis was performed for all 'surface solvent molecules' present at the humps and wells of the rough surface of the liquid (figure 6.2).

To classify the solvent molecules at the liquid surface as belonging to the humps and wells, we consider an XY plane which represents the average surface of the liquid. The position of this plane along the z-axis was determined by averaging the z-coordinates of the 'surface solvent molecules'. A 'surface solvent molecule' is considered to be at the hump, if the distance from the center of the liquid slab to this molecule is greater than the corresponding distance to the average liquid surface. Similarly, the solvent molecules at the wells of the interface were identified as the ones which are nearer than the average liquid surface to the center of the liquid slab.

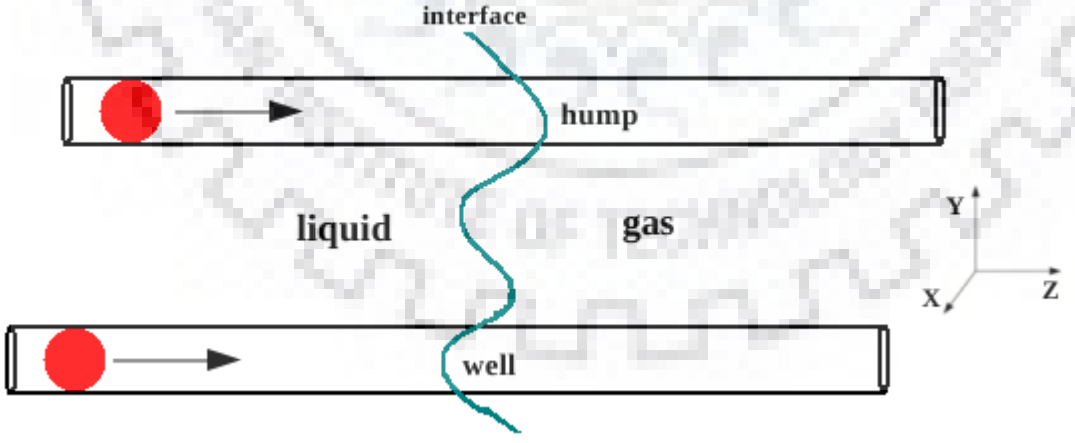

Figure 6.2 Movement of the spherical probe (red) across the interface (cyan) between the methanol-water liquid mixture and methane.

To obtain the number density profile of methane along the z-axis, the cylindrical volume (figure 6.2) covered by the probe was divided into several smaller segments. Within each such segment, the number of methane molecules with which the probe came in contact while passing through the segment was determined. This, when divided by volume of the segment gave number density of methane within that segment at an instant. By repeating this analysis over a larger number of conformations of the simulation system, the average number density profile of CH_4 along the z-direction passing through humps and wells of the liquid surface was determined. The result of this analysis for the interface between methanol-water liquid mixture and methane is shown in figure 6.3 in which, the density of CH_4 is scaled by its value in the bulk gas phase. The number density profile of methane for its interface with pure water is also included in the figure.

In the density profile of methane (figure 6.3), zero on the horizontal axis represents the position of 'surface solvent molecule' at the hump or well of the liquid surface. The distance from the liquid surface is considered to be negative on moving towards the bulk liquid region and positive on moving towards the gas phase. The region lying between a distance of -0.5 nm and 0.3 nm from the surface is referred to as the 'surface region' where, methane is at the surface of methanol-water liquid mixture or just above or beneath it. The region extending from 0.3 nm to 1.5 nm is referred to as the 'local region' where methane molecules which are not in direct contact with the liquid accumulate near its surface. The region beyond 1.5 nm above the 'surface solvent molecule' correspond to the bulk gas phase where there is no enhancement in the density of methane. The bulk liquid region lie at a distance beyond -0.5 nm from the liqiud surface where the density of methane corresponds to its solubility in the liquid. A maximum in the density of methane is observed in the 'local region' above both humps and wells on the liquid surface. This arises from attractive non-bonded interactions between methane and the molecules of methanol-water liquid mixture.

An important observation from the number density profile of methane (figure 6.3) is that, in all the cases, density of methane in the 'surface region' is higher near the humps on the liquid surface compared to that near the wells. This is in contrast to the distribution of methane in the 'local region' where its density is higher above the wells compared to that above the humps. The larger value of density of methane at the 'surface region' near the hump indicates that there is a higher probability for methane to enter the bulk liquid region through the humps of the surface.

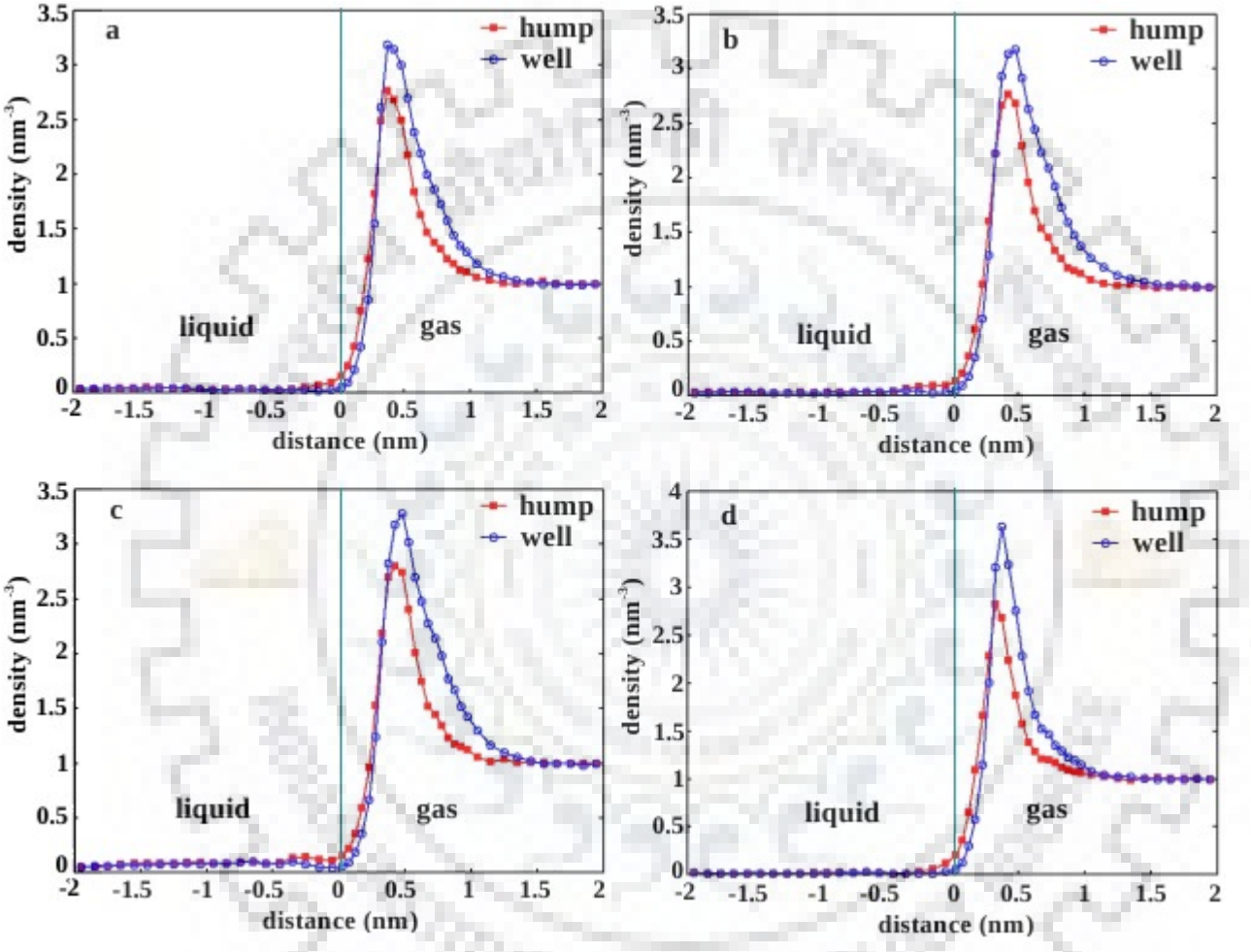

Figure 6.3 Number density profile of CH_4 along the z-direction for the regions corresponding to humps (red) and wells (blue) of the surface of methanol-water mixture containing (a) 400 CH_3OH and 3600 H_2O, (b) 1200 CH_3OH and 2800 H_2O, (c) 2000 CH_3OH and 2000 H_2O molecules. The corresponding density profile for the surface of pure water (d) is also shown. The number density is scaled by its value in the bulk gas phase. The vertical line at zero corresponds to the position of the liquid surface.

Thus, the humps on the liquid surface acts as preferred channels for methane dissolution inspite of the lower density of methane in the 'local region' above the hump. The results suggest that roughness of the liquid-gas interface has an important role in the entry of gas molecules into the liquid.

To understand the distribution of methane molecules at its interface with methanol-water liquid mixture in detail, the number density of methane at various distances from the humps and wells of the liquid surface was examined. For a given distance from the surface of the liquid, the difference between densities of methane corresponding to the humps and wells of the liquid surface was calculated. The difference between corresponding densities of methane at various distances from the humps and wells (d_{hump}-d_{well}) for the systems studied is plotted in figure 6.4. As expected from the number density profiles of methane (figure 6.3), the difference (d_{hump}-d_{well}) is close to zero at distances corresponding to the bulk liquid (< -0.5 nm) and gas (> 1.5 nm) regions. Whereas, d_{hump}-d_{well} is positive at distances corresponding to the 'surface region' and negative at distances corresponding to the 'local region'. It can also be observed from figure 6.4 that the value of d_{hump}-d_{well} changes from negative to positive at a distance of ~0.3 nm from the liquid surface towards the gas phase. This distance is close to the value of the Lennard-Jones distance parameter (0.3730 nm) for methane molecule. This indicates that the difference between densities of methane, d_{hump}-d_{well} change from negative to positive starting from a distance above the liquid surface where methane comes in direct contact with the surface. Thus, the role of humps of the liqiud surface as preferred channels for the entry of methane molecule into the bulk liquid may be related to the interaction of solvent with methane molecules in direct contact with it. To examine this, we determined the average number of solvent molecules in the 'surface region' near the humps and wells for liquid mixtures of various compositions considered. The procedure for this is similar to that applied for determining the density profile of methane (figure 6.2). Here, the number of molecules of the liquid mixture with which the probe comes in contact at the 'surface region' was determined. The results obtained from this analysis is shown in table 6.2 which indicate that more liquid molecules are present in the 'surface region' near the wells on the surface in comparison to the humps. Thus, density of liquid is higher in the region near the wells, which makes it difficult for a methane molecule to enter into the bulk liquid region through the well. This explains the role of humps of the liquid surface as preferred channels for the dissolution of methane.

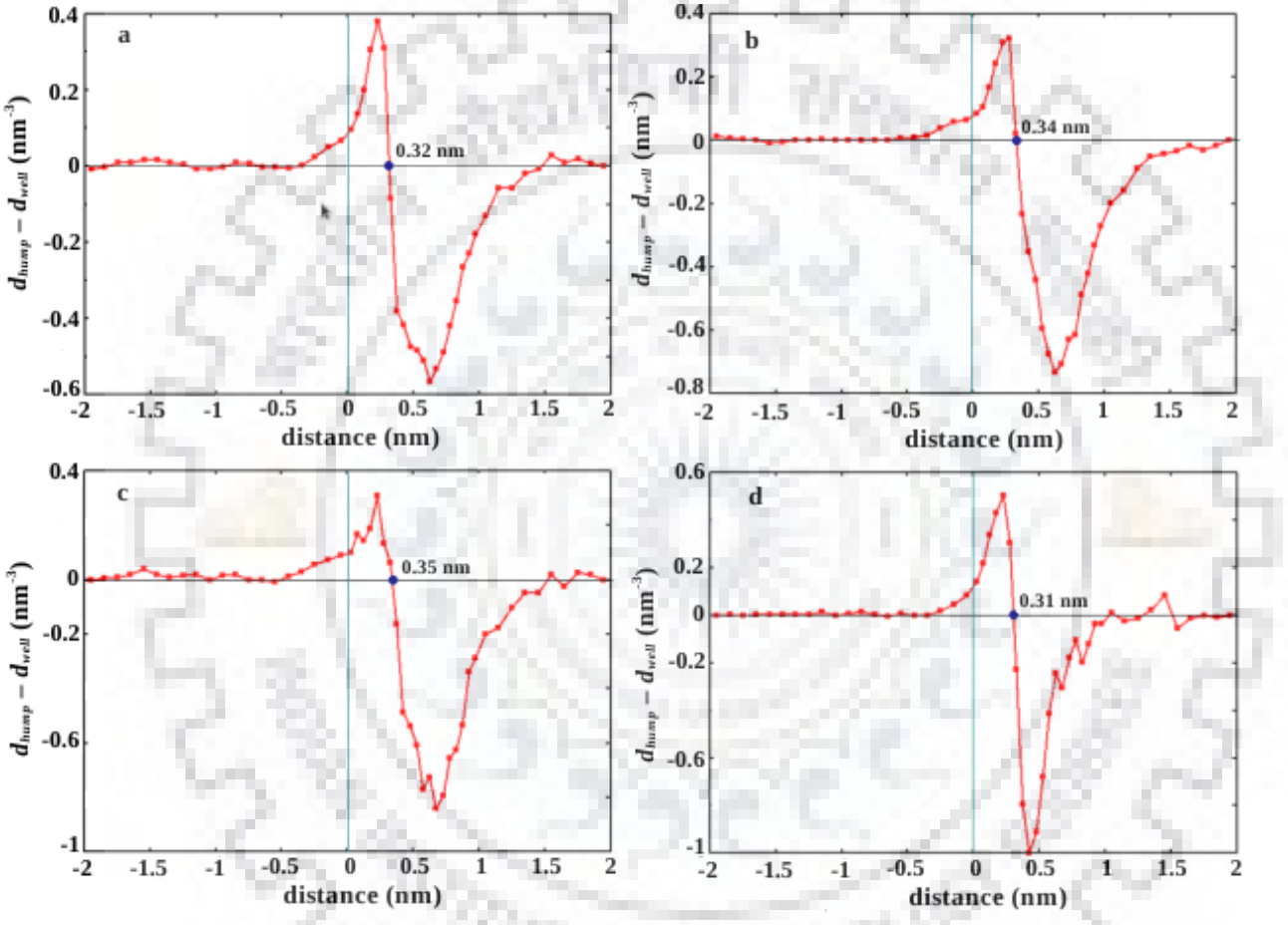

Figure 6.4 Difference between the number densities of methane at various distances from the humps and wells (d_{hump}-d_{well}) for methanol-water mixture containing (a) 400 CH_3OH and 3600 H_2O, (b) 1200 CH_3OH and 2800 H_2O, (c) 2000 CH_3OH and 2000 H_2O molecules. The corresponding plot for the surface of pure water (d) is also shown. The vertical line at zero corresponds to the position of liquid surface.

Table 6.2 Average number of solvent molecules in the 'surface region' near the hump and well at the surface of the liquid mixture containing different concentrations of methanol.

mole fraction of CH_3OH	number of solvent molecules in surface region	
	hump	well
0	6.760	7.322
0.1	6.177	6.827
0.3	5.310	5.868
0.5	4.760	5.108

Considering the role of surface roughness in the dissolution of gas molecule at the surface of methanol-water mixture, we examined the effect of methanol on the molecular level roughness of the liquid surface. A quantitative estimate of surface roughness was made in terms of the amplitude (α) and frequency (γ) of roughness as explained in section 5.3.1 of chapter 5. Amplitude of roughness refers to the height and depth of the humps and wells, respectively, of the surface. The frequency of roughness indicates the closeness of the humps or wells present on the liquid surface. The values of roughness parameters for the liquid mixtures of varying composition was determined from the following analysis as proposed by Pártay *et al.* [129, 140, 260].

For a pair of 'surface solvent molecules', the separation (R) between them in the direction normal to XY plane representing the average surface of the liquid mixture was determined. The lateral separation (S) between the two molecules on the average surface was also calculated. By repeating this procedure over all pairs of 'surface solvent molecules' and over a large number of conformations of the system, the value of R corresponding to various values of S was obtained. The R versus S plots for the surface of liquid mixtures of varying composition considered in the present study are shown in figure 6.5. The figure indicates that the value of R increases almost linearly for small values of S and that the graph becomes flat at larger values of S. The slope of the linear portion gives a measure of frequency (γ) of roughness and the value attained by R at larger values of S represents the amplitude (α) of surface roughness. The values of roughness parameters were obtained by fitting the function [140, 267],

$$R = \frac{\alpha \gamma S}{\alpha + \gamma S} \tag{6.1}$$

to the *R* versus *S* data. The values of α and frequency γ thus obtained for the liquid mixtures of varying composition considered are given in table 6.3. The results indicate that with an increase in the concentration of methanol, the surface of the liquid becomes increasingly rough in terms of both frequency and amplitude.

The number density profile (figure 6.3) of methane along the direction normal to its interface with the methanol-water liquid mixture indicates that there is higher probability for methane molecules to enter into the bulk liquid through the humps of the surface. The above analysis of the molecular level roughness of the liquid surface shows that as the concentration of methanol in the liquid increases, the humps and wells of the surface becomes larger in terms of their height or depth. It is also observed that the humps and wells at the surface becomes closer to each other as the liquid mixture becomes rich in methanol. These results suggest that the larger humps at the surface of methanol rich liquid mixture can facilitate the transfer of methane molecules across the interface between the gas and liquid. Thus, a greater roughness at the surface of methanol-water liquid mixture containing high concentrations of methanol can be considered as a factor which affects the dissolution of methane into the liquid. This can lead to a larger number of CH_4 molecules crossing the liquid-methane interface within a given time in the case of methanol-water liquid mixture containing high concentration of methanol. Thus, due to the roughness at the liquid-methane interface, the distribution of methane molecules between the gas and the liquid phases can reach its equilibrium within a shorter time. For the present simulations, the average number density of methane at various distances from the center of the liquid slab along the direction normal to the interface is plotted in figure 6.6. The figure indicates a greater number density of methane in the bulk liquid at high concentrations of methanol. The maximum in the density of CH_4 adsorbed on the liquid surface shifts to larger distances as the volume of the liquid mixture increases with an increase in the concentration of methanol.

The number density profile of methane (figure 6.3) also showed that the density of methane in the 'local region' above the liquid surface is higher above the wells in comparison with the humps. This can be explained in terms of the non-bonded attractive interaction between the liquid molecules and the methane molecules present in the 'local region' above the surface. The potential energy of interaction between molecules of the methanol-water liquid mixture and the methane molecules in 'local region' above the humps and wells of the liquid surface was calculated. For a given such methane molecule, the potential energy of this interaction is given

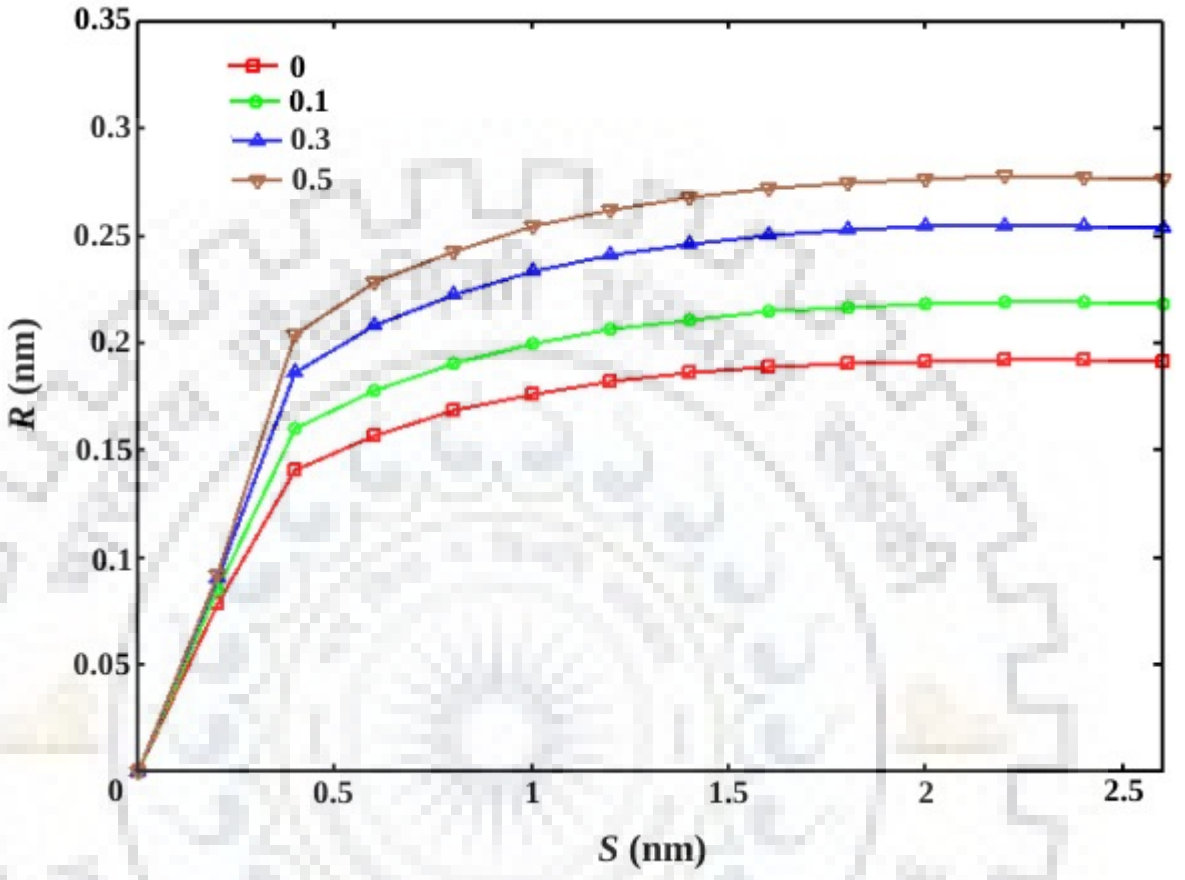

Figure 6.5 Separation between surface solvent molecules in the direction normal (*R*) to the interface plotted against the lateral separation (*S*) between them on the average surface of the methanol-water mixture containing different mole fractions of methanol.

Table 6.3 Values of amplitude (α) and frequency (γ) of surface roughness of the methanol-water mixture containing different mole fractions of methanol.

mole fraction of CH_3OH	amplitude (α) (nm)	frequency (γ)
0	0.218	0.847
0.1	0.249	0.926
0.3	0.292	1.032
0.5	0.320	1.097

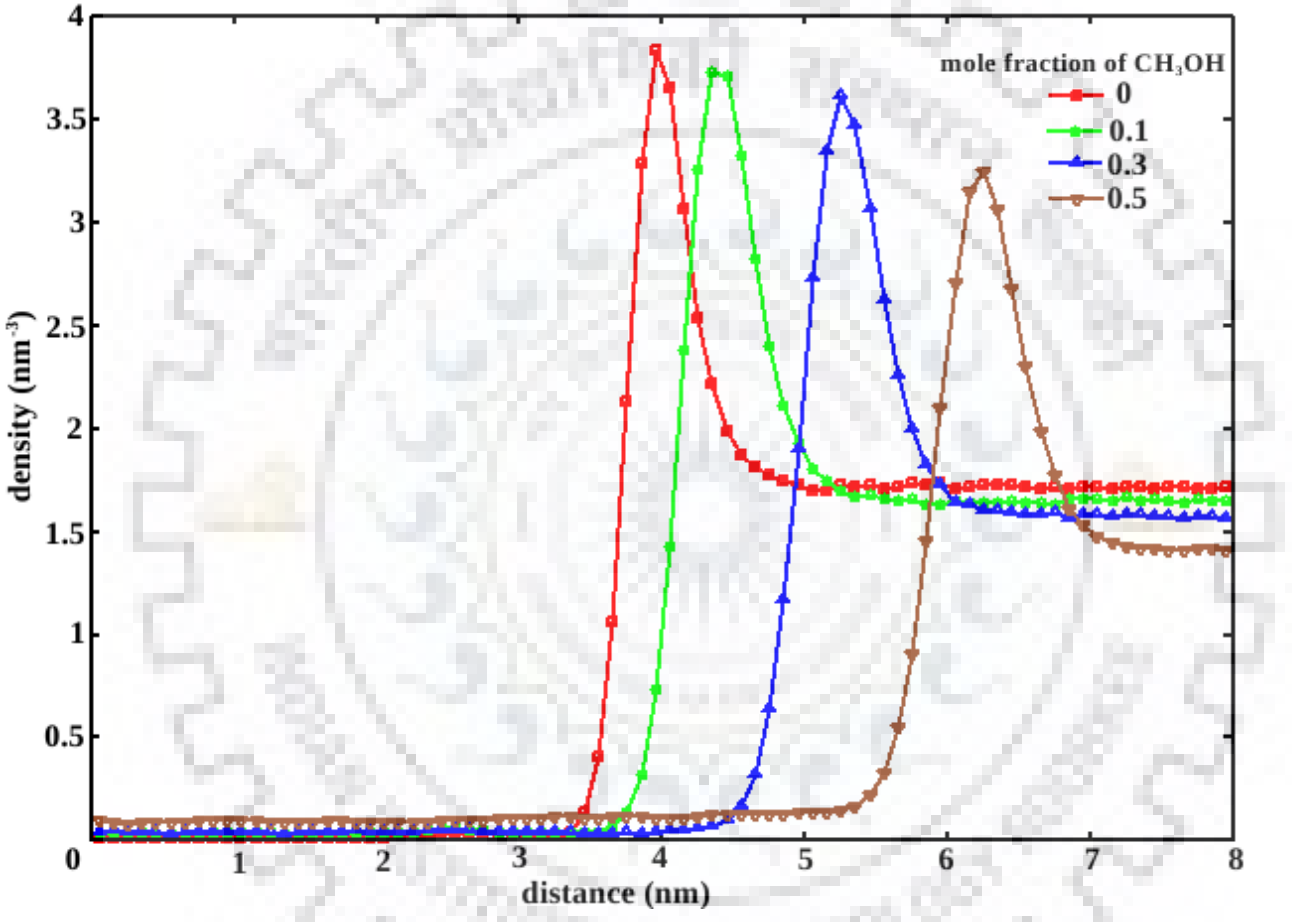

Figure 6.6. Number density profiles of methane in the direction normal to its interface with methanol-water mixture for various mole fractions of methanol. The distance is measured from the center of the liquid slab along the z-axis normal to the interface.

Table 6.4 Difference between potential energy of interaction per CH_4 in the 'local region' above humps ($<PE_{hump}>$) and wells ($<PE_{well}>$) of the surface of the methanol-water mixture for different concentrations of methanol.

mole fraction of CH_3OH	$<PE_{hump}> - <PE_{well}>$ (kJ mol^{-1})
0	1.000
0.1	1.177
0.3	1.308
0.5	1.450

by the sum of the pair interaction Lennard-Jones terms between methane and molecules of the liquid lying within a cutoff distance of 1.2 nm applied in the simulations. The difference between average potential energy of interaction per methane molecule present above the humps ($<PE_{hump}>$) and wells ($<PE_{well}>$) of the liquid surface is given in table 6.4.

The results indicate that the potential energy of interaction between methane and the molecules of the methanol-water mixture is more negative when methane is present in the 'local region' above the wells than the humps of the surface. It is also observed that the difference between potential energies for the regions above the humps and wells increases with an increase in concentration of methanol. These observations can be explained based on the larger amplitude of humps and wells at the surface of the methanol rich liquid mixture. An increase in the height of the hump means that methane molecules within the 'local region' above the hump will in general be farther from the average surface of the liquid. This leads to weaker interaction between solvent moleclues and methane above the humps resulting in the lower density of methane in the 'local region' above the hump compared to the wells (figure 6.3).

6.3.2 Effect of Methane on the Orientation of Interfacial Methanol Molecules

Earlier reported studies of the methanol-water liquid mixture showed that methanol molecules at the surface of the liquid prefer to have their methyl group pointing towards the gas phase with the $O\text{-}CH_3$ bond perpendicular to the average plane representing the liquid surface [129, 131, 140]. It was also reported that the surface of the methanol-water mixture is nearly

saturated with methanol even for low concentrations of methanol in the mixture [129-140]. We examined the orientation of methanol molecules in the first molecular layer at the interface between the methanol-water mixture and methane. Methanol molecules at the interface interact with methane molecules in the gas phase when they come near the liquid surface. To understand the effect of methane on the orientation of interfacial methanol molecules, we identified those methanol molecules at the surface which has atleast one methane molecule within the distance (0.59 nm) corresponding to the first minimum in the CH_4-CH_3OH pair distribution function. The orientation of these interfacial methanol molecules was examined by determining the probability distribution of the cosine of angle (φ) made by the O-CH_3 bond of methanol with the vector which is normal to the average planar surface of the liquid mixture and points towards the gas phase. Similarly, the probability distribution of cos(φ) was determined for interfacial methanol molecules which does not have any methane molecule near them. The result of this analysis for the methanol-water mixtures containing different mole fractions of methanol is shown in figure 6.7.

It can be observed from the figure that the probability is highest for orientations of the O-CH_3 bond corresponding to value of cos(φ) close to unity. This indicates that interfacial methanol molecules of the liquid mixture have a high probability to have its -CH_3 group oriented towards the gas phase. It is also revealed that the probability distribution of orientations of methanol molecules at the interface is affected by the presence of methane near the liquid surface. The probability for an interfacial methanol molecule to have its -CH_3 group oriented towards the gas phase is higher if the molecule has methane near it. The effect of methane on the orientation of interfacial methanol molecules of the methanol-water mixture can be attributed to the interaction between methane and hydrophobic methyl group of methanol. As a methane molecule approaches the liquid surface, it forms non-covalent interactions with the methyl group of methanol thereby enhancing its tendency to be oriented towards the gas phase.

6.4 Conclusions

Classical molecular dynamics simulations were performed to study the adsorption and dissolution of methane at the surface of the methanol-water liquid mixture. The number density profile of methane along the direction normal to its interface with the liquid mixture showed that

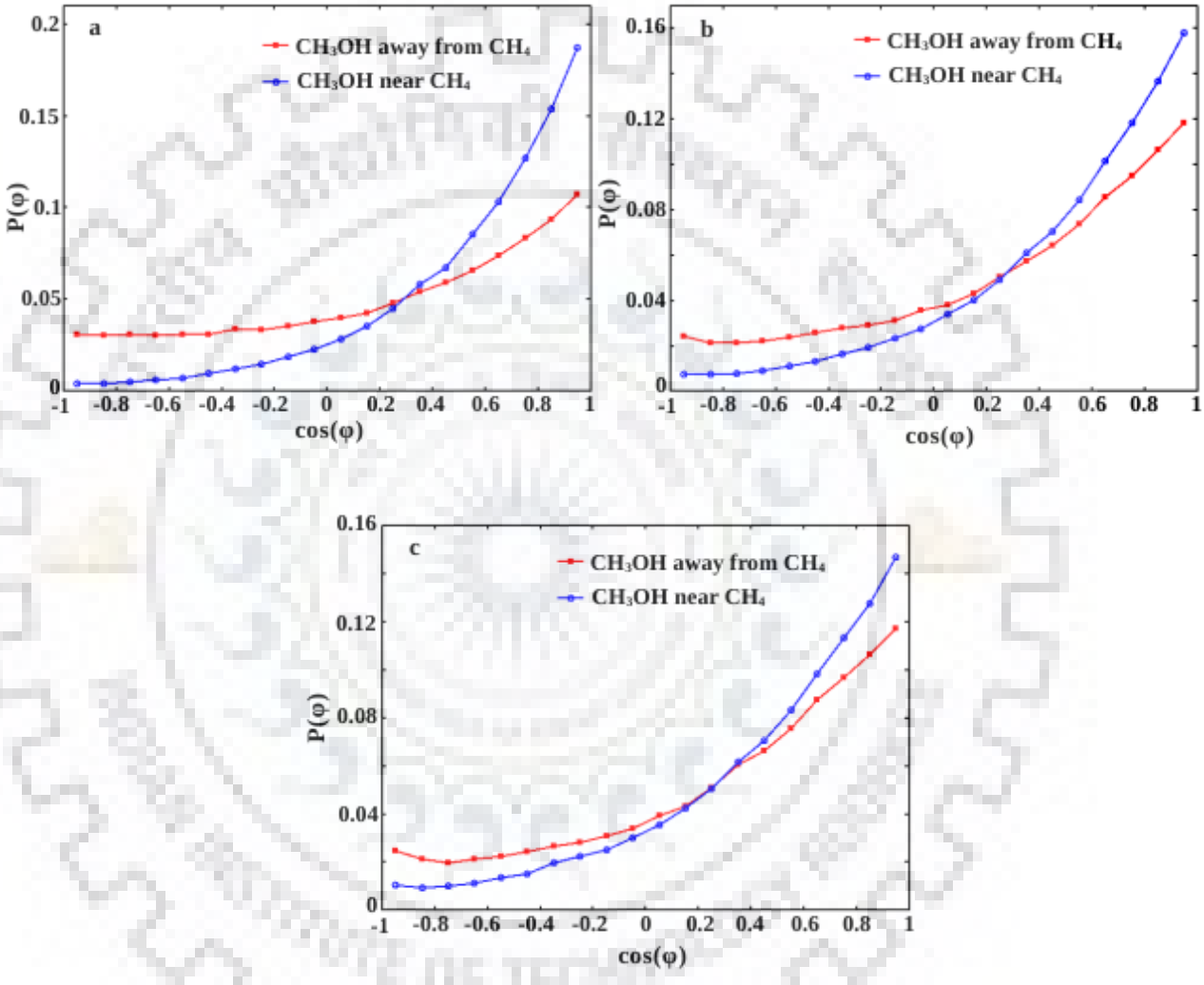

Figure 6.7 Probability distribution of the cosine of the angle (φ) between the O-CH_3 bond of the methanol and the vector normal to the XY plane representing the average surface of the liquid mixture containing (a) 400 CH_3OH and 3600 H_2O, (b) 1200 CH_3OH and 2800 H_2O and (c) 2000 CH_3OH and 2000 H_2O.

a methane molecule is more likely to enter the bulk liquid through the humps of the liquid surface which is rough at a molecular level. Analysis of the density of the liquid mixture near the surface indicated that density is lower at the region below humps compared to the wells. The lower liquid density in the surface region below the hump makes the dissolution of methane molecules easier through the humps.

Examining the effect of composition of the liquid mixture on its surface showed that an increase in concentration of methanol made the liquid surface more rough. The larger humps and wells at the surface of methanol rich mixture can assist the dissolution of methane through the humps which act as preferred channels for the entry of methane molecule into the bulk liquid. Thus, an increase in the surface roughness of methanol-water liquid mixture induced by methanol can lead to greater number of methane molecules crossing the interface between methane and the methanol rich liquid mixture within a given time.

The dependence of the distribution of methane adsorbed above the surface of methanol-water mixture on surface roughness was analyzed and it was observed that the distribution is non uniform with higher density of methane above the wells than the humps of the surface. The non-uniform distribution of adsorbed methane was found to be related to the potential energy of its interaction with the molecules of the liquid mixture. The methane molecules adsorbed above the humps are farther from the average surface of the liquid and therefore interact weakly with liquid molecules compared to those adsorbed above the wells.

The effect of methane on the orientation of interfacial methanol molecules of the methanol-water mixture was also examined. The results indicate that the presence of methane enhanced the tendency of interfacial methanol molecules to be oriented with its methyl group pointing towards the gas phase.

Chapter 7
Conclusions and Future Scope

The aim of the thesis was to apply molecular dynamics simulations to improve the understanding of two important physical systems which are of significance to energy and environment. The first class of system studied was the aqueous solution of hydrate forming gases in water at high concentration which resemble the liquid phase formed during hydrate decomposition.

The CH_4-CO_2-H_2O ternary mixture is known to be formed during extraction of methane from hydrate sediments by the replacement method. The evolution of dissolved gas from this ternary mixture was investigated. The study showed that the presence of CO_2 significantly affects the evolution of dissolved gas molecules by enhancing the formation of nanobubbles. The bubbles formed were found to be of the mixed type containing both CH_4 and CO_2 molecules in it. The role of CO_2 in enhancing the formation of nanobubbles was examined. For this, the distribution of gas molecules in the bubble was analyzed which showed that CO_2 molecules accumulate at the interface between the bubble and the surrounding liquid. The CO_2 molecules present at the interface formed energetically favorable interactions through direct contact with the CH_4 molecules. In addition to this, CO_2 was also observed to reduce surface tension at the interface thereby enhancing the stability of the nanobubble formed. These factors lead to enhanced bubble nucleation in CH_4-CO_2-H_2O system at high concetrations of CO_2. Finally, the state of CH_4 inside the nanobubble was examined which showed that at the conditions applied, methane exist in the supercritical state inside the bubble. Further analysis of the properties of supercritical methane, showed that it forms a repulsive mixture with CO_2 which may have a role in limiting the entry of CO_2 molecules into the interior of the bubble.

An imoportant technique applied in the extraction of natural gas from hydrate sediments involves the injection of thermodynamic hydrate inhibitors into the sediment. The inhibitor induces the dissociation of the hydrate structure leading to the formation of a hydrate melt. To understand the effect of hydrate inhibitors on the evolution of natural gas from the hydrate melt, simulations were performed on the CH_4-H_2O and CH_4-CO_2-H_2O systems containing themodynamic hydrate inhibitors. The role of two commonly used hydrate inhibitors, NaCl and

CH_3OH were considered in the study. An increase in the concentration of these inhibitors were found to promote the formation of nanobubbles in the CH_4-H_2O system. The presence of NaCl was found to assist nanobubble formation by enhancing hydrophobic interactions between the dissolved gas molecules leading to their aggregation. Whereas, the role of CH_3OH as a promoter for nanobubble nucleation is attributed to its amphiphilic nature. On examining the structure of the nanobubble formed in presence of CH_3OH, it was observed that CH_3OH molecules accumulate at the surface of the bubble with its methyl group oriented towards the bubble. The precence of CH_3OH at the bubble-liquid interface was found to reduce the excess pressure inside the bubble as well as the value of surface tension at the interface. This makes the nucleation of nanobubbles energetically favorable in solutions where CH_3OH is present at high concentrations. The study of the evolution of dissolved gas in presence of NaCl and CH_3OH was extended to the case of systems containing both CH_4 and CO_2 dissolved in it. It is observed that for a given concentration of the inhibitor, the presence of CO_2 lead to significant reduction in the induction time preceding bubble nucleation. The role of CO_2 in enhancing bubble nucleation was explained in terms of the distribution of molecules in the bubble. It was observed that CO_2 molecules accumulate at the surface of bubble thereby enhancing its stability. In addition to the effect of NaCl and CH_3OH on the formation and stability of nanobubbles, the role of these inhibitors in influencing the properties of the bubbles formed was examined. It was observed that nanobubbles interact with the surrounding liquid through a continuous exchange of gas molecules between the bubble and the liquid. Both type of inhibitors considered in the study were found to reduce this gas exchange thereby making the bubble less dynamic in nature. The effect of inhibitor molecules on the exchange of gas molecules between the bubble and the surrounding liquid was explained based on the excess pressure inside the bubble and the solubility of gas molecules in the surrounding liquid phase.

The second type of system studied in the thesis is the interface between methane and water which is of significance to gas hydrates and atmospheric chemistry. Classical molecular dynamics simulations were carried out to study the structure of the methane-water interface. A quantitative analysis of the molecular level roughness of the surface of water was performed. The results indicated that an increase in the pressure of methane lead to an increase in the roughness of the water surface in terms of the height and depth of the humps and wells on the surface. The effect of pressure and the strength of water-gas interaction on the surface adsorption of gas was

studied. It was observed that an increase in pressure and stronger gas-water interaction lead to enhanced adsorption of the gas on water surface. The effect of molecular level roughness of the surface on the adsorption of methane was examined. It is revealed that surface roughness influences the distribution of methane adsorbed on the surface. The methane molecules which are in direct contact with the water surface were found to be preferentially adsorbed on the humps of the surface. In contrast, the density of methane adsorbed above the surface molecular layer of methane was found to be higher above the wells than above the humps. The results indicated a clear preference for methane to come in contact with the water surface at the humps. The non uniform distribution of methane over the water surface is explained in terms of the repuslive and attractive components of the methane-water interaction. The attractive component which arises from non-covalent water-gas interaction is dominant in the case of methane molecules above the surface molecular layer of methane. For the methane molecules in direct contact with water, methane-water interaction is dominated by the repulsive component arising from excluded volume effects. The density of water at the humps on the surface is found to be lower than that at the wells which reduces the excluded volume effect at the hump. This leads to a greater fraction of methane molecules in direct contact with water surface to be adsorbed on the humps. The interaction between water and methane above the surface molecular layer of methane is weaker for the region above the humps than that above the wells. This explains the lower density of methane in the region slightly above the humps on the surface.

Several thermodynamic and chemical factors are known to influence the solubility of methane in water. One of the most important chemical species that affects the solubility of methane is methanol. Methanol is the simplest amphiphilic molecule and is also known to act as a cosolvent for methane in water. The effect of methanol on the dissolution of methane at its interface with the methanol-water liquid mixture was examined through molecular dynamics simulations. The average number density profile of methane along the direction normal to the interface was determined which showed that methane molecules prefer to enter the bulk liquid through the humps on the liquid surface which is rough at a molecular level. The role of humps as preferred channels for methane dissolution is explained based on the density of the solvent at the surface region. Solvent density is found to be lower in the region below the hump thereby facilitating the entry of methane into the bulk liquid through the hump. The effect of methanol on the structure of the liquid surface was examined and it is shown that the surface becomes more

rough with an increase in the concentration of methanol. The humps on the surface of methanol rich liquid mixture are larger in amplitude and can facilitate the dissolution of methane by acting as channels for the entry of methane into the liquid. This can lead to a larger number of CH_4 molecules entering across the interface within a given time into the bulk liquid region of the methanol rich mixture. Methanol molecules at the surface of the methanol-water liquid are known to have a tendency to have their methyl group oriented towards the gas phase. The effect of methane on the orientation of methanol moleclues at the surface of the methanol-water liquid mixture was examined. It is observed that the presence of methane near a methanol molecule increases the tendency of surface methanol molecules to orient their methyl group towards the vapor phase.

The studies about the evolution of dissolved gas from the liquid phase formed during hydrate dissociation showed that nanobubbles are formed in the liquid. The formation of nanobubbles is more rapid in the CH_4-CO_2-H_2O mixture which is formed during the replacement of CH_4 in its hydrate by CO_2. The formation of nanobubbles during the replacement process can have significant role in the kinetics of replacement. The nanobubbles capture CO_2 molecules from the liquid thereby reducing their availability for hydrate formation. Further studies are necessary to understand the role of nanobubbles in the replacement mechanism. The study must include long scale simulations of the replacement process and analysis should take into account the properties of the liquid phase formed from hydrate decomposition during the replacement process.

Simulation studies of the water-methane interface provided insight into the effect of surface properties on the adsorption of methane. The effect of aqueous methanol on the properties of the liquid surface was also studied. The study considered the interaction of a single gas species with the surface. The study can be extended to consider the interaction of a mixture of gases with the liquid surface. Understanding the interaction of different gas species with the liquid surface can assist the development of methods for gas separation.

Bibliography

1) Z. R. Chong, S. H. B. Yang, P. Babu, P. Linga, X. S. Li. Review of Natural Gas Hydrates as an Energy Resource: Prospects and Challenges. *Appl. Energy*, 162, 1633-1652, 2016.

2) I. E. A. World Energy outlook. Paris, France. International Energy Agency; 2013.

3) E. D. Sloan. Fundamental Principles and Applications of Natural Gas Hydrates. *Nature*, 426, 353-359, 2003.

4) C. A. Koh, E. D. Sloan, A. K. Sum, D. T. Wu. Fundamentals and Applications of Gas Hydrates. *Annu. Rev. Chem. Biomol. Eng.*, 2, 237-257, 2011.

5) H. Davy. The Bakerian Lecture. On Some of the Combinations of Oxymuriatic Gas and Oxygene, and on the Chemical Relations of these Principles to Inflammable Bodies. *Phil. Trans. R. Soc. Lond.*, 101, 1-35, 1811.

6) E. G. Hammerschmidt. Formation of Gas Hydrates in Natural Gas Transmission Lines. *Ind. Eng. Chem.*, 26, 851-855, 1934.

7) J. S. Gudmundsson, V. Andersson, O. I. Levik, M. Mork. Hydrate Technology for Capturing Stranded Gas. *Ann. N. Y. Acad. Sci.*, 912, 403-410, 2000.

8) L. A. Stern, S. Circone, S. H. Kirby, W. B. Durham. Anomalous Preservation of Pure Methane Hydrate at 1 atm. *J. Phys. Chem. B.*, 105, 1756-1762, 2001.

9) W. L. Mao, H. K. Mao, A. F. Goncharov, V. V. Struzhkin, Q. Guo, J. Hu, J. Shu, R. J. Hemley, M. Somayazulu, Y. Zhao. Hydrogen Clusters in Clathrate Hydrate. *Science*, 297, 2247-2249, 2002.

10) Y. A. Dyadin, E. G. Larionov, A. Y. Manakov, F. V. Zhurko, E. Y. Aladko, T. V. Mikina, V. Y. Komarov. Clathrate Hydrates of Hydrogen and Neon. *Mendeleev Commun.*, 9, 209-210, 1999.

11) A. Chapoy, R. Anderson, B. Tohidi. Low-Pressure Molecular Hydrogen Storage in Semi-clathrate Hydrates of Quaternary Ammonium Compounds. *J. Am. Chem. Soc.*, 129, 746-747, 2007.

12) P. S. R. Prasad, T. Sugahara, A. K. Sum, E. D. Sloan, C. A. Koh. Hydrogen Storage in Double Clathrates with *tert*-Butylamine. *J. Phys. Chem. A*, 113, 6540-6543, 2009.

13) T. Sugahara, J. C. Haag, P. S. R. Prasad, A. A. Warntjes, E. D. Sloan, A. K. Sum, C. A. Koh. Increasing Hydrogen Storage Capacity Using Tetrahydrofuran. *J. Am. Chem. Soc.*, 131, 14616-14617, 2009.

14) G. R. Dickens, M. M. Castillo, J. C. Walker. A Blast of Gas in the Latest Paleocene: Simulating First-order Effects of Massive Dissociation of Oceanic Methane Hydrate. *Geology*, 25, 259-262, 1997.

15) G. R. Dickens, J. R. O'Neil, D. K. Rea, R. M. Owen. Dissociation of Oceanic Methane Hydrate as a Cause of the Carbon Isotope Excursion at the End of the Paleocene. *Paleoceanography*, 10, 965-971, 1995.

16) M. Ota, T. Saito, T. Aida, M. Watanabe, Y. Sato, R. L. Smith, H. Inomata. Macro and Microscopic CH_4-CO_2 Replacement in CH_4 Hydrate Under Pressurized CO_2. *AIChE J.*, 53, 2715-2721, 2007.

17) X. Zhou, S. Fan, D. Liang, J. Du. Replacement of Methane from Quartz Sand-Bearing Hydrate with Carbon Dioxide-in-Water Emulsion. *Energy & Fuels*, 22, 1759-1764, 2008.

18) J. W. Jung, D. N. Espinoza, J. C. Santamarina. Properties and Phenomena Relevant to CH_4-CO_2 Replacement in Hydrate-Bearing Sediments. *J. Geophys. Res.*, 115, B10102, 2010.

19) E. D. Sloan, C. A. Koh. Clathrate Hydrates of Natural Gases. CRC Press: Boca Raton, 2008.

20) P. Englezos, Clathate Hydrates. *Ind. Eng. Chem. Res.*, 32, 1251-1274, 1993.

21) P. Kumar, N. Sathyamurthy. Theoretical Studies of Host-Guest Interaction in Gas Hydrates. *J. Phys. Chem. A*, 115, 14276-14281, 2011.

22) P. Kumar, B. K. Mishra, N. Sathyamurthy. Density Functional Theoretic Studies of Host-Guest Interaction in Gas Hydrates. *Comput. Theor. Chem.*, 1029, 26-32, 2014.

23) P. K. Chattaraj, S. Bandaru, S. Mondal. Hydrogen Storage in Clathrate Hydrates. *J. Phys. Chem. A*, 115, 187-193, 2011.

24) H. K. Srivastava, G. N. Sastry. Viability of Clathrate Hydrates as CO_2 Capturing Agents: A Theoretical Study. *J. Phys. Chem. A*, 115, 7633-7637, 2011.

25) K. R. Ramya, A. Venkatnathan. Stability and Reactivity of Methane Clathrate Hydrates: Insights from Density Functional Theory. *J. Phys. Chem. A*, 116, 7742-7745, 2012.

26) S. P. Kaur, C. N. Ramachandran. Host-Guest and Guest-Guest Interactions in Noble Gas Hydrates. *Mol. Phys.*, 116, 54-63, 2018.

27) N. Sun, Z. Li, N. Qiu, X. Yu, X. Zhang, Y. Li, L. Yang, K.Luo, Q. Huang, S. Du. Ab Initio Studies on the Clathrate Hydrates of Some Nitrogen- and Sulfur- Containing Gases. *J. Phys. Chem. A*, 121, 2620-2626, 2017.

28) A. Khan. *Ab initio* Studies of $(H_2O)_{28}$ Hexakaidecahedral Cluster with Ne, N_2, CH_4, and C_2H_6 Guest Molecules in the Cavity. *J. Chem. Phys.*, 116, 6628, 2002.

29) A. Khan. Theoretical Studies of CH_4 $(H_2O)_{20}$, $(H_2O)_{21}$, $(H_2O)_{20}$, and Fused Dodecahedral and

Tetrakaidecahedral Structures: How do Natural Gas Hydrates Form?. *J. Chem. Phys.*, 110, 11884, 1999.

30) S. Patchkovskii, J. S. Tse. Thermodynamic Stability of Hydrogen Clathrates. *Proc. Natl. Acad. Sci. U. S. A*, 100, 14645-14650, 2003.

31) A. Khan. Stabilization of Hydrate Stucture H by N_2 and CH_4 Molecules in $4^3 5^6 6^3$ and 5^{12} Cavities, and Fused Structure Formation with $5^{12}6^8$ Cage: A Theoretical Study. *J. Phys. Chem. A*, 105, 7429-7434, 2001.

32) S. P. Kaur, C. N. Ramachandran. Effect of Multiple and Adjacent Cage Occupancies on Host-Guest Interaction and NMR Chemical Shifts in Gas Hydrates. *Comput. Theor. Chem.*, 1092, 57-67, 2016.

33) Z. Huo, K. Hester, E. D. Sloan, K. T. Miller. Methane Hydrate Nonstoichiometry and Phase Diagram. *AIChE J.*, 49, 1300-1306, 2003.

34) H. Lu, J. Wang, C. Liu, C. I. Ratcliffe, U. Becker, R. Kumar, J. Ripmeester. Multiple H_2 Occupancy of Cages of Clathrate Hydrate under Mild Conditions. *J. Am. Chem. Soc.*, 134, 9160-9162, 2012.

35) D. Y. Koh, H. Kang, J. Jeon, Y. H. Ahn, Y. Park, H. Kim, H. Lee. Tuning Cage Dimension in Clathrate Hydrates for Hydrogen Multiple Occupancy. *J. Phys. Chem. C*, 118, 3324-3330, 2014.

36) L. G. Tang, R. Xiao, C. Huang, Z. P. Feng, S. S. Fan. Experimental Investigation of Production Behavior of Gas Hydrate under Thermal Stimulation in Unconsolidated Sediment. *Energy Fuels*, 19, 2402-2407, 2005.

37) W. X. Pang, W. Y. Xu, C. Y. Sun, C. L. Zhang, G. J. Chen. Methane Hydrate Dissociation Experiment in a Middle-sized Quiescent Reactor using Thermal Method. *Fuel*, 88, 497-503, 2009.

38) X. Yang, C. Y. Sun, Q. Yuan, P. C. Ma, G. J. Chen. Experimental Study on Gas Production from Methane Hydrate-Bearing Sand by Hot-Water Cyclic Injection. *Energy Fuels*, 24, 5912-5920, 2010.

39) Y. Wang, J. C. Feng, X. S. Li, Y. Zhang. Experimental Investigation of Optimization of Well Spacing for Gas Recovery from Methane Hydrate Reservoir in Sandy Sediment by Heat Stimulation. *Appl. Energ.*, 207, 562-572, 2017.

40) X. S. Li, L. H. Wan, G. Li, Q. P. Li, Z. Y. Chen, K. F. Yan. Experimental Investigation into the Production Behavior of Methane Hydrate in Porous Sediment with Hot Brine Stimulation. *Ind. Eng. Chem. Res.*, 47, 9696-9702, 2008.

41) M. R. Islam. A New Recovery Technique for Gas Production from Alaskan Gas Hydrates. *J. Pet. Sci. Eng.*, 11, 267-281, 1994.

42) D. L. Li, D. Q. Liang, S. S. Fan, X. S. Li, L. G. Tang, N. S. Huang. In situ Hydrate Dissociation using Microwave Heating: Preliminary Study. *Energy Convers. Manage.*, 49, 2207-2213, 2008.

43) M. J. Castaldi, Y. Zhou, T. M. Yegulalp. Down-hole Combustion Method for Gas Production from Methane Hydrates. *J. Pet. Sci. Eng.*, 56, 176-185, 2007.

44) C. Cranganu. *In-situ* Thermal Stimulation of Gas Hydrates. *J. Pet. Sci. Eng.*, 65, 76-80, 2009.

45) G. C. Fitzgerald, M. J. Castaldi, Y. Zhou. Large Scale Reactor Details and Results for the Formation and Decomposition of Methane Hydrates via Thermal Stimulation Dissociation. *J. Pet. Sci. Eng.*, 94-95, 19-27, 2012.

46) H. O. Kono, S. Narasimhan, F. Song, D. H. Smith. Synthesis of Methane Gas Hydrate in Porous Sediments and its Dissociation by Depressurizing. *Powder Technol.*, 122, 239-246, 2002.

47) L. G. Tang, X. S. Li, Z. P. Feng, G. Li, S. S. Fan. Control Mechanisms for Gas Hydrate Production by Depressurization in Different Scale Hydrate Reservoirs. *Energy Fuels*, 21, 227-233, 2007.

48) C. Haligva, P. Linga, J. A. Ripmeester, P. Englezos. Recovery of Methane from a Variable-Volume Bed of Silica Sand/Hydrate by Depressurization. *Energy Fuels*, 24, 2947-2955, 2010.

49) X. S. Li, Y. Zhang, G. Li, Z. Y. Chen, H. J. Wu. Experimental Investigation into the Production Behavior of Methane Hydrate in Porous Sediment by Depressurization with a Novel Three-Dimensional Cubic Hydrate Simulator. *Energy Fuels*, 25, 4497-4505, 2011.

50) K. F. Yan, X. S. Li, Z. Y. Chen, B. Li, C. G. Xu. Molecular Dynamics Simulation of Methane Hydrate Dissociation by Depressurisation. *Mol. Simul.*, 39, 251-260, 2013.

51) B. Li, X. S. Li, G. Li, J. C. Feng, Y. Wang. Depressurization Induced Gas Production from Hydrate Deposits with Low Gas Saturation in a Pilot-Scale Hydrate Simulator. *Appl. Energy*, 129, 274-286, 2014.

52) F. Dong, X. Zang, D. Li, S. Fan, D. Liang. Experimental Investigation on Propane Hydrate Dissociation by High Concentration Methanol and Ethylene Glycol Solution Injection. *Energy Fuels*, 23, 1563-1567, 2009.

53) Y. Qi, W. Wu, Y. Liu, Y. Xie, X. Chen. The Influence of NaCl Ions on Hydrate Structure and Thermodynamic Equilibrium Conditions of Gas Hydrates. *Fluid Phase Equilib.*, 325, 6-10, 2012.

54) J. Lee. Experimental Study on the Dissociation Behavior and Productivity of Gas Hydrate by Brine Injection Scheme in Porous Rock. *Energy Fuels*, 24, 456-463, 2010.

55) S. Fan, Y. Zhang, G. Tian, D. Liang, D. Li. Natural Gas Hydrate Dissociation by Presence of

Ethylene Glycol. *Energy Fuels*, 20, 324-326, 2006.

56) W. Sung, H. Kang. Experimental Investigation of Production Behaviors of Methane Hydrate Saturated in Porous Rock. *Energy Source*, 25, 845-856, 2003.

57) Y. Seo, S. Lee, J. Lee. Experimental Verification of Methane Replacement in Gas Hydrates by Carbon Dioxide. *Chem. Eng. Trans.*, 32, 163-168, 2013.

58) J. Zhao, K. Xu, Y. Song, W. Liu, W. Lam, Y. Liu, K. Xue, Y. Zhu, X. Yu, Q. Li. A Review on Research on Replacement of CH_4 in Natural Gas Hydrates by Use of CO_2. *Energies*, 5, 399-419, 2012.

59) M. Ota, K. Morohashi, Y. Abe, M. Watanabe, R. L. J. Smith, H. Inomata. Replacement of CH_4 in the Hydrate by Use of Liquid CO_2. *Energy Convers. Manage.*, 46, 1680-1691, 2005.

60) H. Lee, Y. Seo, Y. T. Seo, I. L. Moudrakovski, J. A. Ripmeester. Recovering Methane from Solid Methane Hydrate with Carbon Dioxide. *Angew. Chem. Int. Ed.*, 42, 5048-5051, 2003.

61) S. Lee, Y. Lee, J. Lee, H. Lee, Y. Seo. Experimental Verification of Methane-Carbon Dioxide Replacement in Natural Gas Hydrates Using a Differential Scanning Calorimeter. *Environ. Sci. Technol.*, 47, 13184-13190, 2013.

62) K. Ohgaki, K. Takano, H. Sangawa, T. Matsubara, S. Nakano. Methane Exploitation by Carbon Dioxide from Gas Hydrates-Phase Equilibria for CO_2-CH_4 Mixed Hydrate System. *J. Chem. Eng. Jpn.*, 29, 478-483, 1996.

63) N. Goel. In situ Methane Hydrate Dissociation with Carbon Dioxide Sequestration: Current Knowledge and Issues. *J. Pet. Sci. Eng.*, 51, 169-184, 2006.

64) E. M. Yezdimer, P. T. Cummings, A. A. Chialvo. Determination of the Gibbs Free Energy of Gas Replacement in SI Clathrate Hydrates by Molecular Simulation. *J. Phys. Chem. A*, 106,

7982-7987, 2002.

65) P. Dornan, S. Alavi, T. K. Woo. Free Energies of Carbon Dioxide Sequestration and Methane Recovery in Clathrate Hydrates. *J. Chem. Phys.*, 127, 124510, 2007.

66) S. Alavi, T. K. Woo. How much Carbon Dioxide can be Stored in the Structure H Clathrate Hydrates?: A Molecular Dynamics Study. *J. Chem. Phys.*, 126, 044703, 2007.

67) O. Ors, C. Sinayuc. An Experimental Study on the CO_2-CH_4 Swap Process Between Gaseous CO_2 and CH_4 Hydrate in Porous Media. *J. Pet. Sci. Eng.*, 119, 156-162, 2014.

68) J. H. Yoon, T. Kawamura, Y. Yamamoto, T. Komai. Transformation of Methane Hydrate to Carbon Dioxide Hydrate: In Situ Raman Spectroscopic Observations. *J. Phys. Chem. A*, 108, 5057-5059, 2004.

69) D. Bai, X. Zhang, G. Chen, W. Wang. Replacement Mechanism of Methane Hydrate with Carbon Dioxide from Microsecond Molecular Dynamics Simulations. *Energy Environ. Sci.*, 5, 7033-7041, 2012.

70) C. Y. Geng, H. Wen, H. Zhou. Molecular Simulation of the Potential of Methane Reoccupation during the Replacement of Methane Hydrate by CO_2. *J. Phys. Chem. A*, 113, 5463-5469, 2009.

71) J. Zhao, C. Cheng, Y. Song, W. Liu, Y. Liu, K. Xue, Z. Zhu, Z. Yang, D. Wang, M. Yang. Heat Transfer Analysis of Methane Hydrate Sediment Dissociation in a Closed Reactor by a Thermal Method. *Energies*, 5, 1292-1308, 2012.

72) J. Zhao, D. Liu, M. Yang, Y. Song. Analysis of Heat Transfer Effects on Gas Production from Methane Hydrate by Depressurization. *Int. J. Heat Mass Transfer*, 77, 529-541, 2014.

73) J. Zhao, J. Wang, W. Liu, Y. Song. Analysis of Heat Transfer Effects on Gas Production from

Methane Hydrate by Thermal Stimulation. *Int. J. Heat Mass Transfer*, 87, 145-150, 2015.

74) H. Oyama, Y. Konno, Y. Masuda, H. Narita. Dependence of Depressurization-Induced Dissociation of Methane Hydrate Bearing Laboratory Cores on Heat Transfer. *Energy Fuels*, 23, 4995-5002, 2009.

75) S. Circone, S. H. Kirby, L. A. Stern. Thermal Regulation of Methane Hydrate Dissociation: Implications for Gas Production Models. *Energy Fuels*, 19, 2357-2363, 2005.

76) J. Zhao, Z. Zhu, Y. Song, W. Liu, Y. Zhang, D. Wang. Analyzing the Process of Gas Production for Natural Gas Hydrate using Depressurization. *Appl. Energy.*, 142, 125-134, 2015.

77) J. Lee, S. Park, W. Sung. An Experimental Study on the Productivity of Dissociated Gas from Gas Hydrate by Depressurization Scheme. *Energy Convers. Manage.*, 51, 2510-2515, 2010.

78) X. Yang, C. Y. Sun, K. H. Su, Q. Yuan, Q. P. Li, G. J. Chen. A Three-Dimensional Study on the Formation and Dissociation of Methane Hydrate in Porous Sediment by Depressurization. *Energy Convers. Manage.*, 56, 1-7, 2012.

79) H. C. Kim, P. R. Bishnoi, R. A. Heidemann, S. S. H. Rizvi. Kinetics of Methane Hydrate Decomposition. *Chem. Eng. Sci.*, 42, 1645-1653, 1987.

80) S. A. Bagherzadeh, S. Alavi, J. A. Ripmeester, P. Englezos. Evolution of Methane During Gas Hydrate Dissociation. *Fluid Phase Equilib.*, 358, 114-120, 2013.

81) S. Alavi, J. A. Ripmeester. Nonequilibrium Adiabatic Molecular Dynamics Simulations of Methane Clathrate Hydrate Decomposition. *J. Chem. Phys.*, 132, 144703, 2010.

82) S. A. Bagherzadeh, P. Englezos, S. Alavi, J. A. Ripmeester. Molecular Simulation of Non-equilibrium Methane Hydrate Decomposition Process. *J. Chem. Thermodyn.*, 44, 13-19, 2012.

83) S. A. Bagherzadeh, S. Alavi, J. Ripmeester, P. Englezos. Formation of Methane Nano-bubbles during Hydrate Decomposition and their Effect on Hydrate Growth. *J. Chem. Phys.*, 142, 214701, 2015.

84) V. S. Baghel, R. Kumar, S. Roy. Heat Transfer Calculations for Decomposition of Structure I Methane Hydrates by Molecular Dynamics Simulation. *J. Phys. Chem. C*, 117, 12172-12182, 2013.

85) N. J. English, G. M. Phelan. Molecular Dynamics Study of Thermal-driven Methane Hydrate Dissociation. *J. Chem. Phys.*, 131, 074704, 2009.

86) E. M. Myshakin, H. Jiang, R. P. Warzinski, K. D. Jordan. Molecular Dynamics Simulations of Methane Hydrate Decomposition. *J. Phys. Chem. A*, 113, 1913-1921, 2009.

87) S. Sarupria, P. G. Debenedetti. Molecular Dynamics Study of Carbon Dioxide Hydrate Dissociation. *J. Phys. Chem. A*, 115, 6102-6111, 2011.

88) Y. Liu, J. Zhao, J. Xu. Dissociation Mechanism of Carbon Dioxide Hydrate by Molecular Dynamic Simulation and A*b initio* Calculation. *Comput. Theor. Chem.*, 991, 165-173, 2012.

89) S. Das, V. S. Baghel, S. Roy, R. Kumar. A Molecular Dynamics Study of Model SI Clathrate Hydrates: The Effect of Guest Size and Guest-Water Interaction on Decomposition Kinetics. *Phys. Chem. Chem. Phys.*, 17, 9509-9518, 2015.

90) T. Park, D. Kyung, W. Lee. Effect of Organic Matter on CO_2 Hydrate Phase Equilibrium in Phyllosilicate Suspensions. *Environ. Sci. Technol.*, 48, 6597-6603, 2014.

91) D. Kyung, H. K. Lim, H. Kim, W. Lee. CO_2 Hydrate Nucleation Kinetics Enhanced by an Organo-Mineral Complex Formed at the Montmorillonite-Water Interface. *Environ. Sci. Technol.*, 49, 1197-1205, 2015.

92) Y. P. Handa, D. Stupin. Thermodynamic Properties and Dissociation Characteristics of Methane and Propane Hydrates in 70-Å-Radius Silica Gel Pores. *J. Phys. Chem.*, 96, 8599-8603, 1992.

93) J. W. Wilder, K. Seshadri, D. H. Smith. Modeling Hydrate Formation in Media with Broad Pore Size Distributions. *Langmuir*, 17, 6729-6735, 2001.

94) S. A. Bagherzadeh, P. Englezos, S. Alavi, J. A. Ripmeester. Molecular Modeling of the Dissociation of Methane Hydrate in Contact with a Silica Surface. *J. Phys. Chem. B*, 116, 3188-3197, 2012.

95) K. S. Smirnov. A Modeling Study of Methane Hydrate Decomposition in Contact with the External Surface of Zeolites. *Phys. Chem. Chem. Phys.*, 19, 23095-23105, 2017.

96) H. Ji, D. Chen, C. Zhao, G. Wu. Molecular Dynamics Simulation of Methane Hydrate Formation and Dissociation in the Clay Pores With Fatty Acids. *J. Phys. Chem. C*, 122, 1318-1325, 2018.

97) T. Yagasaki, M. Matsumoto, Y. Andoh, S. Okazaki, H. Tanaka. Effect of Bubble Formation on the Dissociation of Methane Hydrate in Water: A Molecular Dynamics Study. *J. Phys. Chem. B*, 118, 1900-1906, 2014.

98) T. Yagasaki, M. Matsumoto, Y. Andoh, S. Okazaki, H. Tanaka. Dissociation of Methane Hydrate in Aqueous NaCl Solutions. *J. Phys. Chem. B*, 118, 11797-11804, 2014.

99) M. Uddin, D. Coombe. Kinetics of CH_4 and CO_2 Hydrate Dissociation and Gas Bubble Evolution via MD Simulation. *J. Phys. Chem. A*, 118, 1971-1988, 2014.

100) T. Uchida, K. Yamazaki, K. Gohara. Generation of Micro- and Nano-bubbles in Water by Dissociation of Gas Hydrates. *Korean J. Chem. Eng.*, 33, 1749-1755, 2016.

101) T. Uchida, K. Yamazaki, K. Gohara. Gas Nanobubbles as Nucleation Acceleration in the Gas-Hydrate Memory Effect. *J. Phys. Chem. C*, 120, 26620-26629, 2016.

102) L. F. Phillips. Processes at the Gas-Liquid Interface. *Int. Rev. Phys. Chem.*, 30, 301-333, 2011.

103) M. Sayou, R. Ishizuka, N. Matubayasi. Energetic Analysis of Adsorption and Absorption of Small Molecule to Nanodroplet of Water. *J. Phys. Chem. B*, 121, 5995-6001, 2017.

104) M. Khurana, Z. Yin, P. Linga. A Review of Clathrate Hydrate Nucleation. *ACS Sustainable Chem. Eng.*, 5, 11176-11203, 2017.

105) H. Ueno, H. Akiba, S. Akatsu, R. Ohmura. Crystal Growth of Clathrate Hydrates Formed with Methane + Carbon Dioxide Mixed Gas at the Gas/Liquid Interface and in Liquid Water. *New J. Chem.*, 39, 8254-8262, 2015.

106) J. D. Lee, M. Song, R. Susilo, P. Englezos. Dynamics of Methane-Propane Clathrate Hydrate Crystal Growth from Liquid Water with or without the Presence of n-Heptane. *Cryst. Growth Des.*, 6, 1428-1439, 2006.

107) T. Koga, J. Wong, M. K. Endoh, D. Mahajan, C. Gutt, S. K. Satija. Hydrate Formation at the Methane/Water Interface on the Molecular Scale. *Langmuir*, 26, 4627-4630, 2010.

108) T. Kodama, R. Ohmura. Crystal Growth of Clathrate Hydrate in Liquid Water in Contact with Methane + Ethane + Propane Gas Mixture. *J. Chem. Technol. Biotechnol.*, 89, 1982-1986, 2014.

109) J. P. Long, E. D. Sloan. Hydrates in the Ocean and Evidence for the Location of Hydrate Formation. *Int. J. Thermophys.*, 17, 1-13, 1996.

110) S. Watanabe, K. Saito, R. Ohmura. Crystal Growth of Clathrate Hydrate in Liquid Water Saturated with a Simulated Natural Gas. *Cryst. Growth Des.*, 11, 3235-3242, 2011.

111) S. L. Li, C. Y. Sun, B. Liu, X. J. Feng, F. G. Li, L. T. Chen, G. J. Chen. Initial Thickness Measurements and Insights into Crystal Growth of Methane Hydrate Film. *AIChE J.*, 59, 2145-2154, 2013.

112) S. Li, C. Sun, B. Liu, Z. Li, G. Chen, A. K. Sum. New Observations and Insights into the Morphology and Growth Kinetics of Hydrate Films. *Sci. Rep.*, 4, 1, 2014.

113) C. Moon, P. C. Taylor, P. M. Rodger. Molecular Dynamics Study of Gas Hydrate Formation. *J. Am. Chem. Soc.*, 125, 4706-4707, 2003.

114) R. W. Hawtin, D. Quigley, P. M. Rodger. Gas Hydrate Nucleation and Cage Formation at a Water/Methane Interface. *Phys. Chem. Chem. Phys.*, 10, 4853-4864, 2008.

115) S. K. Reed, R. E. Westacott. The Interface Between Water and a Hydrophobic Gas. *Phys. Chem. Chem. Phys.*, 10, 4614-4622, 2008.

116) J. Zhang, R. W. Hawtin, Y. Yang, E. Nakagava, M. Rivero, S. K. Choi, P. M. Rodger. Molecular Dynamics Study of Methane Hydrate Formation at a Water/Methane Interface. *J. Phys. Chem. B*, 112, 10608-10618, 2008.

117) E. A. Mastny, C. A. Miller, J. J. de Pablo. The Effect of the Water/Methane Interface on Methane Hydrate Cages: The Potential of Mean Force and Cage Lifetimes. *J. Chem. Phys.*, 129, 034701, 2008.

118) D. Bai, B. Liu, G. Chen, X. Zhang, W. Wang. Role of Guest Molecules on the Hydrate Growth at Vapor-Liquid Interfaces. *AIChE J.*, 59, 2621-2629, 2013.

119) G. J. Guo, M. Li, Y. G. Zhang, C. H. Wu. Why can Water Cages Adsorb Aqueous Methane?

A Potential of Mean Force Calculation on Hydrate Nucleation Mechanisms. *Phys. Chem. Chem. Phys.*, 11, 10427-10437, 2009.

120) C. Liu, Z. Zhang, G. J. Guo. Effect of Guests on the Adsorption Interaction Between a Hydrate Cage and Guests. *RSC Adv.*, 6, 106443-106452, 2016.

121) C. J. Liu, Z. C. Zhang, Z. G. Zhang, Y. G. Zhang, G. J. Guo. Effects of Cage Type and Adsorption Face on the Cage-Methane Adsorption Interaction: Implications for Hydrate Nucleation Studies. *Chem. Phys. Lett.*, 575, 54-58, 2013.

122) A. Y. Galashev. Atomistic Simulations of Methane Interactions with an Atmospheric Moisture. *J. Chem. Phys.*, 139, 124303, 2013.

123) R. Vácha, P. Slavíček, M. Mucha, B. J. Finlayson-Pitts, P. Jungwirth. Adsorption of Atmospherically Relevant Gases at the Air/Water Interface: Free Energy Profiles of Aqueous Solvation of N_2, O_2, O_3, OH, H_2O, HO_2 and H_2O_2. *J. Phys. Chem. A*, 108, 11573-11579, 2004.

124) R. Vácha, P. Jungwirth, J. Chen, K. Valsaraj. Adsorption of Polycyclic Aromatic Hydrocarbons at the Air-Water Interface: Molecular Dynamics Simulations and Experimental Atmospheric Observations. *Phys. Chem. Chem. Phys.*, 8, 4461-4467, 2006.

125) A. Ghoufi, P. Malfreyt. Numerical Evidence of the Formation of a Thin Microscopic Film of Methane at the Water Surface: A Free Energy Calculation. *Phys. Chem. Chem. Phys.*, 12, 5203-5205, 2010.

126) T. Somasundaram, R. M. Lynden-Bell, C. H. Patterson. The Passage of Gases through the Liquid Water/Vapour Interface: A Simulation Study. *Phys. Chem. Chem. Phys.*, 1, 143-148, 1999.

127) E. L. Murina, C. Pastorino, R. Fernández-Prini. Entrance Dynamics of CH_4 Molecules through a Methane-Water Interface. *Chem. Phys. Lett.*, 637, 13-17, 2015.

128) C. J. H. Knox, L. F. Phillips. Capillary-Wave Model of Gas-Liquid Exchange. *J. Phys. Chem. B*, 102, 8469-8472, 1998.

129) L. B. Pártay, P. Jedlovszky, A. Vincze, G. Horvai. Properties of Free Surface of Water-Methanol Mixtures. Analysis of the Truly Interfacial Molecular Layer in Computer Simulation. *J. Phys. Chem. B*, 112, 5428-5438, 2008.

130) M. Matsumoto, Y. Takaoka, Y. Kataoka. Liquid-Vapor Interface of Water-Methanol Mixture. I. Computer Simulation. *J. Chem. Phys.*, 98, 1464, 1993.

131) T. M. Chang, L. X. Dang. Liquid-Vapor Interface of Methanol-Water Mixtures: A Molecular Dynamics Study. *J. Phys. Chem. B.*, 109, 5759-5765, 2005.

132) H. Chen, W. Gan, R. Lu, Y. Guo, H. F. Wang. Determination of Structure and Energetics for Gibbs Surface Adsorption Layers of Binary Liquid Mixture 2. Methanol + Water. *J. Phys. Chem. B*, 109, 8064-8075, 2005.

133) J. Sung, K. Park, D. Kim. Surfaces of Alcohol-Water Mixtures Studied by Sum-Frequency Generation Vibrational Spectroscopy. *J. Phys. Chem. B*, 109, 18507-18514, 2005.

134) K. Wolfrum, H. Graener, A. Laubereau. Sum-frequency Vibrational Spectroscopy at the Liquid-Air Interface of Methanol.Water solutions. *Chem. Phys. Lett.*, 213, 41-46, 1993.

135) C. D. Stanners, Q. Du, R. P. Chin, P. Cremer, G. A. Somorjai, Y. R. Shen. Polar Ordering at the Liquid-Vapor Interface of *n*-Alcohols (C_1-C_8). *Chem. Phys. Lett.*, 232, 407-413, 1995.

136) G. Raina, G. U. Kulkarni, C. N. R. Rao. Surface Enrichment in Alcohol-Water Mixtures. *J. Phys. Chem. A*, 105, 10204-10207, 2001.

137) L. Pártay, P. Jedlovszky, A. Vincze, G. Horvai. Structure of the Liquid-Vapor Interface of Water-Methanol Mixtures as Seen from Monte Carlo Simulations. *J. Phys. Chem. B*, 109,

20493-20503, 2005.

138) S. Paul, A. Chandra. Hydrogen Bond Properties and Dynamics of Liquid-Vapor Interfaces of Aqueous Methanol Solutions. *J. Chem. Theory Comput.*, 1, 1221-1231, 2005.

139) J. R. Choudhuri, A. Chandra. Hydrogen Bonded Structure, Polarity, Molecular Motion and Frequency Fluctuations at Liquid-Vapor Interface of a Water-Methanol Mixture: An *Ab initio* Molecular Dynamics Study. *J. Chem. Phys.*, 141, 134703, 2014.

140) M. Darvas, L. B. Pártay, P. Jedlovszky, G. Horvai. Computer Simulation and ITIM Analysis of the Surface of Water-Methanol Mixtures Containing Traces of Water. *J. Mol. Liq.*, 153, 88-93, 2010.

141) T. Yagasaki, M. Matsumoto, H. Tanaka. Effects of Thermodynamic Inhibitors on the Dissociation of Methane Hydrate: A Molecular Dynamics Study. *Phys. Chem. Chem. Phys.*, 17, 32347-32357, 2015.

142) M. P. Allen, D. J. Tildesley. Computer Simulation of Liquids. Oxford University Press: New york, 1991.

143) R. Tripathi, N. N. Nair. Mechanism of Acyl-Enzyme Complex Formation from the Henry-Michaelis Complex of Class C β-Lactamases with β-Lactam Antibiotics. *J. Am. Chem. Soc.*, 135, 14679-14690, 2013.

144) V. Imandi, N. N. Nair. The Wacker Oxidation of Allyl Alcohol along Cyclic-Intermediate Routes: An *Ab initio* Molecular Dynamics Investigation. *Chem. Phys. Lett.*, 660, 111-116, 2016.

145) R. Tripathi, N. N. Nair. Mechanism of Meropenem Hydrolysis by New Delhi Metallo β-Lactamase. *ACS Catal.*, 5, 2577-2586, 2015.

146) T. K. Ghosh, N. N. Nair. Alumina-supported Rh, Rh2, and Rh1(CO) as Catalysts for

Hydrogen Evolution from Water. *Surf. Sci.*, 632, 20-27, 2015.

147) S. Biswas, T. Dasgupta, B. S. Mallik. Proton Transfer from Water to Ketyl Radical Anion: Assessment of Critical Size of Hydrated Cluster and Free Energy Barrier in Solution from First Principles Simulations. *Chem. Phys.*, 477, 46-51, 2016.

148) S. Biswas, B. S. Mallik. Proton Transfer from Water to Anion: Free Energy Profile from First Principles Metadynamics Simulations. *J. Mol. Liq.*, 219, 810-814, 2016.

149) S. Biswas, B. S. Mallik. A Delicate Case of Unidirectional Proton Transfer from Water to an Aromatic Heterocyclic Anion. *Phys. Chem. Chem. Phys.*, 18, 29979-29986, 2016.

150) P. Dopieralski, J. Ribas-Arino, P. Anjukandi, M. Krupicka, D. Marx. Unexpected Mechanochemical Complexity in the Mechanistic Scenarios of Disulfide Bond Reduction in Alkaline Solution. *Nat. Chem.*, 9, 164-170, 2017.

151) P. Dopieralski, J. Ribas-Arino, P. Anjukandi, M. Krupicka, J. Kiss, D. Marx. The Janus-faced Role of External Forces in Mechanochemical Disulfide Bond Cleavage. *Nat. Chem.*, 5, 685-691, 2013.

152) Y. Kubota, T. Ohnuma, T. Bučko. Carbon Dioxide Capture in 2-aminoethanol Aqueous Solution from A*b initio* Molecular Dynamics Simulations. *J. Chem. Phys.*, 146, 094303, 2017.

153) Z. Mester, A. Z. Panagiotopoulos. Mean Ionic Activity Coefficients in Aqueous NaCl Solutions from Molecular Dynamics Simulations. *J. Chem. Phys.*, 142, 044507, 2015.

154) M. Hellström, J. Behler. Structure of Aqueous NaOH Solutions: Insights from Neural-network-based Molecular Dynamics Simulations. *Phys. Chem. Chem. Phys.*, 19, 82-96, 2017.

155) S. Yadav, A. Chandra. Preferential Solvation, Ion Pairing, and Dynamics of Concentrated

Aqueous Solutions of Divalent Metal Nitrate Salts. *J. Chem. Phys.*, 147, 244503, 2017.

156) S. Prasad, C. Chakravarty, H. K. Kashyap. Concentration-dependent Structure and Dynamics of Aqueous LiCl Solutions: A Molecular Dynamics Study. *J. Mol. Liq.*, 225, 240-250, 2017.

157) S. Kaur, H. K. Kashyap. Three-dimensional Morphology and X-ray Scattering Structure of Aqueous *tert*-Butanol Mixtures: A Molecular Dynamics Study. *J. Chem. Sci.*, 129, 103-116, 2017.

158) M. Chopra, N. Choudhury. Effect of Uranyl Ion Concentration on Structure and Dynamics of Aqueous Uranyl Solution: A Molecular Dynamics Simulation Study. *J. Phys. Chem. B*, 118, 14373-14381, 2014.

159) S. Borah, P. Padma Kumar. *Ab initio* Molecular Dynamics Investigation of Structural, Dynamic and Spectroscopic Aspects of Se(VI) Species in the Aqueous Environment. *Phys. Chem. Chem. Phys.*, 18, 14561-14568, 2016.

160) S. Borah, P. Padma Kumar. *Ab initio* Molecular Dynamics Study of Se(IV) Species in Aqueous Environment. *Phys. Chem. Chem. Phys.*, 18, 26755-26763, 2016.

161) P. Padma Kumar, A. G. Kalinichev, R. J. Kirkpatrick. Hydrogen-Bonding Structure and Dynamics of Aqueous Carbonate Species from Car-Parrinello Molecular Dynamics Simulations. *J. Phys. Chem. B*, 113, 794-802, 2009.

162) T. A. Pham, T. Ogitsu, E. Y. Lau, E. Schwegler. Structure and Dynamics of Aqueous Solutions from PBE-based First-Principles Molecular Dynamics Simulations. *J. Chem. Phys.*, 145, 154501, 2016.

163) Y. G. Bushuev, S. V. Davletbaeva, O. I. Koifman. Molecular Dynamics Simulations of Aqueous Glycine Solutions. *CrystEngComm*, 19, 7197-7206, 2017.

164) K. R. Ramya, P. Kumar, A. Venkatnathan. Molecular Simulations of Anion and Temperature Dependence on Structure and Dynamics of 1-Hexyl-3-methylimidazolium Ionic Liquids. *J. Phys. Chem. B*, 119, 14800-14806, 2015.

165) K. R. Ramya, P. Kumar, A. Kumar, A. Venkatnathan. Interplay of Phase Separation, Tail Aggregation, and Micelle Formation in the Nanostructured Organization of Hydrated Imidazolium Ionic Liquid. *J. Phys. Chem. B*, 118, 8839-8847, 2014.

166) S. Sharma, A. Gupta, D. Dhabal, H. K. Kashyap. Pressure-dependent Morphology of Trihexyl(tetradecyl)phosphonium Ionic Liquids: A Molecular Dynamics Study. *J. Chem. Phys.*, 145, 134506, 2016.

167) C. D. Wick, L. X. Dang, P. Jungwirth. Simulated Surface Potentials at the Vapor-Water Interface for the KCl Aqueous Electrolyte Solution. *J. Chem. Phys.*, 125, 024706, 2006.

168) C. D. Wick, L. X. Dang. Computational Investigation of the Influence of Organic-Aqueous Interfaces on NaCl Dissociation Dynamics. *J. Chem. Phys.*, 132, 044702, 2010.

169) R. C. Dutta, S. K. Bhatia. Structure and Gas Transport at the Polymer-Zeolite Interface: Insights from Molecular Dynamics Simulations. *ACS Appl. Mater. Interfaces*, 10, 5992-6005, 2018.

170) S. Sharma, H. K. Kashyap. Interfacial Structure of Pyrrolidinium Cation Based Ionic Liquids at Charged Carbon Electrodes: The Role of Linear and Nonlinear Alkyl Tails. *J. Phys. Chem. C*, 121, 13202-13210, 2017.

171) N. R. Tummala, S. Liu, D. Argyris, A. Striolo. Interfacial Water Properties in the Presence of Surfactants. *Langmuir*, 31, 2084-2094, 2015.

172) P. Bhauriyal, A. Mahata, B. Pathak. Graphene-like Carbon-Nitride Monolayer: A Potential

Anode Material for Na- and K-Ion Batteries. *J. Phys. Chem. C*, 122, 2481-2489, 2018.

173) S. R. Subramanian, E. R. A. Singam, M. Berinski, V. Subramanian, R. C. Wade. Identification of an Electrostatic Ruler Motif for Sequence-Specific Binding of Collagenase to Collagen. *J. Phys. Chem. B*, 120 , 8580-8589, 2016.

174) L. Baweja, K. Balamurugan, V. Subramanian, A. Dhawan. Effect of Graphene Oxide on the Conformational Transitions of Amyloid Beta Peptide: A Molecular Dynamics Simulation Study. *J. Mol. Graphics Modell.*, 61, 175-185, 2015.

175) S. Sarkar, S. Ghosh, R. Chakrabarti. Ammonium Based Stabilizers Effectively Counteract Urea-induced Denaturation in a Small Protein: Insights from Molecular Dynamics Simulations. *RSC Adv.*, 7, 52888-52906, 2017.

176) S. Ghosh, N. Patel, R. Chakrabarti. Probing the Salt Concentration Dependent Nucleobase Distribution in a Single-Stranded DNA-Single-Walled Carbon Nanotube Hybrid with Molecular Dynamics. *J. Phys. Chem. B*, 120 , 455-466, 2016.

177) S. Paul, S. Taraphder. Determination of the Reaction Coordinate for a Key Conformational Fluctuation in Human Carbonic Anhydrase II. *J. Phys. Chem. B*, 119, 11403-11415, 2015.

178) A. Roy, S. Taraphder. Identification of Proton-Transfer Pathways in Human Carbonic Anhydrase II. *J. Phys. Chem. B*, 111, 10563-10576, 2007.

179) S. Goyal, A. Chattopadhyay, K. Kasavajhala, U. D. Priyakumar. Role of Urea-Aromatic Stacking Interactions in Stabilizing the Aromatic Residues of the Protein in Urea-Induced Denatured State. *J. Am. Chem. Soc.*, 139, 14931-14946, 2017.

180) S. Padhi, U. D. Priyakumar. Urea-Aromatic Stacking and Concerted Urea Transport: Conserved Mechanisms in Urea Transporters Revealed by Molecular Dynamics. *J. Chem. Theory Comput.*, 12, 5190-5200, 2016.

181) M. Gupta, P. Khatua, C. Chakravarty, S. Bandyopadhyay. Hydration Behavior along the Folding Pathways of Trpzip4, Trpzip5 and Trpzip6. *J. Phys. Chem. B*, 122, 1560-1572, 2018.

182) M. Gupta, P. Khatua, C. Chakravarty, S. Bandyopadhyay. The Sensitivity of Folding Free Energy Landscapes of Trpzips to Mutations in the Hydrophobic Core. *Phys. Chem. Chem. Phys.*, 19, 22813-22825, 2017.

183) K. Chakraborty, S. Bandyopadhyay. Correlated Dynamical Crossovers of the Hydration Layer of a Single-Stranded DNA Oligomer. *J. Phys. Chem. B*, 118, 413-422, 2014.

184) M. Khatua, S. Pan, P. K. Chattaraj. Movement of Ng_2 Molecules Confined in a C_{60} cage: An Ab initio Molecular Dynamics Study. *Chem. Phys. Lett.*, 610-611, 351-356, 2014.

185) S. Paul, T. G. Abi, S. Taraphder. Structure and Dynamics of Water Inside Endohedrally Functionalized Carbon Nanotubes. *J. Chem. Phys.*, 140, 184511, 2014.

186) S. Paul, S. Taraphder. Functionalized Single Walled Carbon Nanotubes as Template for Water Storage Device. *Chem. Phys.*, 479, 42-52, 2016.

187) M. Chopra, N. Choudhury. Comparison of Structure and Dynamics of Polar and Nonpolar Fluids through Carbon Nanotubes. *J. Phys. Chem. C*, 117, 18398-18405, 2013.

188) S. Pantawane, D. Bandyopadhyay, N. Choudhury. Generic Mechanism for Pattern Formation in the Solvation Shells of Buckminsterfullerene. *ACS Omega*, 3, 1060-1068, 2018.

189) N. Choudhury. Dynamics of Water in Solvation Shells and Intersolute Regions of C_{60}: A Molecular Dynamics Simulation Study. *J. Phys. Chem. C*, 111, 2565-2572, 2007.

190) N. Choudhury. A Molecular Dynamics Simulation Study of Buckyballs in Water: Atomistic Versus Coarse-Grained Models of C_{60}. *J. Chem. Phys.*, 125, 034502, 2006.

191) M. Matsumoto, S. Saito, I. Ohmine. Molecular Dynamics Simulation of the Ice Nucleation and Growth Process Leading to Water Freezing. *Nature*, 416, 409-413, 2002.

192) J. Y. Yan, G. N. Patey. Molecular Dynamics Simulations of Ice Nucleation by Electric Fields. *J. Phys. Chem. A*, 116, 7057-7064, 2012.

193) M. Fitzner, G. C. Sosso, S. J. Cox, A. Michaelides. The Many Faces of Heterogeneous Ice Nucleation: Interplay Between Surface Morphology and Hydrophobicity. *J. Am. Chem. Soc.*, 137, 13658-13669, 2015.

194) A. J. B. di Lorenzo, M. A. Carignano, R. G. Pereyra. A Statistical Study of Heterogeneous Nucleation of Ice by Molecular Dynamics. *Chem. Phys. Lett.*, 635, 45-49, 2015.

195) L. Lupi, A. Hudait, V. Molinero. Heterogeneous Nucleation of Ice on Carbon Surfaces. *J. Am. Chem. Soc.*, 136, 3156-3164, 2014.

196) E. Pluhařová, L. Vrbka, P. Jungwirth. Effect of Surface Pollution on Homogeneous Ice Nucleation: A Molecular Dynamics Study. *J. Phys. Chem. C*, 114, 7831-7838, 2010.

197) D. Quigley, P. M. Rodger. Metadynamics Simulations of Ice Nucleation and Growth. *J. Chem. Phys.*, 128, 154518, 2008.

198) T. Li, D. Donadio, G. Russo, G. Galli. Homogeneous Ice Nucleation from Supercooled Water. *Phys. Chem. Chem. Phys.*, 13, 19807-19813, 2011.

199) E. Sanz, C. Vega, J. R. Espinosa, R. Caballero-Bernal, J. L. F. Abascal, C. Valeriani. Homogeneous Ice Nucleation at Moderate Supercooling from Molecular Simulation. *J. Am. Chem. Soc.*, 135, 15008-15017, 2013.

200) J. R. Espinosa, G. D. Soria, J. Ramirez, C. Valeriani, C. Vega, E. Sanz. Role of Salt,

Pressure, and Water Activity on Homogeneous Ice Nucleation. *J. Phys. Chem. Lett.*, 8, 4486-4491, 2017.

201) M. R. Walsh, C. A. Koh, E. D. Sloan, A. K. Sum, D. T. Wu. Microsecond Simulations of Spontaneous Methane Hydrate Nucleation and Growth. *Science*, 326, 1095-1098, 2009.

202) L. C. Jacobson, W. Hujo, V. Molinero. Amorphous Precursors in the Nucleation of Clathrate Hydrates. *J. Am. Chem. Soc.*, 132, 11806-11811, 2010.

203) J. Vatamanu, P. G. Kusalik. Observation of Two-Step Nucleation in Methane Hydrates. *Phys. Chem. Chem. Phys.*, 12, 15065-15072, 2010.

204) S. Sarupria, P. G. Debenedetti. Homogeneous Nucleation of Methane Hydrate in Microsecond Molecular Dynamics Simulations. *J. Phys. Chem. Lett.*, 3, 2942-2947, 2012.

205) Z. He, P. Linga, J. Jiang. What are the Key Factors Governing the Nucleation of CO_2 Hydrate? *Phys. Chem. Chem. Phys.*, 19, 15657-15661, 2017.

206) Y. T. Tung, L. J. Chen, Y. P. Chen, S. T. Lin. The Growth of Structure I Methane Hydrate from Molecular Dynamics Simulations. *J. Phys. Chem. B*, 114, 10804-10813, 2010.

207) J. Vatamanu, P. G. Kusalik. Molecular Insights into the Heterogeneous Crystal Growth of sI Methane Hydrate. *J. Phys. Chem. B*, 110, 15896-15904, 2006.

208) Y. T. Tung, L. J. Chen, Y. P. Chen, S. T. Lin. Growth of Structure I Carbon Dioxide Hydrate from Molecular Dynamics Simulations. *J. Phys. Chem. C*, 115, 7504-7515, 2011.

209) S. Liang, P. G. Kusalik. Crystal Growth Simulations of H_2S Hydrate. *J. Phys. Chem. B*, 114, 9563-9571, 2010.

210) Y. T. Tung, L. J. Chen, Y. P. Chen, S. T. Lin. Molecular Dynamics Study on the Growth of

Structure I Methane Hydrate in Aqueous Solution of Sodium Chloride. *J. Phys. Chem. B*, 116, 14115-14125, 2012.

211) S. Liang, D. Rozmanov, P. G. Kusalik. Crystal Growth Simulations of Methane Hydrates in the Presence of Silica Surfaces. *Phys. Chem. Chem. Phys.*, 13, 19856-19864, 2011.

212) K. F. Yan, X. S. Li, Z. Y. Chen, Z. M. Xia, C. G. Xu, Z. Zhang. Molecular Dynamics Simulation of the Crystal Nucleation and Growth Behavior of Methane Hydrate in the Presence of the Surface and Nanopores of Porous Sediment. *Langmuir*, 32, 7975-7984, 2016.

213) M. E. Tuckerman. *Ab initio* Molecular Dynamics: Basic Concepts, Current Trends and Novel Applications. *J. Phys.: Condens. Matter*, 14, R1297, 2002.

214) D. van der Spoel, E. Lindahl, B. Hess, and the GROMACS development team, *GROMACS User Manual version 4.6.5*, www.gromacs.org, 2013.

215) S. J. Weiner, P. A. Kollman, D. A. Case, U. C. Singh, C. Ghio, G. Alagona, S. Jr. Profeta, P. Weiner. A New Force Field for Molecular Mechanical Simulation of Nucleic Acids and Proteins. *J. Am. Chem. Soc.*, 106, 765-784, 1984.

216) W. D. Cornell, P. Cieplak, C. I. Bayly, I. R. Gould, K. M. Merz, D. M. Ferguson, D. C. Spellmeyer, T. Fox, J. W. Caldwell, P. A. Kollman. A Second Generation Force Field for the Simulation of Proteins, Nucleic Acids, and Organic Molecules. *J. Am. Chem. Soc.*, 117, 5179-5197, 1995.

217) B. R. Brooks, R. E. Bruccoleri, B. D. Olafson, D. J. States, S. Swaminathan, M. Karplus. CHARMM: A Program for Macromolecular Energy, Minimization, and Dynamics Calculations. *J. Comput. Chem.*, 4, 187-217, 1983.

218) W. L. Jorgensen, D. S. Maxwell, J. Tirado-Rives. Development and Testing of the OPLS All-Atom Force Field on Conformational Energetics and Properties of Organic Liquids. *J. Am.*

Chem. Soc., 118, 11225-11236, 1996.

219) J. D. Bernal, R. H. Fowler. A Theory of Water and Ionic Solution, with Particular Reference to Hydrogen and Hydroxyl Ions. *J. Chem. Phys.*, 1, 515, 1933.

220) H. J. C. Berendsen, J. P. M. Postma, W. F. van Gunsteren, J. Hermans. Interaction Models for Water in Relation to Protein Hydration. In *Intermolecular Forces*, Pullman, B., Ed., Reidel: Dordrecht, The Netherlands, 14, 331-342, 1981.

221) W. L. Jorgensen, J. Chandrasekhar, J. D. Madura, R. W. Impey, M. L. Klein. Comparison of Simple Potential Functions for Simulating Liquid Water. *J. Chem. Phys.*, 79, 926, 1983.

222) M. W. Mahoney, W. L. Jorgensen. A Five-Site Model for Liquid Water and the Reproduction of the Density Anomaly by Rigid, Nonpolarizable Potential Functions. *J. Chem. Phys.*, 112, 8910, 2000.

223) H. J. C. Berendsen, J. R. Grigera, T. P. Straatsma. The Missing Term in Effective Pair Potentials. *J. Phys. Chem.*, 91, 6269-6271, 1987.

224) H. W. Horn, W. C. Swope, J. W. Pitera, J. D. Madura, T. J. Dick, G. L. Hura, T. Head-Gordon. Development of an Improved Four-Site Water Model for Biomolecular Simulations: TIP4P-Ew. *J. Chem. Phys.*, 120, 9665, 2004.

225) J. L. F. Abascal, C. Vega. A General Purpose Model for the Condensed Phases of Water: TIP4P/2005. *J. Chem. Phys.*, 123, 234505, 2005.

226) A. V. Onufriev, S. Izadi. Water Models for Biomolecular Simulations. *WIREs Comput. Mol. Sci.*, 8, 2018, doi: 10.1002/wcms.1347.

227) E. Sanz, C. Vega, J. L. F. Abascal, L. G. MacDowell. Phase Diagram of Water from Computer Simulation. *Phys. Rev. Lett.*, 92, 255701, 2004.

228) E. Sanz, C. Vega, J. L. F. Abascal, L. G. MacDowell. Tracing the Phase Diagram of the Four-Site Water Potential (TIP4P). *J. Chem. Phys.*, 121, 1165, 2004.

229) W. L. Jorgensen, J. Tirado-Rives. Potential Energy Functions for Atomic-Level Simulations of Water and Organic and Biomolecular Systems. *Proc. Natl. Acad. Sci. U.S.A.*, 102, 6665-6670, 2005.

230) J. G. Harris, K. H. Yung. Carbon Dioxide's Liquid-Vapor Coexistence Curve And Critical Properties as Predicted by a Simple Molecular Model. *J. Phys. Chem.*, 99, 12021-12024, 1995.

231) H. J. C. Berendsen, J. P. M. Postma, W. F. van Gunsteren, A. DiNola, J. R. Haak. Molecular Dynamics with Coupling to an External Bath. *J. Chem. Phys.*, 81, 3684, 1984.

232) S. Nosé. A Unified Formulation of the Constant Temperature Molecular Dynamics Methods. *J. Chem. Phys.*, 81, 511, 1984.

233) W. G. Hoover. Canonical Dynamics: Equilibrium Phase-Space Distributions. *Phys. Rev. A: At., Mol., Opt. Phys.*, 31, 1695, 1985.

234) H. C. Andersen. Molecular Dynamics Simulations at Constant Pressure and/or Temperature. *J. Chem. Phys.*, 72, 2384, 1980.

235) M. Parrinello, A. Rahman. Polymorphic Transitions in Single Crystals: A New Molecular Dynamics Method. *J. Appl. Phys.*, 52, 7182-7190, 1981.

236) J. Qin, R. J. Rosenbauer, Z. Duan. Experimental Measurements of Vapor-Liquid Equilibria of the H_2O + CO_2 + CH_4 Ternary System. *J. Chem. Eng. Data*, 53, 1246-1249, 2008.

237) S. Z. S. Al Ghafri, E. Forte, G. C. Maitland, J. J. Rodriguez-Henríquez, J. P. M. Trusler. Experimental and Modeling Study of the Phase Behavior of (Methane + CO_2 + Water) Mixtures.

J. Phys. Chem. B, 118, 14461-14478, 2014.

238) W. L. Jorgensen, J. D. Madura, C. J. Swenson. Optimized Intermolecular Potential Functions for Liquid Hydrocarbons. *J. Am. Chem. Soc.*, 106, 6638-6646, 1984.

239) X. Li, D. A. Ross, J. P. M. Trusler, G. C. Maitland, E. S. Boek. Molecular Dynamics Simulations of CO_2 and Brine Interfacial Tension at High Temperatures and Pressures. *J. Phys. Chem. B*, 117, 5647-5652, 2013.

240) Z. Duan, Z. Zhang. Equation of State of the H_2O, CO_2, and H_2O-CO_2 Systems up to 10 GPa and 2573.15 K: Molecular Dynamics Simulations with *Ab Initio* Potential Surface. *Geochim. Cosmochim. Acta*, 70, 2311-2324, 2006.

241) B. Hess, C. Kutzner, D. van der Spoel, E. Lindahl. GROMACS 4: Algorithms for Highly Efficient, Load-Balanced, and Scalable Molecular Simulation. *J. Chem. Theory Comput.*, 4, 435-447, 2008.

242) J. E. Basconi, M. R. Shirts. Effects of Temperature Control Algorithms on Transport Properties and Kinetics in Molecular Dynamics Simulations. *J. Chem. Theory Comput.*, 9, 2887-2899, 2013.

243) B. Hess, H. Bekker, H. J. C. Berendsen, J. G. E. M. Fraaije. LINCS: A Linear Constraint Solver for Molecular Simulations. *J. Comput. Chem.*, 18, 1463-1472, 1997.

244) S. Miyamoto, P. A. Kollman. Settle: An Analytical Version of the SHAKE and RATTLE Algorithm for Rigid Water Models. *J. Comput. Chem.*, 13, 952-962, 1992.

245) P. S. Epstein, M. S. Plesset. On the Stability of Gas Bubbles in Liquid-Gas Solutions. *J. Chem. Phys.*, 18, 1505-1509, 1950.

246) K. Ohgaki, N. Q. Khanh, Y. Joden, A. Tsuji, T. Nakagawa. Physicochemical Approach to

Nanobubble Solutions. *Chem. Eng. Sci.*, 65, 1296-1300, 2010.

247) J. H. Weijs, J. R. T. Seddon, D. Lohse. Diffusive Shielding Stabilizes Bulk Nanobubble Clusters. *ChemPhysChem*, 13, 2197-2204, 2012.

248) G. J. Guo, P. M. Rodger. Solubility of Aqueous Methane under Metastable Conditions: Implications for Gas Hydrate Nucleation. *J. Phys. Chem. B*, 117, 6498-6504, 2013.

249) I. Skarmoutsos, L. I. Kampanakis, J. Samios. Investigation of the Vapor-Liquid Equilibrium and Supercritical Phase of Pure Methane via Computer Simulations. *J. Mol. Liq.*, 117, 33-41, 2005.

250) L. Yi, D. Liang, S. Liang, X. Zhou. Molecular Dynamics Study of CH_4-CO_2 Mixed Hydrate Dissociation. *Asia-Pac. J. Chem. Eng.*, 10, 823-832, 2015.

251) D. E. Smith, L. X. Dang. Computer Simulations of NaCl Association in Polarizable Water. *J. Chem. Phys.*, 100, 3757, 1994.

252) W. L. Jorgensen. Optimized Intermolecular Potential Functions for Liquid Alcohols. *J. Phys. Chem.*, 90, 1276-1284, 1986.

253) W. Humphrey, A. Dalke, K. Schulten. VMD: Visual Molecular Dynamics. *J. Mol. Graphics*, 14, 33-38, 1996.

254) N. Choudhury. Effect of Salt on the Dynamics of Aqueous Solution of Hydrophobic Solutes: A Molecular Dynamics Simulation Study. *J. Chem. Eng. Data*, 54, 542-547, 2009.

255) V. V. Zakharov, E. N. Brodskaya, A. Laaksonen. Surface Tension of Water Droplets: A Molecular Dynamics Study of Model and Size Dependencies. *J. Chem. Phys.*, 107, 10675, 1997.

256) G. Vázquez, E. Alvarez, J. M. Navaza. Surface Tension of Alcohol+Water from 20 to 50 °C.

J. Chem. Eng. Data, 40, 611-614, 1995.

257) F. Biscay, A. Ghoufi, P. Malfreyt. Surface Tension of Water-Alcohol Mixtures from Monte Carlo Simulations. *J. Chem. Phys.*, 134, 044709, 2011.

258) Q. Xu, M. Nakajima, S. Ichikawa, N. Nakamura, P. Roy, H. Okadome, T. Shiina. Effects of Surfactant and Electrolyte Concentrations on Bubble Formation and Stabilization. *J. Colloid Interface Sci.,* 332, 208-214, 2009.

259) R. Sakamaki, A. K. Sum, T. Narumi, R. Ohmura, K. Yasuoka. Thermodynamic Properties of Methane/Water Interface Predicted by Molecular Dynamics Simulations. *J. Chem. Phys.*, 134, 144702, 2011.

260) L. B. Pártay, G. Hantal, P. Jedlovszky, A. Vincze, G. Horvai. A New Method for Determining the Interfacial Molecules and Characterizing the Surface Roughness in Computer Simulations. Application to the Liquid-Vapor Interface of Water. *J. Comput. Chem.*, 29, 945-956, 2008.

261) P. E. Mason. Molecular Dynamics Study on the Microscopic Details of the Evaporation of Water. *J. Phys. Chem. A*, 115, 6054-6058, 2011.

262) S. Strazdaite, J. Versluis, H. J. Bakker. Water Orientation at Hydrophobic Interfaces. *J. Chem. Phys.*, 143, 084708, 2015.

263) J. Grdadolnik, F. Merzel, F. Avbelj. Origin of Hydrophobicity and Enhanced Water Hydrogen Bond Strength Near Purely Hydrophobic Solutes. *Proc. Natl. Acad. Sci. U. S. A.*, 114, 322-327, 2017.

264) E. Ruckenstein, Y. S. Djikaev. Effect of Hydrogen Bonding between Water Molecules on Their Density Distribution near a Hydrophobic Surface. *J. Phys. Chem. Lett.*, 2, 1382-1386, 2011.

265) Y. S. Djikaev, E. Ruckenstein. Probabilistic Approach to the Length-Scale Dependence of the Effect of Water Hydrogen Bonding on Hydrophobic Hydration. *J. Phys. Chem. B*, 117, 7015-7025, 2013.

266) Y. S. Djikaev, E. Ruckenstein. Temperature Dependence of the Evaporation Lengthscale for Water Confined Between Two Hydrophobic Plates. *J. Colloid Interface Sci.*, 449, 226-235, 2015.

267) P. Jedlovszky, M. Darvas, G. Horvai. Relation Between the Surface Tension and Roughness of the Intrinsic Liquid Surface. *Z. Naturforsch., A*, 68, 123-129, 2013.

268) F. Biscay, A. Ghoufi, V. Lachet, P. Malfreyt. Monte Carlo Calculation of the Methane-Water Interfacial Tension at High Pressures. *J. Chem. Phys.*, 131, 124707, 2009.

269) D. Chandler. Interfaces and the Driving Force of Hydrophobic Assembly. *Nature*, 437, 640-647, 2005.

270) K. Lekvam, P. R. Bishnoi. Dissolution of Methane in Water at Low Temperatures and Intermediate Pressures. *Fluid Phase Equilib.*, 131, 297-309, 1997.

271) P. Servio, P. Englezos. Measurement of Dissolved Methane in Water in Equilibrium with Its Hydrate. *J. Chem. Eng. Data*, 47, 87-90, 2002.

272) K. Y. Song, G. Feneyrou, F. Fleyfel, R. Martin, J. Lievois, R. Kobayashi. Solubility Measurements of Methane and Ethane in Water at and near Hydrate Conditions. *Fluid Phase Equilib.*, 128, 249-260, 1997.

273) S. Yamamoto, J. B. Alcauskas, T. E. Crozier. Solubility of Methane in Distilled Water and Seawater. *J. Chem. Eng. Data*, 21, 78-80, 1976.

274) T. D. O'Sullivan, N. O. Smith. The Solubility and Partial Molar Volume of Nitrogen and

Methane in Water and in Aqueous Sodium Chloride from 50 to 125° and 100 to 600 Atm. *J. Phys. Chem.*, 74, 1460-1466, 1970.

275) Y. Wang, B. Han, H. Yan, R. Liu. Solubility of CH_4 in the Mixed Solvent *t*-Butyl Alcohol and Water. *Thermochim. Acta*, 253, 327-334, 1995.

276) J. Kiepe, S. Horstmann, K. Fischer, J. Gmehling. Experimental Determination and Prediction of Gas Solubility Data for Methane + Water Solutions Containing Different Monovalent Electrolytes. *Ind. Eng. Chem. Res.*, 42, 5392-5398, 2003.

277) Z. Duan, N. Møller, J. Greenberg, J. H. Weare. The Prediction of Methane Solubility in Natural Waters to High Ionic Strength from 0 to 250°C and from 0 to 1600 bar. *Geochim. Cosmochim. Acta*, 56, 1451-1460, 1992.

278) Y. S. Kim, B. D. Lim, J. E. Lee, C. S. Lee. Solubilities of Carbon Dioxide, Methane, and Ethane in Sodium Chloride Solution Containing Gas Hydrate. *J. Chem. Eng. Data*, 53, 1351-1354, 2008.

279) M. Wise, A. Chapoy, R. Burgass. Solubility Measurement and Modeling of Methane in Methanol and Ethanol Aqueous Solutions. *J. Chem. Eng. Data*, 61, 3200-3207, 2016.

280) H. Docherty, A. Galindo, C. Vega, E. Sanz. A Potential Model for Methane in Water Describing Correctly the Solubility of the Gas and the Properties of the Methane Hydrate. *J. Chem. Phys*, 125, 074510, 2006.

281) O. Konrad, T. Lankau. Solubility of Methane in Water: The Significance of the Methane-Water Interaction Potential. *J. Phys. Chem. B*, 109, 23596-23604, 2005.

282) L. C. Jacobson, V. Molinero. A Methane-Water Model for Coarse-Grained Simulations of Solutions and Clathrate Hydrates. *J. Phys. Chem. B*, 114, 7302-7311, 2010.

283) A. Phan, D. R. Cole, A. Striolo. Aqueous Methane in Slit-Shaped Silica Nanopores: High Solubility and Traces of Hydrates. *J. Phys. Chem. C*, 118, 4860-4868, 2014.